Detection and Spectroscopy of Single CdSe Nanocrystallite Quantum Dots

by

Stephen A. Empedocles

B.A. Chemistry/Psychology
University of Colorado, Boulder, 1991

Submitted to the Department of Chemistry
in partial fulfillment of the requirements for
the degree of

DOCTOR OF PHILOSOPHY

at the

MASSACHUSETTS INSTITUTE OF TECHNOLOGY

June 1999

Signature of Author _____
Department of Chemistry
April 20, 1999

Certified by _____
Moungi G. Bawendi
Professor of Chemistry
Thesis Supervisor

Accepted by _____
Dietmar Seyferth
Chairman, Departmental Committee on Graduate Students

This doctoral thesis has been examined by a committee of the Department of Chemistry as follows:

Professor Robert W. Field _____
Chairman

Professor Moungi G. Bawendi _____
Thesis Supervisor

Professor Robert J. Silbey _____

Detection and Spectroscopy of Single CdSe Nanocrystallite Quantum Dots

by

Stephen Empedocles

Submitted to the Department of Chemistry on April 20, 1999 in partial fulfillment of the requirements for the degree of Doctor of Philosophy in Chemistry.

Abstract

Semiconductor nanocrystallites, with size dependent optical properties that have generated considerable interest over the past 10 years, are intrinsically difficult to study due to inhomogeneities in ensemble samples. In this thesis, I describe the motivation and development of an experimental program designed to detect and spectrally resolve the fluorescence from single CdSe nanocrystallites. Through these experiments, we uncover many new and unexpected physical phenomena such as ultra-narrow emission linewidths, fluorescence blinking on a timescale of seconds, and spectral shifting over a wide range of time and energy scales (from seconds to minutes and from less than 100μeV to greater than 80meV). Ionization is found to play an important role in the optical characteristics of single nanocrystallites by quenching luminescence and by producing large local electric fields. Stark measurements of single nanocrystallites are able to directly measure local electric fields around individual nanocrystallites, and measure changes in the field that occur coincident with spectral shifts. Stark experiments also reveal a highly polarizable excited state (~10^5Å^3) with a large induced excited state dipole (~80 Debye). Single nanocrystallite line shapes are found to primarily reflect fluctuations in the local field over time, which can be controlled by adjusting the excitation intensity, wavelength, sample temperature, and sample preparation. Measured linewidths can also be controlled by adjusting the integration time or by adding an applied electric field. Polarization spectroscopy is used to probe the nature of the transition dipole from the emitting state, uncovering a degenerate dipole that is oriented isotropically in the x-y plane of the nanocrystallite. The 2-dimensional nature of this dipole allows us to use polarization spectroscopy to directly measure the 3-dimensional orientation of each nanocrystallite within a sample. These experiments have provided a new perspective on the physics and dynamics of CdSe nanocrystallites that has been unavailable in ensemble experiments.

Thesis Supervisor: Moungi G. Bawendi, Ph. D.
Title: Professor of Chemistry

To my best friend and the love of my life,

Marianne

Table of Contents

Chapter 1: Introduction

One of the most basic and yet fascinating postulates of quantum mechanics is wave-particle duality, the idea that everything can be described simultaneously as both a wave and a particle. Light, for instance, obeys many physical laws indicating wave-like character (e.g. diffraction), however, at the same time, many aspects can only be described as a particle effect (e.g. photoelectron effect). In the same way, objects that are typically considered to be a particle, such as an electron, are also found to have wave-like character.

While wave-particle duality has been demonstrated experimentally, it is not an effect that is normally observed in everyday life. The reason is that a particle's wavelength is inversely proportional to its momentum, so that macroscopic objects have such short wavelengths that their wave-like character is unobservable. It is only when objects are small compared to a characteristic length scale, defined by the particle's wavelength, that the wavelike character of a particle becomes a dominant effect. At this point, classical mechanics breaks down and the system can only be described in terms of quantum mechanics.

1.1 Quantum Confinement

It is the transition from the classical to the quantum mechanical regime that has encouraged the study of quantum confined systems; systems in which one or more dimensions have been made intentionally small compared to the characteristic length-scale of the material. A well studied example is quantum confined semiconductor structures. When a semiconductor is illuminated by light of sufficient energy, an

electron can be excited from the valence band into the conduction band, leaving behind a positively charged hole. In quantum confined semiconductors, this electron-hole pair, also referred to as an exciton, is physically confined into a region that is smaller than its characteristic length-scale (i.e. the Bohr exciton diameter). Depending on the geometry of the structure (figure 1.1 b-d), the exciton can be confined in one, two or all three dimensions (quantum wells, quantum wires and quantum dots respectively). Two dimensional quantum wells are structures that are extended in 2 dimensions, while the third dimension remains small (like a disk). When an electron-hole pair is excited, it feels a free lattice potential within the plane of the quantum well, but sees a quantum confined "particle in a box" potential in the third dimension. Along the confined direction, only certain wavelengths are stable, so the energy levels in this dimension are quantized. As a result, quantum wells have a distinctly different density of states than what is found in the bulk material (figure 1.1f).

Quantum dots, the zero-dimensional analogue of quantum wells, represent the ultimate in semiconductor quantum confined systems[1,2]. In these structures, the electron and hole see a "particle in a box" potential in all three dimensions (figure 1.1d). Theory predicts that quantum confinement in all three dimensions leads to a collapse of the bulk band structure into discrete, atomic-like states (figure 1.1 h)[3,4]. As a result, quantum dots are often referred to as "artificial atoms".

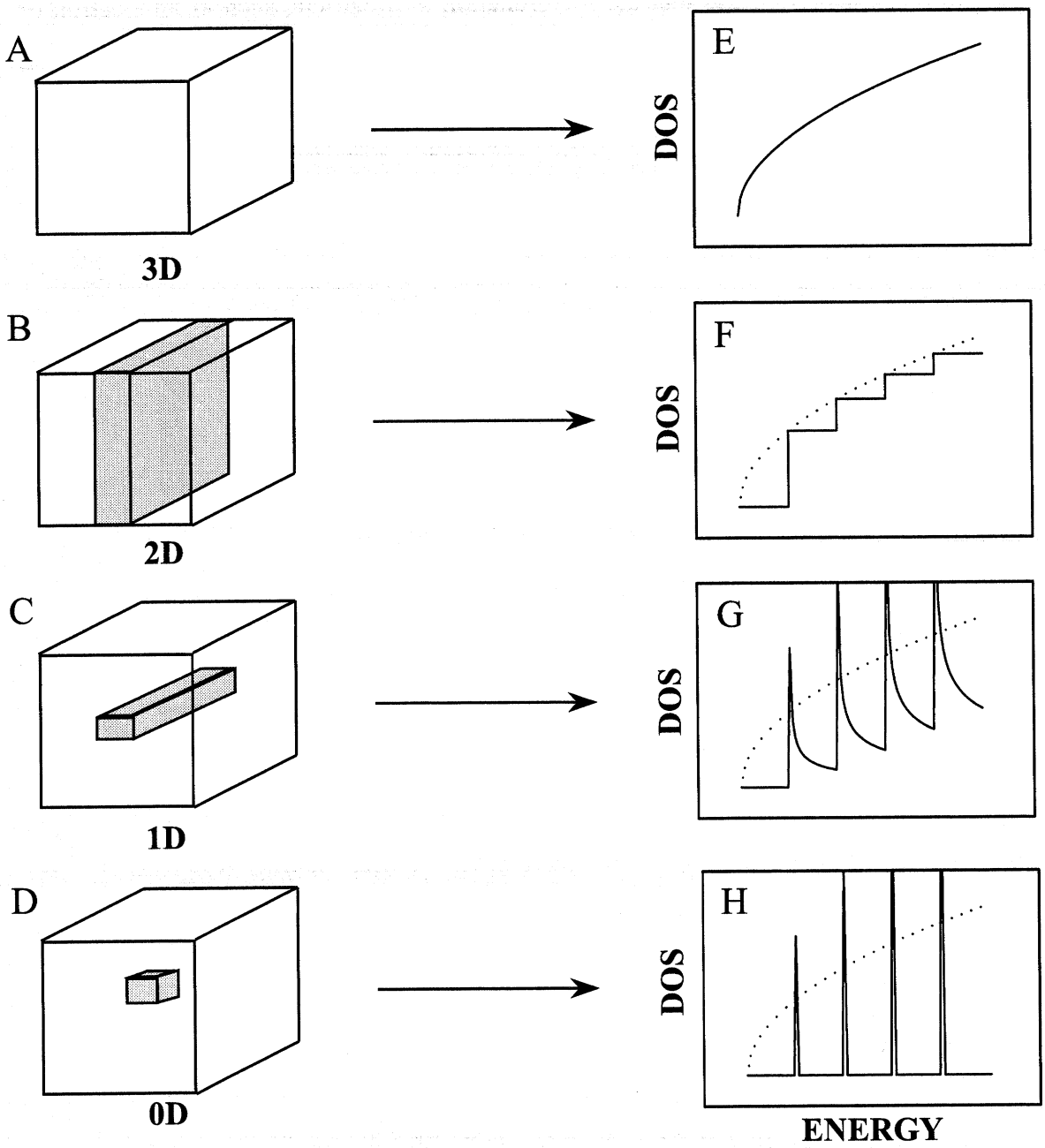

Figure 1.1: Quantum Confinement. Graphic representations of bulk material (A), a 2D quantum well (B), a 1D quantum wire (C) and a 0D quantum dot (D). Also included (E-H) are examples of the corresponding density of states calculated for each system (solid lines) along with the corresponding bulk density of states (dotted lines).

1.2 Quantum Dots - Electronic Structure

Bloch's theorem states that the wavefunction of a particle, such as an electron or hole, $[\psi_{e(h)}(r)]$ in a periodic potential can be described as the product of a unit cell function $[u_{e(h)}(r)]$ times an envelope function $[\varphi_{e(h)}(r)]$: $[\psi_{e(h)}(r)=u_{e(h)}(r)\cdot\varphi_{e(h)}(r)]$. In bulk semiconductors, the envelope function is simply that of a free particle $[\varphi_{e(h)}(r)=\exp(i\cdot\mathbf{k}\cdot\mathbf{r})]$, where **r** and **k** are the position and wavevector of the particle respectively. In the case of a quantum dot, the envelope function describes the "particle in a box" wavefunctions defined by the size and shape of the quantum dot structure. For spherical quantum dots, the envelope functions are the hydrogenic solutions to a "particle in a sphere"[5], and can be written as the product of a radial and an angular component:

$$\varphi_{n,l,m}^{e(h)} \propto \frac{j_l(k_{n,l}r)}{r}\cdot Y_l^m(\theta,\phi),$$

where n, l, and m are the radial, angular momentum and magnetic quantum numbers, r is the radial position, $k_{n,l}$ is the momentum vector, $j_l(k_{n,l}r)$ is the l^{th} order spherical Bessel function, and $Y_l^m(\theta,\phi)$ are the spherical harmonics. In this equation, $k_{n,l}$ is quantized due to the boundary conditions imposed by the quantum dot surface, such that $j_l(k_{n,l}R)=0$, where R is the radius of the sphere. These wavefunctions resemble those of a hydrogen atom, with angular momentum states that can be described as S, P, D, etc., further reinforcing the picture of these structures as "artificial atoms".

The energies of the "particle in a sphere" wavefunctions are the same as those for a free particle with the exception that $k_{n,l}$ is quantized as described above. For the lowest exciton state in a spherical quantum dot, the energy is:

$$E_{exciton} = \frac{\hbar^2 \pi^2}{2m_e R^2} + \frac{\hbar^2 \pi^2}{2m_h R^2} + E_g ,$$

where E_g is the intrinsic bandgap energy of the bulk semiconductor material, R is the radius of the quantum dot, $m_{e(h)}$ is the electron (hole) effective mass, and $\hbar = \frac{h}{2\pi}$ where h is Plank's constant. Within this model, the energy of the lowest excited state changes as the inverse square of the quantum dot radius.

While this simple model neglects effects such as the Coulomb and exchange interactions between the electron and hole, as well as the symmetry of the crystal structure and exact (potentially non-spherical) shape of the quantum dot, these effects are usually small compared to the confinement energy imposed by the size of the quantum dot. In most cases, these effects can be added as perturbations to the "particle in a sphere" model.

This simple picture of a "particle in a box" portrays two of the most fundamental characteristics of quantum dots: 1) The electronic structure of a quantum dot is quantized into discrete states and 2) The energy of these states is dependent on the size of the quantum dot. As an example of these effects, figure 1.2 shows absorption spectra of a series of different size CdSe quantum dots. These spectra clearly reveal the discrete, size dependent nature of the electronic states that is characteristic of zero-dimensional quantum confined structures. It is these features that have generated such interest in quantum dots over the past few years, both for the opportunity to study the fundamental physics of quantum confinement, as well as for use in potential devices such as highly efficient quantum dot lasers, optical switches, and infrared detectors[6].

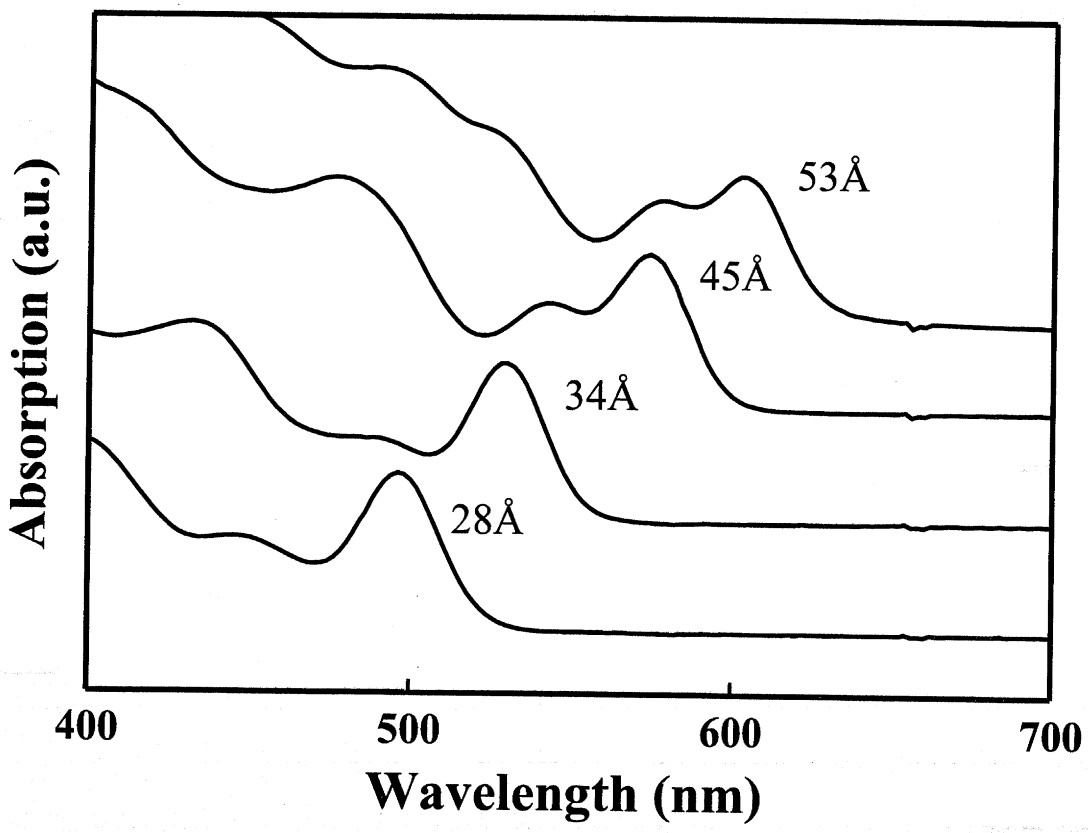

Figure 1.2: Zero-dimensional quantum confinement. Absorption spectra from 4 ensemble quantum dot samples, revealing the evolution of the electronic structure as a function of size. Spectra have been normalized to the height of the first absorption peak and have been vertically offset for clarity. Inset numbers correspond to the average diameter of the quantum dots within each ensemble sample.

1.3 Nanocrystallite Quantum Dots

Quantum dots can be made from many different semiconductor materials (CdSe[7], CdS[7-9], CdTe[7], ZnS[10], GaAs[11,12], InGaAs[13], InAs[14], InP[15-17], Ge[18], and Si[19] among others) and by many different techniques including photo- and electron-beam lithography[13], ion implantation[20], strained epitaxial growth[14,17,21], heat treatment of doped glasses[22,23], sol gel[9], and wet chemical synthesis[7,8,10,15,16,19]. One type of quantum dot structure that has been extensively studied is nanocrystallite quantum dots, which are synthesized as nanometer sized

colloids in solution[7,10,15,16]. Nanocrystallites are a particularly flexible type of quantum dot system due to the ease with which these free-standing colloidal structures can be physically manipulated.

Nanocrystallite quantum dots have been fabricated from a variety of materials (group IV, III-V, II-VI), however, the most common are the II-VI semiconductors. In particular, CdSe nanocrystallites have been extensively studied as a prototypical quantum dot system due to the existence of highly advanced synthetic procedures[7] which allow the fabrication of nanocrystallites with a well defined size and shape, in macroscopic quantities.

1.3.1 Synthesis

One particularly successful synthetic route to the fabrication of CdSe nanocrystallites was developed by Murray *et al.* [7]. The organometallic precursors for CdSe (di-methyl cadmium and tri-n-octyl phosphine selenide in a solvent of tri-octyl phosphine) are injected into a coordinating solvent [tri-octyl phosphine oxide (TOPO)] at 350°C. The high concentration of precursors in solution results in the rapid, homogeneous nucleation of CdSe seed crystals which are then allowed to grow via Ostwald ripening[24] at a temperature of ~300°C. Once the desired size is reached, the reaction solution is cooled, halting further growth.

1.3.2 Physical Properties

The as-synthesized nanocrystallites have a single crystal core with a wurtzite crystal structure. They are slightly prolate, with an aspect ratio of 1.1-1.2, and with the

long axis of the nanocrystallite parallel to the c-axis of the internal crystal structure. Intrinsic to the synthetic procedure, the surface of each nanocrystallite is surrounded by a layer of organic ligands (figure 1.3). This ligand layer can be chemically modified to adjust the solubility of the nanocrystallites in a variety of solvents ranging from long-chain hydrocarbons to water. The ability to dissolve nanocrystallites in such a wide range of solvents makes them a very flexible material for study and incorporation into quantum dot heterostructures.

While the synthetic procedure described above produces a relatively homogeneous distribution of nanocrystallite sizes, further reduction of the size distribution can be achieved through size selective precipitation. The relative stability of nanocrystallites in solution is a strong function of size, with larger nanocrystallites tending to be less soluble than smaller ones. By slowly adding a non-solvent such as methanol to a solution of nanocrystallites dispersed in hexane, the largest sizes can be selectively precipitated and separated from the initial solution as a solid phase. The solid phase nanocrystallites can then be redispersed in hexane, yielding a solution with a

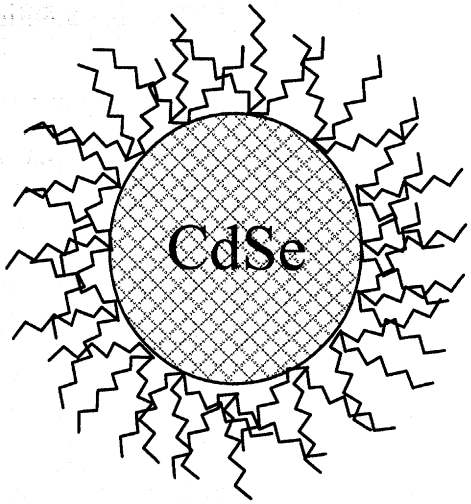

Figure 1.3: Graphic representation of a nanocrystallite, depicting the layer of organic ligands surrounding the crystalline CdSe core (TOPO/TOPSe is the native capping group)

reduced size distribution. Multiple precipitation cycles can yield size distributions as narrow as 5% rms. Figure 1.4 shows a TEM image of a distribution of 50Å nanocrystallites, revealing how uniform these samples are in size and shape.

The diameter of the nanocrystallites can be controlled during synthesis within a size range from ~15 to 100Å. In this range, the physical size of the nanocrystallites is smaller than the diameter of the bulk Bohr exciton (112Å), making them truly zero dimensional structures. The effect of quantum confinement is most evident in the energy of the band edge absorption and emission, which can be tuned with size across most of the visible region of the electromagnetic spectrum (~400-700nm). The absorption spectra displayed in figure 1.2 are from solution phase samples of CdSe nanocrystallites.

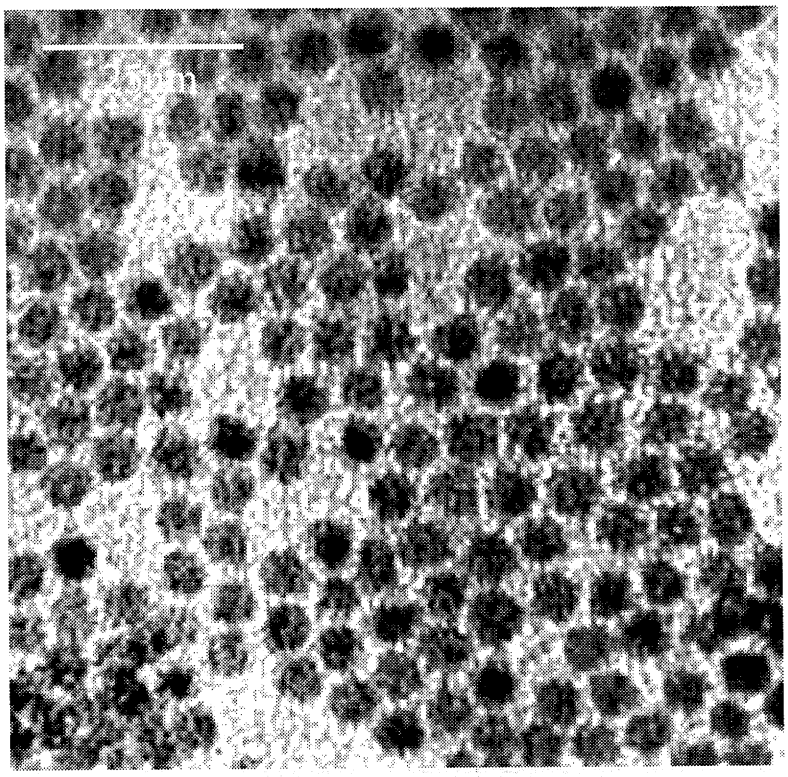

Figure 1.4: TEM image of a sample of CdSe nanocrystallites with a diameter of 50Å dispersed in hexane on a carbon substrate.

1.3.3 Fluorescence Properties

In addition to affecting solubility, the surface layer of organic ligands surrounding each nanocrystallite also serves to passivate non-radiative surface defects. This greatly increases the fluorescence quantum yield over the non-passivated value. While non-passivated nanocrystallites have an unmeasurably low quantum yield, TOPO capped nanocrystallites can have quantum yields as high as 20% at room temperature[25]. This quantum yield is found to increase dramatically at cryogenic temperatures and has been measured as high as 90%[26].

The fluorescence quantum yield in CdSe nanocrystallites can be further increased through the addition of a shell of ZnS to the outside of the CdSe core (figure 1.5) [27,28]. These "overcoated" nanocrystallites can have quantum yields as high as 50% at room temperature[27,28]. At the same time, the ZnS overcoating is found to have only a minor

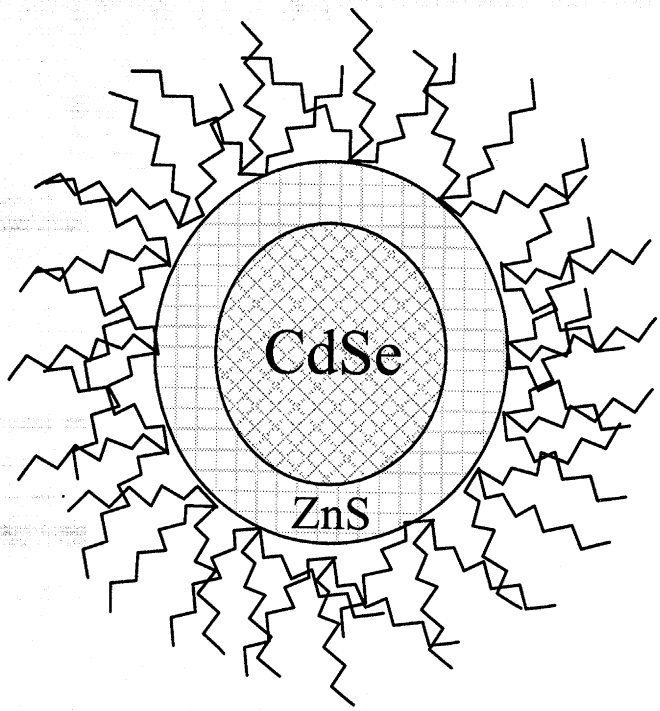

Figure 1.5: Graphic representation of a CdSe nanocrystallite with a ZnS shell and an organic surface passivation layer.

effect on the electronic structure of the nanocrystallites[28]. This suggests that while the ZnS shell adds significant volume to the nanocrystallite, the exciton wavefunction remains largely confined within the CdSe core. This is consistent with theoretical predictions which indicate that the higher bandgap ZnS should confine both the electron and hole within the lower energy CdSe core. The increase in quantum yield observed in overcoated nanocrystallites is likely to be the result of moving the surface of the nanocrystallite away from the CdSe core, reducing the interaction of the exciton with nonradiative surface defects.

Overcoated and non-overcoated nanocrystallites both have the same organic surface layer. In this thesis, nanocrystallites will be identified by whether they are overcoated or non-overcoated, as well as by the average diameter of the CdSe core within the ensemble sample. For non-overcoated nanocrystallites, this diameter corresponds to the total diameter of the nanocrystallite, while for overcoated nanocrystallites, this size refers to the diameter of the CdSe core within the core/shell structure.

In addition to being a tunable chromophore with discrete electronic transitions, both overcoated and non-overcoated nanocrystallites are extremely photo-stable. Figure 1.6 shows a comparison between the fluorescence intensity of a solution of nanocrystallites that emit at ~542nm, and a solution of fluorescein molecules that emit at ~520nm as a function of time. In this experiment, the concentration of the two solutions was matched, and the excitation intensities were adjusted to account for differences in the absorption cross-section of each chromophore. In this way, the number of excitations per chromophore per unit time was matched, insuring an appropriate comparison of the photo-degradation probability per excitation. As can be seen, while the emission from

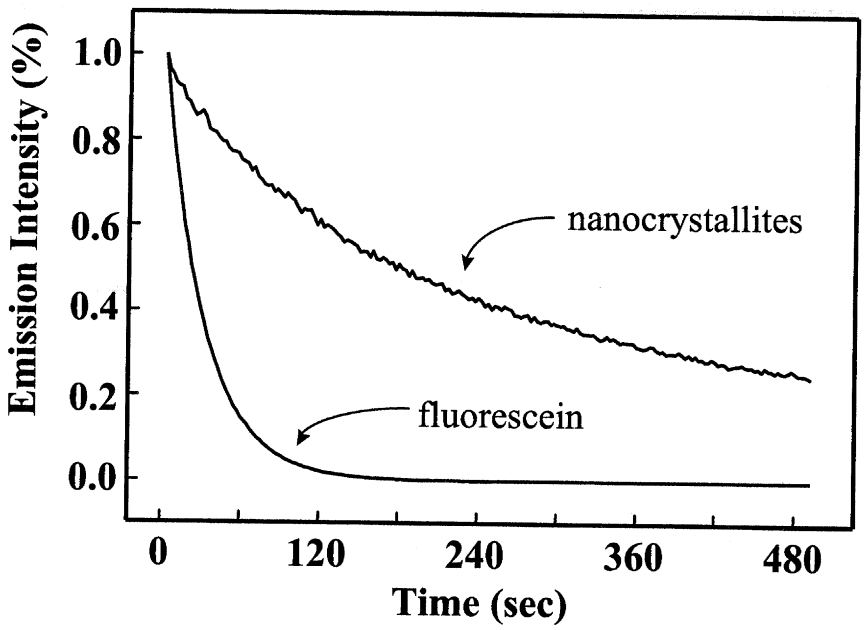

Figure 1.6: Relative emission intensity for an ensemble sample of fluorescein molecules and water soluble CdSe nanocrystallites as a function of time. The excitation intensity for each sample (15.7W/cm^2 for fluorescein and 19.5W/cm^2 for nanocrystallites) has been adjusted in order to equate the number of excitations per nanocrystallite per unit time. Plotted intensities have been normalized to the intensity of the first measurement so that a fair comparison of the relative photo-degradation rates can be made.

fluorescein quickly drops to zero under the excitation conditions of this experiment, the nanocrystallite fluorescence decays far more slowly. This photo-stability makes CdSe nanocrystallites an appealing fluorophore for applications such as LEDs[29,30] and multi-color fluorescent labels for use in biological systems[31,32].

1.3.4 Process Flexibility

The free standing, colloidal nature of these nanocrystallites makes them easy to manipulate into a number of different geometries. They can be embedded into a variety of polymers or incorporated into thin films of other bulk semiconductors such as ZnS [33,34]. In addition, they can be manipulated into close packed glassy thin films[35],

ordered three dimensional superlattices (colloidal crystals)[36] and even linked to form quantum dot molecules[37]. Such a high degree of flexibility and control makes CdSe nanocrystallites ideally suited for the study of zero-dimensional physics, as well as for potential use in quantum confined optical and electronic devices.

1.4 Summary

The study of quantum confined semiconductor structures such as quantum dots, represents an opportunity to harness the physical effects of wave-particle duality on the macroscopic level, providing scientists with the ability to control the physical, optical and electronic properties of solid state materials. In particular, nanocrystallite quantum dots, synthesized as colloids in solution, are a particularly flexible material for the study of quantum confined structures. Unfortunately, many effects, intrinsic to ensemble nanocrystallite samples, make these structures inherently difficult to study. As will be discussed in the next chapter, these effects can, in principle, be eliminated by studying single nanocrystallites, one at a time. The ease of manipulation, high fluorescence quantum yield and exceptional photo-stability described in this chapter make CdSe nanocrystallites an ideal candidate for detection on the single chromophore level.

1.5 References

[1] L. Brus, Appl. Phys. A, **53**, 456 (1991).
[2] A.P. Alivisatos, Science **271**, 933 (1996).
[3] Efros, Al.L.; Efros, A.L. Sov. Phys. Semicond., **16**(7), 772 (1982)
[4] Brus, L.E. J. Chem. Phys. **80**, 4403 (1984).
[5] S. Flugge, *Practical Quantum Mechanics* (Springer, Berlin, 1971) Vol. 1, p. 155.
[6] Weisbuch, J. of Cryst. Growth **138**, 776 (1994).
[7] Murray, C.B.; Norris, D.J.; Bawendi, M.G. J. Am. Chem. Soc. **115**, 8706 (1993).
[8] A. Eychmuller, A. Hasselbarth, L. Katsikas, and H. Weller, Ber Bunsen Phys Chem **95**(1), 79 (1991).
[9] Y.H. Kau, K. Hayashi, L. Yu, M. Yamane, and J.D. Mackenzie, SPIE Proc. **2288**, 752 (1994).
[10] M.A. Hines and P. Guyot-Sionnest, J. Phys. Chem. B, **102**(19), 3655 (1998).
[11] D. Gammon, B.V. Shanabrook, and D.S. Katzer, Appl. Phys. Lett. **57**, 2710 (1990).
[12] D. Gammon, B.V. Shanabrook, and D.S. Katzer, Phys. Rev. Lett. **67**, 1547 (1991)
[13] R. Steffen, A. Forchel, T.L. Reinecke, T. Koch, M. Albrecht, J. Oshinowo, and F. Faller, Phys. Rev. B **54**(3), 1510 (1996).
[14] E. Dekel, D. Gershoni, E. Ehrenfreund, D. Spektor, J.D. Garcia, and P.M. Petroff, Phys. Rev. Lett. **80**(22), 4991 (1998).
[15] D. Bertram, O.I. Micic, and A.J. Nizik, Phys. Rev. B. **57**(8), R4265 (1998).
[16] A.A. Guzelian et al, J. Phys. Chem. **100**, 7212 (1996).
[17] N. Carlsson, W. Deifert, A. Petersson, P. Castrillo, W.E. Pistol, and L.Samuelson, Appl. Phys. Lett. **65**, 3039 (1994).
[18] J.G. Couillard, H.G. Craighead, J. Mater. Sci, **33**(23), 5665 (1998).
[19] K.A. Littau, P.J. Szajawkski, A.J. Muller, A.R. Kortan, and L.E. Brus, J. Phys. Chem. **97**, 1224 (1993).
[20] J.D. Budai, C.W. White, S.P. Withrow, M.F. Chisholm, J. Zhu, and R.A. Zuhr, Nature **390**[7], 384 (1997).
[21] Y. Nagamune, H. Watabe, M. Hishioka, And Y. Arakawa, Appl. Phys. Lett. **67**, 3257 (1995).
[22] A.I. Ekimov and A.A. Onushchenko, Sov. Phys. Semicond. **16**, 775 (1982).
[23] N.F. Borelli, D.W. Hall, H.J. Holland, and D.W. Smith, . Appl. Phys. **61**, 5399 (1987).
[24] A.L. Smith, *Particle Growth in Suspensions*, (Academic Press, london, 1983), p. 3.
[25] C.B Murray, Thesis (M.I.T.), 1995.
[26] D.J. Norris, A. Sacra, C.B. Murray, and M.G. Bawendi, Phys. Rev. Lett. **72**, 2612 (1994).
[27] Hines, M.A.; Guyot-Sionnest, P. J. Phys. Chem. **100**, 468 (1996).
[28] Dabbousi, B.O. et al., J. Phys Chem B **101**, 9463 (1997).
[29] V. Colvin, M. Schlamp, and A.P. Alivisatos, Nature **370**, 354 (1994).
[30] B.O. Dabbousi, M.G. Bawendi, O. Onitsuka, and M.F. Rubner, Appl. Phys. Lett. **66**(11), 1316 (1995).
[31] Bruchez Jr., M. et al, Science, 281, 2013-2016 (1998).

[32] Chan, C.W. and Nie, S., Science **381**, 2016-2018 (1998).
[33] Danek, M. et al., J. Cryst. Growth **145**, 714 (1994).
[34] Danek, M. et al., Chem. Mater. **8**(1), 173 (1996).
[35] Kagan, C.R. et al., Phys. Rev. Lett. **76**(9), 1517 (1996).
[36] Murray, C.B.; Kagan, C.R.; Bawendi, M.G. Science **270**, 1335 (1995).
[37] Peng, X., Wilson, T.E., Alivisatos, A.P., Shultz, P.G. Angew. Chem. Int. Ed. Engl., **36**(1-2), 145 (1997).

Chapter 2: Optical Spectroscopy

2.1 Introduction

Optical spectroscopy is an important technique for studying nanocrystallites as well as other quantum dot structures. Simple experiments such as absorption and emission spectroscopy in both the time and frequency regimes, as well as the application of perturbations such as electric and magnetic fields, have allowed researchers to study the underlying physics of quantum confinement and determine potential applications for these materials. Unfortunately, fundamental difficulties exist in the study of ensemble nanocrystallite samples that have made it very difficult to understand and exploit the novel physical properties that result from quantum confinement. While this chapter discusses nanocrystallites, the effects described here are quite general, and exist in all types of quantum dots. Two issues of primary concern are inhomogeneous broadening and ensemble averaging.

2.2 Inhomogeneous Broadening

Nanocrystallites are primarily of interest for their size dependent optical properties. Unfortunately, the characteristics that make nanocrystallites interesting also make them inherently difficult to study. Since the electronic structure of each nanocrystallite is strongly dependent on its size and shape, inhomogeneities in these characteristics (mostly size) can result in broadening of the ensemble spectrum (figure 2.1). Even a relatively narrow distribution of sizes within an ensemble can result in spectral broadening which is many orders of magnitude larger than the theoretical linewidth predicted for a single nanocrystallite[1-5]. As an example, the lifetime of the

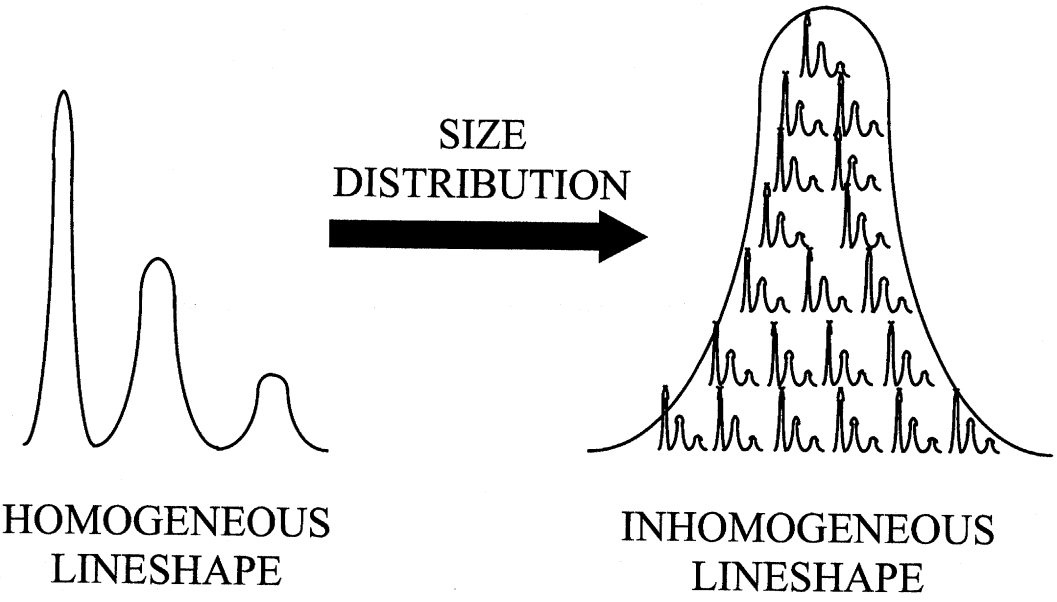

Figure 2.1: Inhomogeneous broadening. Measured ensemble emission and absorption spectra are a convolution of the single nanocrystallite lineshape with the distribution of sizes within the ensemble sample.

lowest excited state in CdSe nanocrystallites is extremely long (~100ns at 10K). This places a lower bound of ~10^{-9}eV on the intrinsic linewidth of the emitting state (although there may be other effects which broaden this state, such as dephasing due to phonon interactions*). Figure 2.2 reveals, however, that the emission linewidth measured in these samples (~10^{-1}eV) is significantly larger than this. Broad ensemble linewidths are the result of inhomogeneous broadening†, and often complicate the interpretation of ensemble nanocrystallite experiments.

* Theoretical calculations predict linewidths on the order of 10^{-5}eV resulting from phonon dephasing of the lowest excited state in GaAs quantum dots [D. Gammon, E.S. Snow and D.S. Katzer, Surface Science **361/362**, 814 (1996)].

† As we will see in chapter 7, there are other contributions to the linewidth measured in ensemble spectra that can only be revealed through the detection of single nanocrystallites.

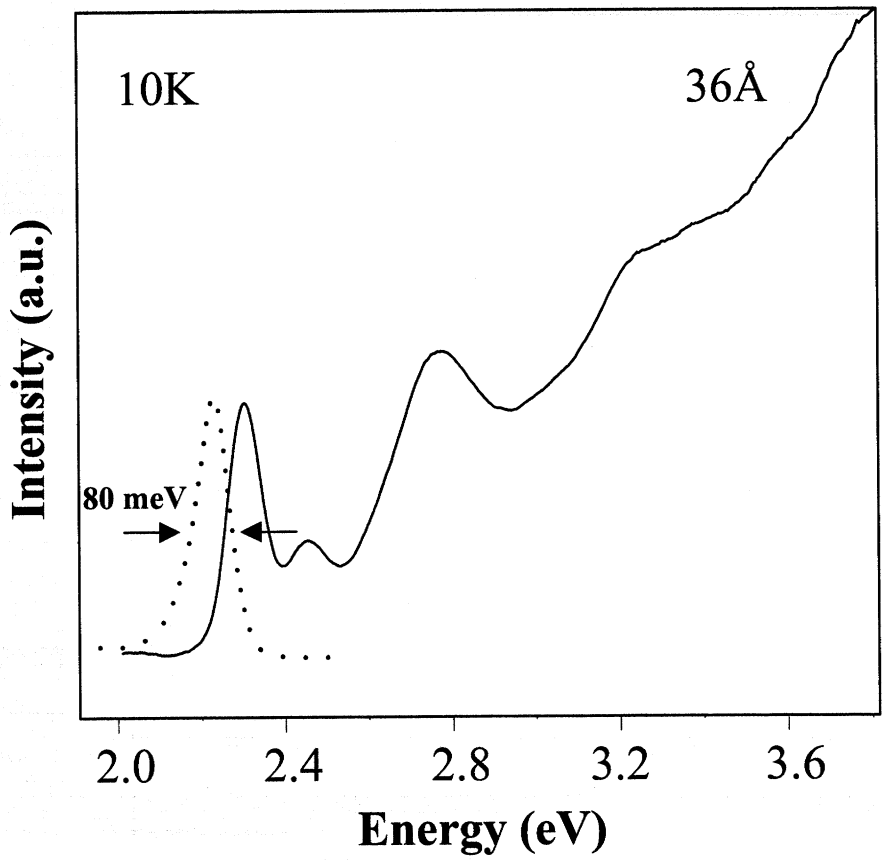

Figure 2.2: Inhomogeneously broadened excitation and emission spectra (solid and dotted lines respectively) for a 36Å ensemble nanocrystallite sample.

2.3 Ensemble Averaging

A second effect that can often obscure important spectral information in ensemble nanocrystallite samples is ensemble averaging. Ensemble averaging is inherent in any ensemble measurement, and refers to the fact that when a characteristic is probed in an ensemble, what is measured is the average of that characteristic throughout the sample. As a result, information can be lost about the individual components of the ensemble. For instance, the individual spectra represented in figures 2.3a and 2.3b could potentially result in identical measured spectra when averaged over the ensemble*.

* Inhomogeneous broadening is simply a special case of ensemble averaging (figure 2.3b).

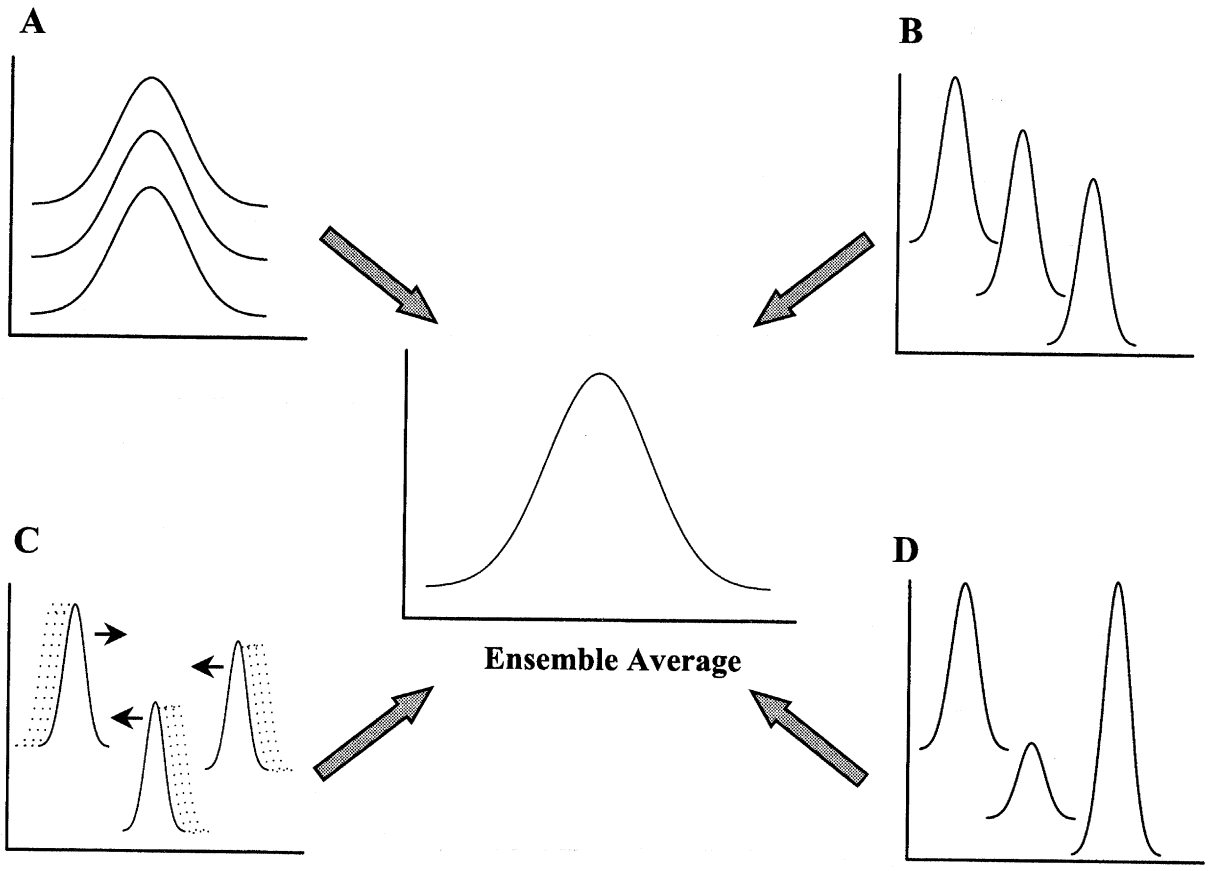

Figure 2.3: Ensemble Averaging. Graphic representations of single nanocrystallite characteristics that could potentially result in identical ensemble spectra. (A) All single nanocrystallite spectra are the same and are the same as the ensemble average. (B) All single nanocrystallite spectra are different, and are different than the ensemble average. (C) Single nanocrystallite spectra shift incoherently over time relative to each other. (D) Individual nanocrystallites emit with different intensities, or change emission intensity over time.

Another effect of ensemble averaging is to obscure orientation dependent information when there is no alignment between the individual components of the ensemble. Interactions with a directional perturbation or light field can be hidden in these cases. For instance, emission from an ensemble of *randomly* oriented molecules (or nanocrystallites), each with a uniaxial transition dipole moment, appears non-polarized when averaged over the ensemble.

Ensemble averaging can also hide dynamical effects within an ensemble. This occurs when no coherence exists between the dynamics of the individual components of the ensemble. For instance, imagine that individual spectra within an ensemble shift in energy as a function of time, oscillating back and forth within some finite energy range (figure 2.3c). If all of the spectra shift coherently, the ensemble average will also shift as a function of time. On the other hand, if individual spectra within the ensemble shift incoherently, the ensemble average may show no change as a function of time. In this case, important information about the dynamics of the system is lost.

Differences in emission intensity between individual components of an ensemble can also be hidden in an ensemble average (figure 2.3d). This can obscure information about the effects of local environments on dynamics, lifetimes and quantum yields. Similarly, dynamical changes in emission intensity *within* individual nanocrystallites (e.g. changes in emission intensity over time) can also be hidden if no coherence exists throughout the ensemble.

As we will see in the following chapters, effects such as the spectral shifting and fluorescence blinking described above are actually very common in CdSe nanocrystallites and can be observed on the single nanocrystallite level. These effects, however, were unexpected prior to these single nanocrystallite experiments since they are completely obscured in ensemble measurements due to ensemble averaging.

2.4 Ensemble Techniques

In the past, ensemble experiments have been designed in order to minimize the effects of inhomogeneous broadening and ensemble averaging. For instance, size

selective optical techniques such as fluorescence line narrowing[6,7] have been used in an attempt to reduce the extent of inhomogeneous broadening. This is done by optically selecting a small subset of the size distribution to be studied. By exciting a narrow range of energies along the low energy side of the band edge absorption peak, it is possible to monitor emission from only the largest nanocrystallites in the sample. This effectively reduces the size distribution being probed and can significantly reduce the effects of inhomogeneous broadening (figure 2.4). Experiments using fluorescence line narrowing have revealed significantly narrower emission linewidths as well as new spectral features such as a series of peaks corresponding to a longitudinal optical (LO) phonon progression, with a peak spacing that is comparable to the bulk LO phonon frequency. However, while these experiments have provided valuable information about ensemble nanocrystallite samples, they are still ensemble measurements and linewidths are found to be significantly broader than what is predicted by theory. This suggests that residual inhomogeneities may exist, which are not optically selected by this technique. Similar results are also obtained when looking at the absorption spectrum of ensemble nanocrystallite samples using size selective techniques such as photoluminescence excitation[8] and spectral hole burning[9].

In some cases, the dynamics within an ensemble can be synchronized, reducing the effects of ensemble averaging. For instance, fluorescence lifetime measurements are routinely performed in which a pulsed excitation synchronizes the entire ensemble of nanocrystallites[10,11]. These experiments are still ensemble measurements, however,

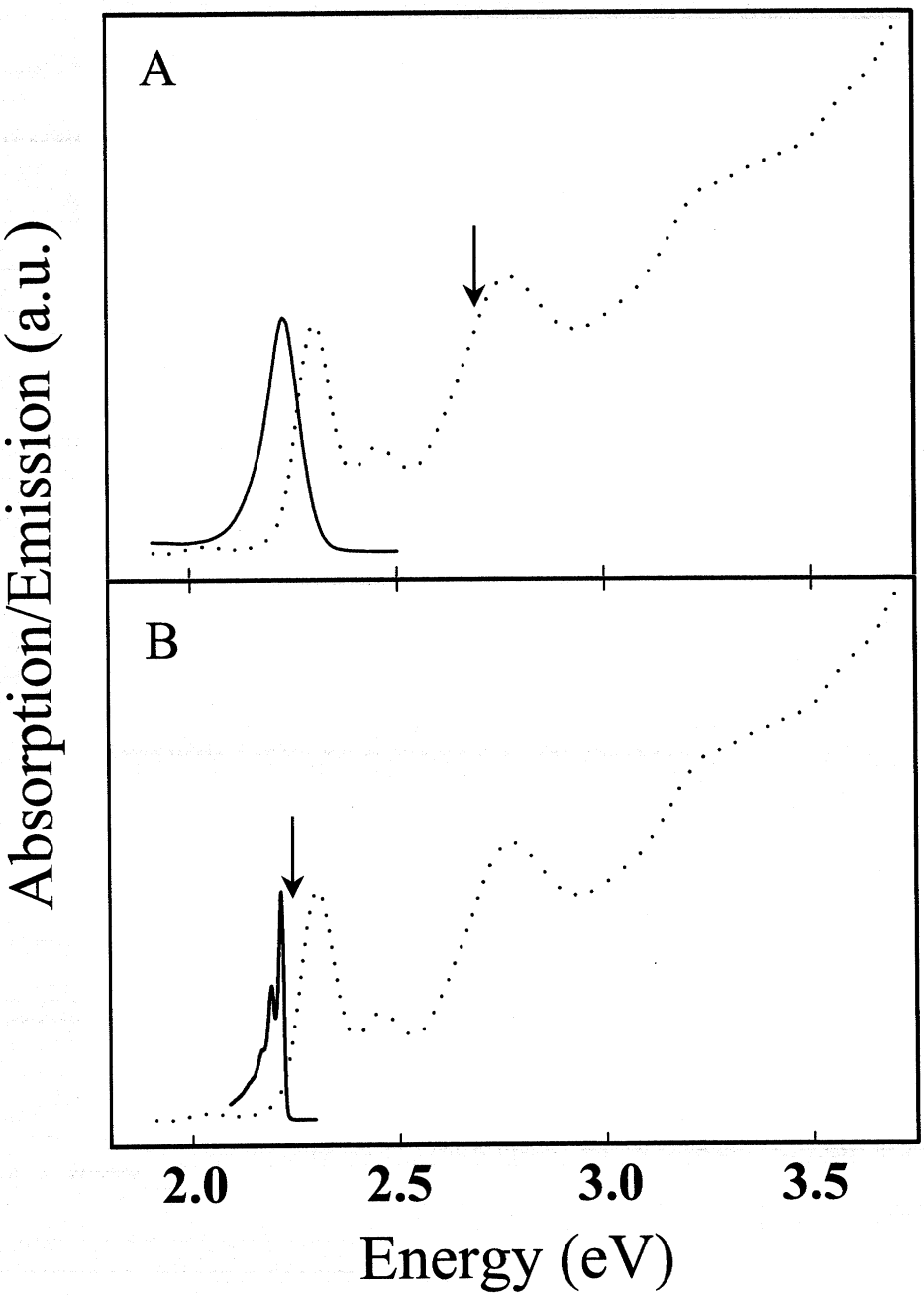

Figure 2.4: Inhomogeneous broadening and fluorescence line narrowing. (A) Excitation and emission spectra (dotted and solid lines respectively) for an ensemble sample of nanocrystallites. Excitation for the emission spectrum in (A) was above the band edge peak, exciting the entire population of nanocrystallites. (B) Excitation and fluorescence line narrowed emission spectra (dotted and solid lines respectively) from the same nanocrystallite sample, with excitation on the low energy side of the band-edge absorption peak, selectively exciting only a small subset of the size distribution. Arrows indicate the excitation energy for each emission spectrum.

and residual inhomogeneities can lead to the loss of information. For instance, a multi-exponential fluorescence decay may indicate an ensemble of identical nanocrystallites with multiple relaxation pathways, or it may indicate a population of nanocrystallites made up of several sub-groups, each with a different single exponential decay.

2.5 Single Chromophore Detection

While the optical selection techniques described above have provided valuable insight into the physics of nanocrystallites, much information still remains hidden. The only way to truly eliminate the effects of inhomogeneous broadening and ensemble averaging is to collect spectra from single nanocrystallites, one at a time. By avoiding the averaging effects of ensemble spectroscopy, single nanocrystallite detection should, in principle, yield far more detailed information.

At the inception of the experiments described in this thesis, the field of single chromophore detection was in its infancy. Several groups had demonstrated that it was possible to see single molecules[12-18], however, the majority of the publications were proof of principle experiments, designed to show the feasibility of different types of single molecule detection. Our study of single nanocrystallites represents one of the first examples of a practical application of this new technology to a system of interest for reasons other than our ability to detect it on the single chromophore level. In addition, due to the structural inhomogeneities in nanocrystallites, the effects of inhomogeneous broadening and ensemble averaging in this system are significantly more pronounced than what is observed in other, more traditional molecules[19]. This means that nanocrystallites are an ideal candidate for detection on the single chromophore level.

2.6 Summary

Optical spectroscopy is a powerful tool that has been used for years to understand the physics and potential applications of semiconductor nanocrystallites. While detailed spectroscopic information is, in principle, available, the effects of averaging spectral information over many nanocrystallites simultaneously often results in a loss of important information. As a result, ensemble spectroscopy is ultimately limited in the level of detail that it can uncover. While techniques such as fluorescence line narrowing and pulsed excitation exist, which can reduce the distribution of characteristics being probed, these measurements are still made on an ensemble, and will necessarily be characterized by ensemble averaged results. As such, effects such as inhomogeneous broadening and ensemble averaging will always exist to some extent in an ensemble measurement. In order to truly eliminate these effects, it is necessary to avoid averaging by probing single nanocrystallites, one at a time.

2.7 References

[1] Al.L. Efros and A.L. Efros, Sov. Phys. Semicond. **16**(7), 772 (1982).
[2] L.E. Brus, J. Chem. Phys. **80**, 4403 (1984).
[3] D.J. Norris et al., Phys. Rev. B **53**, 16347 (1996).
[4] D.J. Norris and M.G. Bawendi, Phys. Rev. B **53**, 16338 (1996).
[5] Al.L. Efros et al., Phys. Rev. B, **54**(7), 1 (1996).
[6] A.P. Alivisatos et al., J. Chem. Phys. **90**(7), 3463 (1989).
[7] M. Nirmal, D.J. Norris, M. Kuno, and M.G. Bawendi, Phys. Rev. Lett. **75**(20), 3728 (1995).
[8] D.J. Norris, A. Sacra, C.B. Murray and M.G. Bawendi, Phys. Rev. Lett. **72**(16), 2612 (1994).
[9] A.P. Alivisatos, A.L. Harris, N.J. Levinos, M.L. Steigerwald, and L.E. Brus, J. Chem. Phys. **89**(7), 4001 (1988).
[10] M.G. Bawendi, P.J. Carrol, W. L. Wilson, and L.E. Brus, J. Chem. Phys. **96**(2), 946 (1992).
[11] V.I. Klimov and D.W. McBranch, Phys. Rev. Lett. **80**(18), 4028 (1998).
[12] L. Kador, D.E. Horne, and W. E. Moerner, J. Phys. Chem. **94**, 1237 (1990).
[13] M. Orrit and J. Bernard, Phys. Rev. Lett. **65**, 2716 (1990).
[14] W.P. Ambrose and W.E. Moerner, Nature **349**, 225 (1991).
[15] T. Basche and W.E. Moerner, Nature **355**, 335 (1992).
[16] U.P. Wild, F. Guttler, M. Pirotta, and A. Renn, Chem. Phys. Lett. **193**, 451 (1992).
[17] A. Zumbusch et al, Phys. Rev. Lett. **70**, 3584 (1993).
[18] F. Guttler et al, J. Lumin. **56**, 29 (1993).
[19] W.P. Ambrose, T. Basche, and W.E. Moerner, J. Chem. Phys. **95**(10), 7150 (1991).

Chapter 3: Single Nanocrystallite Microscopy

3.1 Introduction

When the work for this thesis began in 1994, the field of single chromophore detection was still very new. As such, much of the work involved in the completion of this thesis was devoted to developing techniques and an apparatus capable of detecting the fluorescence from single nanocrystallites. By the completion of this work, however, single chromophore spectroscopy had become a relatively common tool, used in the study of many physical systems[1-13]. Therefore, while much of the success of this project involved simply being able to detect single nanocrystallites, what is truly interesting about this work is not how the experiments were done, but what was learned and what insight was gained. As such, an emphasis will be placed on the results of these single nanocrystallite experiments and their bearing on the field of quantum confined nanostructures. While the important experimental details will be discussed, the trivial details of the experimental development will be omitted.

3.2 Single Molecule Detection

The first demonstration of single molecule detection was performed by W.E. Moerner's group in 1989[14,15]. In these landmark experiments, it was demonstrated that absorption spectra from single pentacene impurities in a crystalline p-terphenyl matrix could be obtained at liquid helium temperatures by using a combination of frequency modulation and Stark modulation absorption spectroscopy. This was an extremely important result since

the detection of 1.66 yoctomol* of pentacene molecules represents the ultimate limit in detection sensitivity (it is hard to imagine detecting fewer than one of something).

While these results were very exciting, the experiments were prohibitively difficult and, to my knowledge, have never been reproduced. The following year, however, the group of Michele Orrit demonstrated that *fluorescence* could also be detected from single pentacene impurities[16]. While fluorescence detection is far less general than absorption spectroscopy (i.e. the molecule of interest must be fluorescent), single molecule fluorescence detection is far simpler due to the zero-baseline nature of the measurement. As such, fluorescence detection has become the method of choice for the majority of single molecule applications.

In addition to absorption and emission spectroscopy, more sophisticated experiments such as two-photon excited fluorescence[17,18], time resolved fluorescence[19,20], and Raman scattering[21,22] from single molecules have also been demonstrated in recent years. These experiments, and others, have strongly demonstrated the power of single chromophore detection in uncovering the hidden details of ensemble systems. One of the most valuable aspects of single chromophore spectroscopy is that by eliminating ensemble effects, simple experimental procedures such as Stark and polarization spectroscopy become far more powerful than they are in ensemble experiments. As such, complex information can be uncovered using relatively simple experimental tools. As mentioned in chapters 1 and 2, CdSe nanocrystallites are particularly well suited for study on the single chromophore level, and would benefit greatly from such experiments.

* The SI prefix "yocto" corresponds to 10^{-24}. It may seem odd that someone would have made the effort to formally create a prefix that represents such a small number, however, "yocto" was only adopted recently, during the 1991 meeting of the Conférence Générale des Poids et Mesures, *after* the first evidence of single chromophore detection.

3.3 Requirements for Single Nanocrystallite Detection

There are two primary issues that must be addressed in order to achieve single nanocrystallite detection. The first is that it must be possible to resolve, or separate in some way, the signal from adjacent nanocrystallites. The second is that there must be a sufficiently high signal to noise ratio to be able to detect the fluorescence from each nanocrystallite.

3.3.1 Resolution

Resolving the fluorescence from individual nanocrystallites can be done by either reducing the concentration of nanocrystallites within the sample or reducing the excitation volume being probed so that the number of nanocrystallites detected within the spatial resolution of the detection system is less than 1 (i.e. there are either 1 or 0 nanocrystallites detected at any time). The resolution of the far-field optical microscope used in these experiments is limited at the lower end by the diffraction limit of light ($\sim\frac{\lambda}{2}$, although in reality the measured diffraction limit of this system is ~0.5μm at λ=600nm). Therefore, in order to be able to resolve the fluorescence from individual nanocrystallites, it is necessary for the nanocrystallites to be spatially separated by at least this distance. This is accomplished by spin casting an extremely dilute solution of nanocrystallites ($\sim 10^{-9}$M) in poly(methyl methacrylate) (0.5% PMMA by weight, dissolved in toluene). This procedure produces a uniform PMMA film that is ~200Å thick with an areal density of less than 1 nanocrystallite per μm^2.

At cryogenic temperatures, it is also possible to use *spectral* resolution to distinguish between different nanocrystallites. If two nanocrystallites fall within the same diffraction limited detection area, differences in emission energy can often be used

to resolve the individual nanocrystallites (an example of this is shown later, in chapter 6, figure 6.5). When necessary, this allows the detection of single nanocrystallites in samples where the concentration is significantly higher than described above.

3.3.2 Signal to Noise

The second issue that must be addressed when considering the detection of single nanocrystallites is signal to noise: Is there enough light emitted from a single nanocrystallite to be detected above the background of the sample and detection system? Obviously, the answer to this question must be "yes" or the remainder of this thesis would be fairly uninteresting. It is important, however, to understand how close to the detection limit we are, in order to evaluate the potential quality of our data (i.e. will the data from these experiments be noisy or clear?)

Since the signal from a single chromophore arises from a single quantum system, which can only emit one photon per excitation, it is necessary to excite the chromophore many times in order to collect enough photons to detect it above the noise of the detection system. For this reason, excitation intensities used in single chromophore experiments are relatively high when compared to the intensities used in comparable ensemble measurements. In order to avoid additional complications, however, the excitation rate must also be significantly slower than the excited state lifetime. This reduces effects resulting from the presence of bi-excitons (two excitons in the nanocrystallite at the same time). The radiative lifetime of CdSe nanocrystallites is surprisingly long as a result of emission from a spin-forbidden "dark exciton" state[23] (~100ns at 10K). At room

temperature, the lifetime is about one order of magnitude shorter. An excitation rate of ~10^5-10^6 per second should therefore be appropriate for these experiments.

In order to confirm that an excitation rate of $10^6 s^{-1}$ is feasible in these experiments, an experimentally measured absorption cross-section per nanocrystallite of ~10^5 $M^{-1}cm^{-1}$ ($1.66x10^{-16}$ cm^2) is used*. With 514nm excitation, an excitation rate of $10^6 s^{-1}$ would correspond to an excitation intensity of ~250W/cm^2 or 1.75mW focused to a spot size of ~30μm. This is an easily obtainable excitation power. Conservatively assuming a quantum yield of 50% (at 10K) and a detection efficiency of 5% (percentage of the total photons emitted), it should be possible to detect ~2500 photons/second! This is more than 2 orders of magnitude higher than the detection noise for a standard liquid nitrogen cooled CCD camera.

Clearly, single nanocrystallite detection should be possible. In fact, the calculation above suggests that it would be feasible to reduce the quantum efficiency or excitation rate by almost 2 orders of magnitude and still have sufficient signal to noise. This is true, however, only if the background level is negligible as well. In fact, the biggest challenge in the detection of single chromophores is not in the efficient collection of the fluorescent signal, but rather the efficient rejection of stray light resulting from other sources.

* An absorption spectrum was taken from a well washed sample of nanocrystallites in hexane. The solvent was then evaporated, and the sample was heated to 370 °C to burn off the organic surface layer. This sample was then weighted. Using the average nanocrystallite size, as measured by TEM, the number of nanocrystallites was calculated and used to determine the absorption cross-section per nanocrystallite in the original sample.

3.3.3 Background

Several sources of stray light exist in these experiments: 1) Stray room light, 2) resonantly scattered excitation light, 3) non-resonant fluorescence from components of the optical system, 4) raman scatter from the microscope optics, and 5) fluorescence from within the sample or the sample substrate.

Stray room light can be easily eliminated by placing the experimental apparatus inside a light-tight box. Resonantly scattered excitation light can be efficiently removed through the use of high optical density (O.D. > 4.0), non-fluorescent filters such as wavelength specific holographic notch filters, dielectric long-pass or band-pass filters, or low fluorescence colored glass long-pass filters. Fluorescence from the optical components of the microscope system can be eliminated through the use of standard, low-fluorescence optics, since even slight fluorescence from these components is not located in a focal plane of the microscope and will not be efficiently collected into the detection system. Similarly, Raman scatter from the microscope optics is also fairly low, however, it may account for ~3-10 counts/pixel/second detected evenly across the detector, depending on the excitation intensity. While this is not a prohibitive background, it is likely to be the largest source of stray light in our system, and cannot be eliminated by the use of higher quality optics. The largest *potential* source of background light is from fluorescent impurities within the sample or sample substrate, since these are located in or very near the focal plane of the microscope. As such, any impurity fluorescence is efficiently collected. By using high purity polymers and ultraviolet grade, low fluorescence quartz substrates, this sample/substrate fluorescence can be reduced to a couple of counts per second.

3.4 Detection Techniques

Now that the feasibility of single nanocrystallite detection has been established, a detection technique must be selected. While there are many ways to detect the fluorescence from single chromophores, we are interested in imaging, as well as spectroscopy, of single nanocrystallite samples and are therefore restricted to three general techniques: Wide-field microscopy, scanning confocal microscopy, and near-field scanning optical microscopy.

3.4.1 Wide-Field Microscopy

Wide-field microscopy uses standard microscope optics to illuminate and collect the fluorescent image from a wide field of view within the sample. This technique is relatively simple, since no moving parts are necessary to acquire an image. One significant advantage of wide-field microscopy is that it is possible to collect data from an entire image simultaneously (no scanning required), allowing massively parallel data acquisition. The disadvantage of wide-field microscopy is that it is the least capable of rejecting stray light. As such, wide-field microscopy could potentially have the largest background level of the single chromophore techniques.

3.4.2 Scanning Confocal Microscopy

Scanning confocal microscopy only illuminates and collects light from a diffraction limited area of the sample, which is confocal with an aperture in front of the detection system[24]. Images are obtained by scanning the excitation across the sample, and collecting the fluorescence intensity at each position. An image is then created by plotting emission intensity as a function of position. While the spatial resolution of a

confocal microscope is roughly the same as a wide-field microscope in the x-y plane, the resolution in the z-direction is much higher (smaller depth of field). The advantage of confocal microscopy is that the restricted depth of field eliminates stray light that originates from outside the sample plane. This means that fluorescence from impurities in the sample matrix or substrate that are not exactly in focus are eliminated. This results in a significant increase in the signal to noise ratio. The disadvantage of scanning confocal microscopy is that data collection is very slow. Images taken by scanning the confocal probe can take many minutes to acquire and it is impossible to observe more than one position on the sample at once, precluding the possibility of parallel data acquisition.

3.4.3 Near-Field Scanning Optical Microscopy

Near-Field Scanning Optical Microscopy (NSOM) restricts the excitation resolution in all three dimensions by passing excitation light through a sub-diffraction limit sized aperture (usually a tapered, metal coated optical fiber)[25]. The light that passes through the aperture is no longer a propagating wave, and decays exponentially as a function of distance from the aperture[26]. Lateral resolution is determined primarily by the diameter of the aperture[25]. Depth resolution is determined by the depth of the evanescent field. Spatial resolution of ~10nm can be obtained with this technique. The NSOM tip (aperture) is then scanned over the sample as in confocal microscopy. The increased resolution of NSOM creates two distinct advantages: First, stray light from the sample is virtually eliminated. Second, high lateral resolution allows the detection of single chromophores at a concentration that is significantly higher than with far-field microscopy. As with confocal microscopy, NSOM data acquisition is slow and there is

no possibility of parallel acquisition. A second disadvantage is that the NSOM tip must be very close to the chromophore of interest (~10nm)[25]. A metal coated tip in such close proximity can interact with the chromophore being studied, altering the physical characteristics being probed and potentially affecting the measurements[19]. Also, since the tip must be close to the chromophore, NSOM is inappropriate for use in a number of sample environments such as thick films or rough surfaces. Finally, NSOM is experimentally more complex and problematic than the other two techniques.

3.5 Single Nanocrystallite Detection System

For the experiments described in this thesis, a wide-field detection geometry was selected. The primary motivation for this decision was the ability to perform highly parallel data acquisition. Since one of the motivations for doing single nanocrystallite spectroscopy was the wide range of inhomogeneities present in these samples, it is necessary for us to study enough single nanocrystallite that we can probe the extent of these inhomogeneities. In order to understand ensemble data, it is often desirable to reconstruct ensemble results using single nanocrystallite data. It is also important to demonstrate that what is seen on the single nanocrystallite level is consistent with ensemble results. For instance, recall figure 2.1, which shows a graphic representation of an ensemble spectrum that is reproduced by the distribution of single chromophore spectra within the sample. We will find that there are many instances in which similar comparisons between actual single nanocrystallite and ensemble data can be made. The ability to collect data from many single nanocrystallites at once allows us to perform

these types of statistical comparisons on a regular basis. Scanning probe techniques, such as NSOM and confocal microscopy) require far more effort to obtain far less data.

The primary disadvantage of wide-field microscopy is the potential background signal. By using an extremely thin polymer matrix, as described in section 3.2.1, however, the depth of field is automatically restricted to this width, and very low background levels can be achieved.

3.5.1 Microscope

The optical design of the single nanocrystallite microscope is based on a standard microscope, with modifications intended to optimize light collection and minimize the detection of stray light. Figure 3.1 is a schematic drawing of the significant optical components. Excitation light from a laser source (514nm Ar^+ unless otherwise stated) is

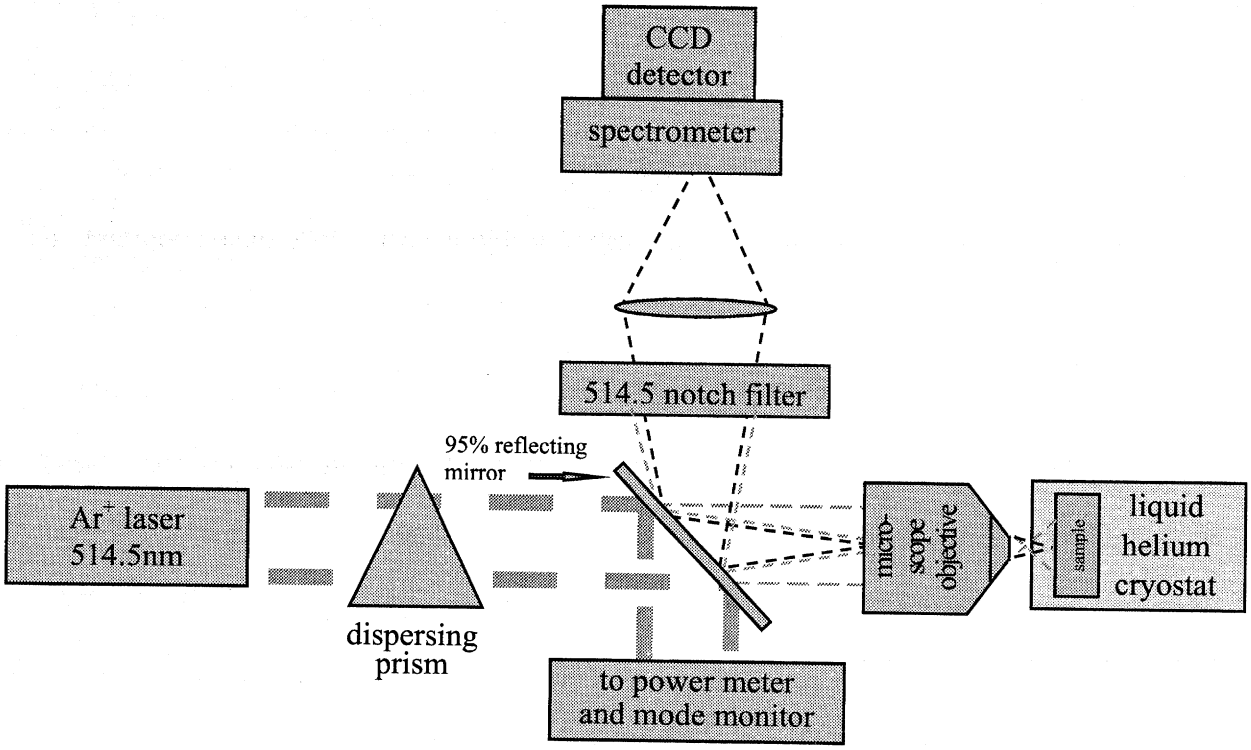

Figure 3.1: Far-field epifluorescence microscope (described in text).

transmitted through a 95% reflecting broadband mirror* (at an angle of 45°) and then focused by a long working distance microscope objective (NA=0.7) onto the sample surface. The microscope objective has a working distance of ~3mm and a designated tube length of 160mm. The collimated excitation light is focused in front of the focal plane of the microscope and is diverging when it passes through the sample surface. As a result, a ~30μm diameter spot on the sample surface is illuminated. Excitation of the nanocrystallites at a wavelength above the band gap causes them to fluoresce. The fluorescent image is then collected by the same objective lens[Ŧ]. The image reflects off the 95% reflecting mirror, passes through a wavelength specific filter to remove any excitation light[#], is focused with a projection eyepiece onto the entrance slit of a spectrometer and detected with a 2-dimensional charge coupled device (CCD) camera. For imaging purposes, the entrance slit of the spectrometer is opened to 7mm and the diffraction grating is replaced with a silvered mirror at an angle of 0 degrees. As a result, the image is *not* spectrally dispersed and is simply refocused onto the CCD. Spectra are obtained by closing the entrance slit on the spectrometer and reinstalling the diffraction grating. Further discussion of the procedure for spectral acquisition will be included in chapter 6.

---

* The choice of a 95% reflecting, broadband mirror (silver coated), instead of a dichroic mirror, was made to avoid wavelength specificity in the excitation and emission pathways. This allows the use of multiple excitation wavelengths and the collection of arbitrary emission wavelengths, greatly increasing the flexibility of this system.

Ŧ Since excitation and emission follow the same optical path, this is referred to as an epifluorescence microscope.

\# For standard Ar^+ wavelengths, an appropriate holographic notch filter was used (OD>6, blocking width ~5nm). For arbitrary wavelength excitation using a tunable dye laser, an appropriate combination of dielectric and colored glass long pass filters were used.

3.5.2 Detectors

Two different CCD cameras were used in these experiments. Unless otherwise noted, data was acquired using a Princeton Instruments back-illuminated liquid nitrogen cooled CCD camera. This camera has an extremely low dark count rate (~1cnt/pixel/hr) and high quantum efficiency in the visible region of the electromagnetic spectrum (~80%). A Princeton Instruments 'Pentamax' camera with an intensified CCD chip and a readout rate of 15 frames/second was used for experiments where short integration times and/or fast readout rates were necessary. By binning pixels on the CCD, it was possible to continuously acquire images at a rate of greater than 30 frames/second. This camera, however, has a smaller dynamic range, lower quantum efficiency (~30%) and significantly higher dark count rate than the liquid nitrogen cooled CCD. As such, it was not used in applications where long integration times (>5 sec) were possible.

3.5.3 Cryostat

In order to avoid thermal effects which can easily disrupt subtle spectroscopic data, single nanocrystallite images and spectra were typically taken at a temperature of ~10K (unless otherwise noted). The sample substrate was housed in a liquid helium cold-finger cryostat. In order to image the sample using a microscope objective that was mounted outside of the cryostat, a special attachment was added to extend one cryostat window into the center of the cryostat. With this attachment, it was possible to bring the sample substrate within the working distance of the microscope objective.

In order to minimize vibrations of the sample within the cryostat, low thermal conductivity stabilizing rings were mounted between the cold-finger and the heat-shield, and between the heat-shield and the outer shroud of the cryostat (figure 3.2). With these stabilizers in place, thermal drift and mechanical vibrations could be reduced to the point where a single nanocrystallite image or spectrum could be monitored for more than 2 hours without moving out of focus or out of the detection region, once thermal equilibrium was reached.

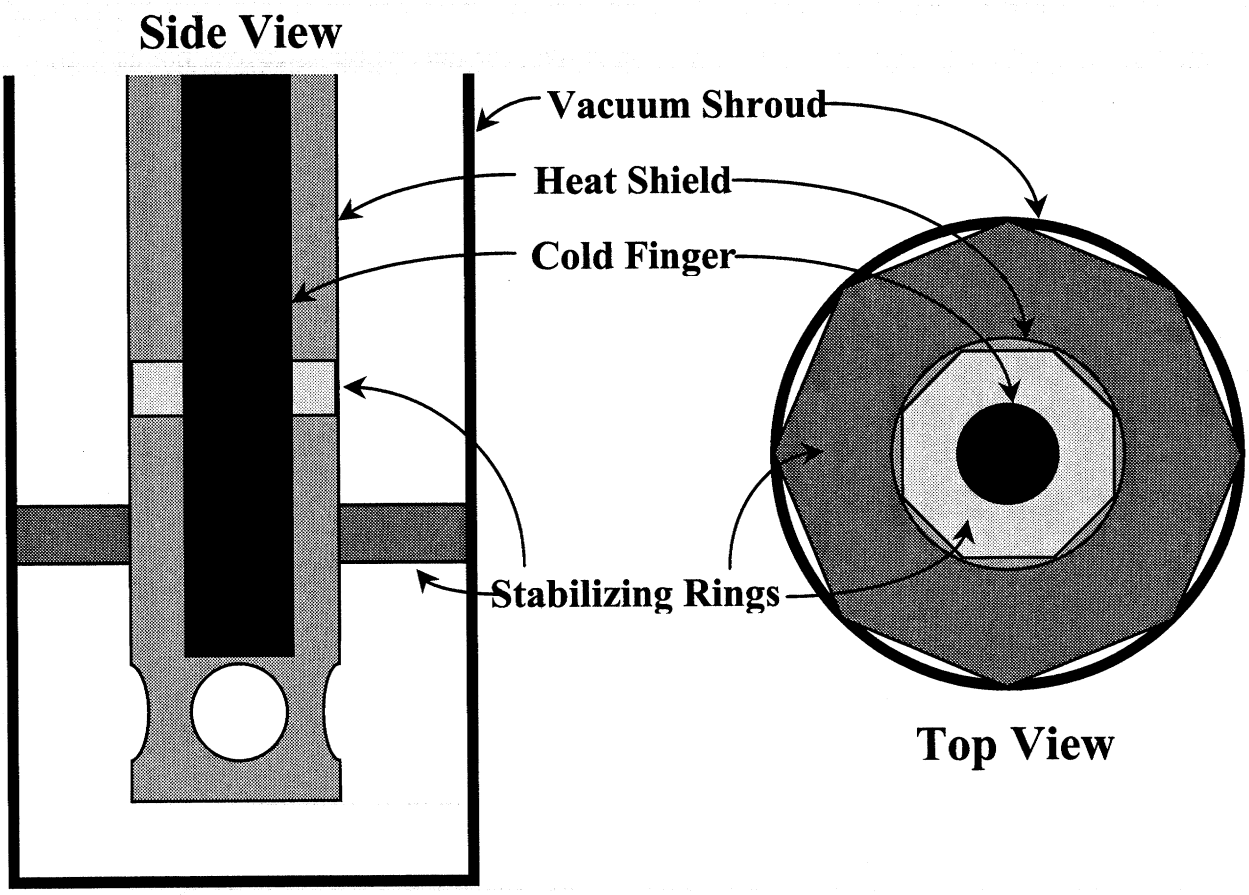

Figure 3.2: Vibration reduction. Stabilizing rings dampened vibration of the cold-finger relative to the heat shield, and the heat shield relative to the outer vacuum shroud, as shown in the side view. Top view illustrates how minimum thermal contact was made between the components. Stabilizing rings were made from low thermal conductivity *phenolic*.

In order to insure that the entire sample reached a temperature of ~10K, the substrate used in these experiments was made from single crystal quartz, which has a thermal conductivity similar to sapphire ($\kappa \approx 10$W/cm·K at 10K) but far less impurity fluorescence. After spin-coating, the sample substrate was mounted into a specially designed copper sample holder that was attached to the end of the liquid helium cold finger. Since thermal conductivity is related to the cross-sectional area, sample substrates were designed to be at least 2mm thick. Direct measurements of the substrate surface confirmed that it was possible to cool the center of the sample to temperatures at or below 10K. It should be noted that the thermal conductivity of amorphous quartz is not as high as crystalline quartz, and temperatures only as low as ~25K were reached with these substrates. Cover slips and amorphous substrates were not used for cryogenic measurements.

3.6 Summary

With the experimental apparatus described in this chapter, it is possible to image and take spectra from single nanocrystallites (or other single chromophores) in a spectral range from ~400nm to ~800nm and in a temperature range from 10K to room temperature. Data can be acquired with acquisition times as short as 10ms, and with a repetition rate as high as ~30 frames/sec. As will be shown in chapters 4 and 6, both images and spectra can be obtained from multiple sources simultaneously, allowing massively parallel data acquisition on the single nanocrystallite level.

3.7 References

1 J.J. Macklin, J.K. Trautman, T.D. Harris, and L.E. Brus, Science **272**, 255 (1996).
2 T. Ha et al., Phys. Rev. Lett. **77**, 3979 (1996).
3 I. Sase, H. Miyata, S. Ishiwata, and K. Kinosita, Proc. Natl. Acad. Sci. USA **94**, 5646 (1997).
4 S. Nie and S.R. Emory, Science **275**, 1102 (1997).
5 R.M. Dickson, A.B. Cubitt, R.Y. Tsien, and W.E. Moerner, Nature **388**, 355 (1997).
6 D. Gammon et al, Science **277**, 85 (1997).
7 B. Lounis, F. Jelezko, and M. Orrit, Phys. Rev. Lett. **78**, 3673 (1997).
8 D. A. Vanden Bout et al, Science **277**, 1074 (1997).
9 A. Ishijima et al, Cell **92**, 161 (1998).
10 Ch. Brunel, B. Lounis, Ph. Tamarat, and M. Orrit, Phys. Rev. Lett. **81**, 2679 (1998).
11 M.D. Mason, G. M. Credo, K. D. Weston, and S.K. Buratto, Phys. Rev. Lett. **80**, 5405 (1998).
12 K. Kinosita et al, Cell **93**, 21 (1998).
13 T. Ha et al., Proc. Natl. Acad. Sci. USA **96**, 893 (1999).
14 W.E. Moerner and L. Kador, Phys. Rev. Lett. **62**, 2535 (1989).
15 L. Kador, D.E. Horne, and W.E. Moerner, J. Phys. Chem. **94**, 1237 (1990).
16 M. Orrit and J. Bernard, Phys. Rev. Lett. **65**, 2716 (1990).
17 D. Walser, T. Plakhotnik, a. Renn, and U.P. Wild, Chem. Phys. Lett. **270**, 16 (1997).
18 E.J. Sanchez, L. Novotny, G.R. Holtom, and X.S. Xie, J. Phys. Chem. A **101**(38), 7019 (1997).
19 X.S. Xie and R. C. Dunn, Science **265**, 361 (1994).
20 J.J Macklin, J.K. Trautman, T.D. Harris, and L.E. Brus, Science **272**, 255 (1996).
21 S. Nie and S.R. Emory, Science **275**, 1102 (1997).
22 K. Kneipp, Y. Wang, H. Kneipp, L.T. Perelman, I. Itzkan, R.R. Dasari, and M.S. Feld, Phys. Rev. Lett. **78**(9), 1667 (1997).
23 Al.L. Efros, M. Rosen, M. Kuno, M. Nirmal, D.J. Norris, and M.G. Bawendi, Phys. Rev. B **54**(7), 1 (1996).
24 C. Sheppard, *Confocal laser scanning microscopy* (Springer, in association with the Royal Microscopical Society, 1997, Oxford)
25 E. Betzig and J.K. Trautman, Science **257**, 189 (1992).
26 U. Durig, D.W. Pohl, and F Rohner, J. Appl. Phys. **59**, 3318 (1986).

Chapter 4: Single Nanocrystallite Imaging

4.1 Introduction

The first step in the detection and spectroscopy of single nanocrystallite is to image the sample. As described in chapter 3, a far-field epifluorescence microscope is used to image extremely dilute solutions of nanocrystallites imbedded in a thin PMMA film. Individual nanocrystallites within the film are separated by more than the diffraction limit of light, allowing the fluorescence from each nanocrystallite to be spatially resolved using far-field optics. This allows us to image individual nanocrystallites even though their physical size is smaller than the diffraction limit of visible light*. Once we are able to image single nanocrystallite samples, it is also necessary to verify that the fluorescence being collected actually originates from single nanocrystallites. After that, we can shift our attention to studying the interesting physics revealed through this technique.

4.2 Images

A typical image of 39Å non-overcoated nanocrystallites can be seen in figure 4.1a. Each bright spot corresponds to the fluorescence from a single nanocrystallite. As can be seen, nanocrystallites within the same image fluoresce with different intensities. Variations in fluorescence intensity are primarily the result of physical difference between individual

* This is analogous to looking at the sky at night. Stars appear as an array of identically sized spots, each a point source of light. This is because their physical size is smaller than the diffraction limit of your eye. In many cases, however, they are separated by a distance that is greater than this limit, allowing the individual stars to be resolved.

nanocrystallites, resulting in different non-radiative relaxation rates as well as differences in fluorescence intermittency (described below). While there was no noticeable difference in the images of different sized non-overcoated nanocrystallites, there was a dramatic increase in the fluorescence signal when overcoated samples were detected (~5x). This difference is attributed to an increased resistance to surface degradation of overcoated nanocrystallites[1,2] and a decrease in fluorescence intermittency.

The nanocrystallites seen in images such as figure 4.1a appear to be quite robust, allowing us to monitor the fluorescence from some nanocrystallites for more than 1 hour.

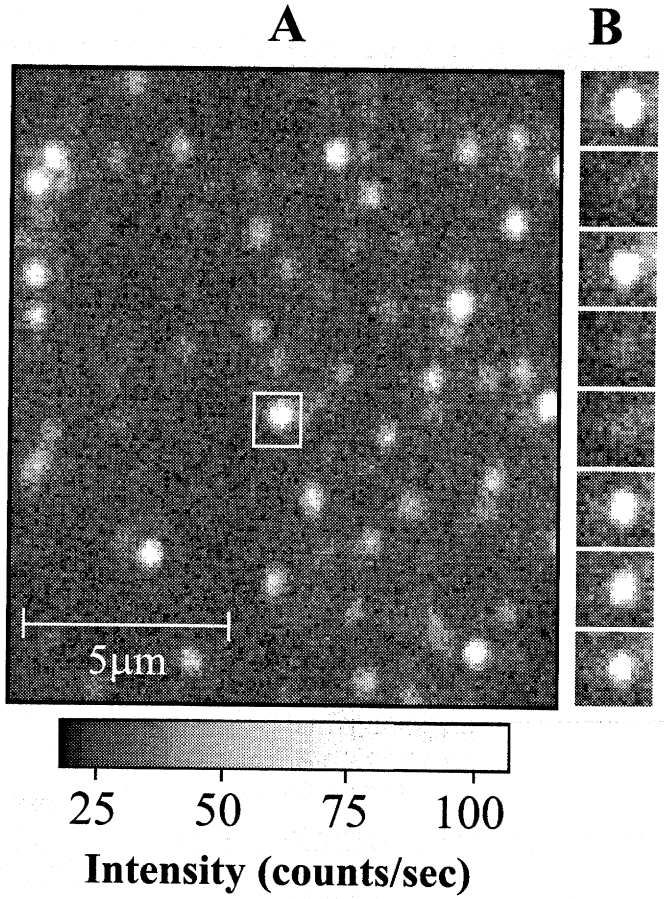

Figure 4.1: Single nanocrystallite image. (A) Image of single 45Å non-overcoated nanocrystallites taken with a 0.5 second integration time and an excitation intensity of 60W/cm^2. (B) Consecutive 0.5 second images of the nanocrystallite indicated by the white box in (A). The images in (B) show binary fluorescence blinking over time.

Over time, however, the fluorescence from individual nanocrystallites is seen to photo-bleach, causing the fluorescence to turn off in a sudden, single-step fashion. While some nanocrystallites are very photo-stable and do not appear to change in fluorescence intensity over periods of time as long as minutes to hours, others bleach rapidly, on a time scale of several seconds. For non-overcoated or lightly overcoated nanocrystallites (<6Å shell), the photo-degradation rate within a particular sample is qualitatively similar to that seen in the ensemble photo-bleaching data of figure 1.6. Some nanocrystallites bleach quickly while others appear to survive indefinitely. The difference between these

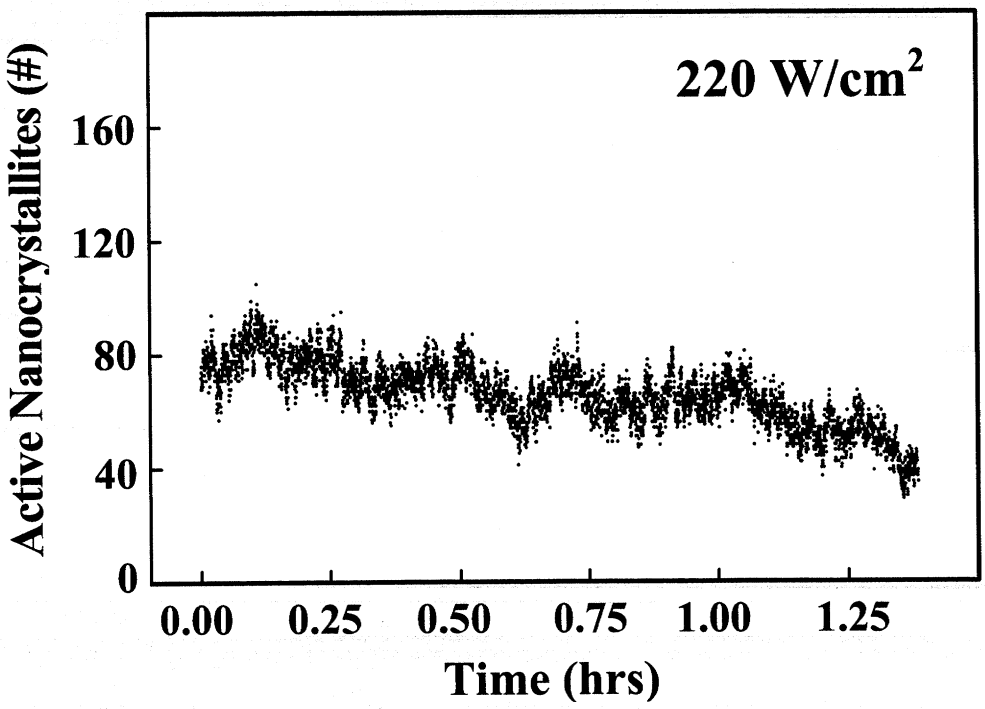

Figure 4.2: Photostability of a sample of 46Å overcoated nanocrystallites as a function of time. The y-axis plots the total number of single nanocrystallites that were visible within an image vs the time of the measurement. Over ~1.4 hours, 220 different nanocrystallites were observed, however, only ~80 nanocrystallites were visible in any given image due to fluorescence blinking of the individual nanocrystallites. Although individual nanocrystallites blinked on and off over time, the average number of visible nanocrystallites remained fairly constant, suggesting very little photodegradation over time.

individual nanocrystallites may be the result of differences in surface passivation. Consistent with this, heavily overcoated nanocrystallites (>6Å shell) show significantly slower photo-degradation rates, with the number of nanocrystallites visible in an image changing very little over time (figure 4.2).

4.3 Evidence for Single Nanocrystallite Detection

On the timescale of a single image (<0.5 second), the fluorescence from individual nanocrystallites is often seen to flicker on and off (figure 4.1b). While the period of time that the nanocrystallites are off ("off times") are typically quite short, on the order of several seconds, some single nanocrystallites are seen to turn off for as long as 10 minutes or more. This effect, referred to as "fluorescence intermittency" was very surprising, since no equivalent effect has been observed in ensemble experiments. The reason: Ensemble averaging. This binary fluorescent blinking, rather than a stepwise or continuous dimming of the emission from a single point, is strong evidence that the spots seen in figure 4.1a originate from single nanocrystallites. For instance, if each spot within the image originated from multiple nanocrystallites, then a stepwise dimming of the fluorescence would be expected as individual nanocrystallites turned off independently. Similarly, the binary photo-bleaching described above is also strong evidence for single nanocrystallite detection.

It should be noted that while fluorescence intermittency indicates that the fluorescence detected in these images arises from a single chromophore, it does not specifically identify this chromophore as a CdSe nanocrystallite. Spectral information presented in chapter 6, such as size dependent changes in the emission energy and

spectral characteristics common to ensemble CdSe nanocrystallite spectra, however, clearly identify these chromophores as CdSe nanocrystallites. In addition, the total emission rate detected for the brightest nanocrystallites is within a factor of 3 of the calculated value at 10K. This evidence, combined with evidence that will be presented in chapters 6 and 7, strongly suggests that what is detected in these experiments is the fluorescence emitted from single CdSe nanocrystallites.

The measured density of nanocrystallites seen in images such as figure 4.1a is very close to the density estimated from the concentration of the starting solution. This implies that what is observed in these experiments is not just fluorescence from single nanocrystallites, but fluorescence from a significant percentage of the total nanocrystallite population. As a result, information obtained from single nanocrystallites should be representative of the ensemble distribution. Additional evidence presented throughout this thesis will further demonstrate that what is measured in single nanocrystallites is consistent with results obtained in ensemble experiments. Since this evidence, as well as additional evidence for the detection of single nanocrystallites, is dispersed throughout this thesis, the main points have been compiled in Appendix 1.

4.4 Fluorescence Intermittency

In addition to providing evidence for single nanocrystallite detection, the fluorescence intermittency observed in figure 4.1b is of interest for other reasons. The pattern of fluorescence blinking is found to be strongly dependent on the particular nanocrystallite as well as the excitation intensity, temperature and the presence of a ZnS overcoating. Nirmal *et al.* studied some of these effects in detail at room temperature[3]

and concluded that intermittency is the result of photo-induced ionization of the nanocrystallites. By adjusting the excitation intensity, the rate that the fluorescence turned off, which is measured as the average "on-time", was found to change dramatically. As the excitation intensity was increased, the average "on-time" decreased. At the same time, there was no change in the average "off-time", indicating that the rate that the fluorescence turned back on was not excitation intensity dependent.

4.4.1 Mechanism

The mechanism proposed by Nirmal *et al.* is based on the well known effect of photo-darkening in ensemble semiconductor doped glasses[4], which are essentially nanocrystallites embedded in a glassy matrix. In these samples, degradation of the ensemble fluorescence intensity at cryogenic temperatures occurs as a result of ionization of the individual nanocrystallites. An ionized nanocrystallites is one in which a single charge from an excited electron-hole pair is ejected from the nanocrystallite, leaving the remaining charge delocalized in the core. Without the complimentary charge, the remaining charge has no way to relax from the lowest excited state, and can remain delocalized in the core indefinitely. In this singly charged state, emission resulting from the excitation of future electron-hole pairs is quenched due to rapid, non-radiative relaxation via Auger scattering between the excited exciton and the delocalized charge[4]. Emission resumes only when the core of the nanocrystallite is neutralized, by either the return of the ejected carrier or the removal of the remaining charge. In semiconductor doped glasses at cryogenic temperatures, ionization results in a decrease in ensemble fluorescence over time when the nanocrystallites ionize with no available neutralization pathway. In single CdSe nanocrystallites, Nirmal *et al.*

concluded that ionization and thermal return of ejected charges was responsible for the observed fluorescence intermittency at room temperature.

The excitation intensity dependence of the on-times indicates that ionization is photo-induced. From room temperature data, however, it is impossible to determine the mechanism of ionization. Possibilities include: 1) photoionization through bi-exciton formation, followed by Auger recombination of one electron-hole pair and ionization of a scattered charge from the second pair, 2) thermal ionization from a singly excited state, or 3) ionization of a single exciton through the absorption of a second photon. Note that 1 and 3 correspond to different processes: In one case, two excitons are excited; in the other, a single exciton is excited twice.

Recent results by Banin *et al.*[5], on the intermittency of single CdSe nanocrystallites over a range of temperatures between 15K and room temperature, suggests that for CdS overcoated CdSe nanocrystallites, the ionization mechanism involves both thermal and bi-excitation effects ("bi-excitation" refers to either a bi-exciton or doubly excited single exciton) . While a complete temperature dependence study is required in order to conclusively determine the mechanism of ionization in non-overcoated and ZnS overcoated nanocrystallites, it is likely that similar results will be found. Preliminary evidence for this includes: 1) room temperature "on-times" vary linearly with excitation intensity, consistent with thermal ionization from a singly excited state, 2) on-times observed at 10K are significantly increased over those observed at room temperature, consistent with thermal ionization, however, 3) at 10K, even in the absence of substantial thermal energy, fluorescence intermittency is still a common occurrence (although the frequency is significantly reduced). This suggests a contribution from bi-excitation or other photo-induced effects.

4.4.2 Room Temperature vs Cryogenic Results

The excitation intensity *independence* of the "off-times" at room temperature suggest that, in this temperature range, the neutralization process is spontaneous[3]. In this case, neutralization is likely to occur through the thermally activated return of the ionized charge. This does not, however, explain the intermittency results observed in our lab at cryogenic temperatures. At 10K, measured "off-times" for CdSe and ZnS overcoated CdSe nanocrystallites are not infinite, even in the absence of the thermal energy necessary for the return of the ionized charge*. This suggests that a second neutralization pathway exist: photo-induced ionization of the remaining charge. This pathway leaves a neutral core with both charges located outside of the nanocrystallite. In support of this model, additional evidence suggests that charges do, in fact, collect around individual nanocrystallites. These results will be discussed in chapters 8, 9 and 10.

While at room temperature, thermal return of the ionized charge appears to be the dominant recombination pathway, this proposed "bi-ionization" model would suggest that an excitation intensity dependence of the off-times should exist at cryogenic temperatures. Preliminary data taken in our lab indicates that this is the case. Figure 4.3 plots fluorescence intensity as a function of time for the same single nanocrystallite at two different excitation intensities at 10K. The fluorescence time-traces clearly demonstrate the binary nature of the fluorescence blinking. As can be seen, the average

* Banin *et al.* report extremely long (perhaps infinite) "off times" for CdS overcoated CdSe nanocrystallites at 20K. This is different than what is observed for ZnS overcoated nanocrystallites, which frequently blink on and off at low temperature. One possible explanation for this difference is that the confinement of the electron and hole within the CdSe core is different for CdS and ZnS overcoatings. CdS confines the hole more strongly than the electron, allowing ionization of the electron but not the hole. This would eliminate the proposed low-temperature neutralization pathway, resulting in extremely long "off times". ZnS overcoating, however, confines both the electron and hole equally, potentially allowing bi-ionization.

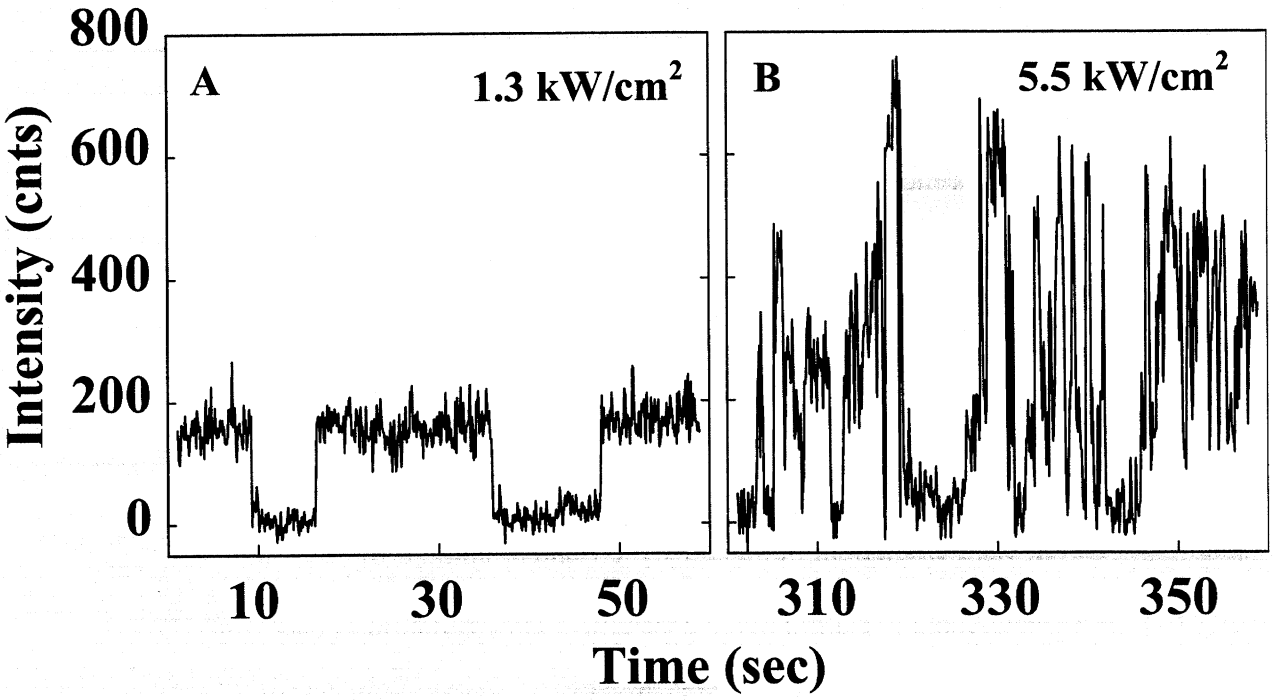

Figure 4.3: Affect of excitation intensity on fluorescence intermittency. Time traces plot the emission intensity from the same single nanocrystallite at two different excitation intensities. Changes in both the average on- and off-times are clearly observed. Emission was collected with an integration time of 100ms.

duration of both the on- and off-times appears to decrease as the excitation intensity is increased. This is consistent with the proposed mechanism.

4.4.3 Effect of ZnS overcoating

Within the model described above, the pattern of fluorescence intermittency can be explained as the result of ionization and neutralization of a nanocrystallite as a function of time. To confirm this hypothesis, Nirmal *et al.* studied overcoated nanocrystallites with varying ZnS thickness at room temperature. ZnS, which has a higher bandgap than CdSe, acts as a barrier to ionization, and should decrease the rate of both ionization and thermal return of external charges. As expected, an increase in both the "on" and "off times" was observed as the thickness of the ZnS shell was increased.

4.4.4 Implications of Intermittency on Ensemble Measurements

While fluorescence intermittency cannot be observed directly on the ensemble level, this effect will contribute to characteristics measured in ensemble experiments. one example relates to the measured quantum yield for an ensemble sample. The binary nature of fluorescence intermittency might suggest that measured quantum yields are influenced not only by the competition between radiative and non-radiative relaxation pathways during each excitation, but also by the relative amount of "on" and "off time" experienced by each nanocrystallite in the ensemble. The excitation intensity dependence of intermittency, however, suggests that this should be a relatively insignificant effect at the low excitation intensities typically used in quantum yield measurements.

One area in which fluorescence intermittency will play a more significant role is in ensemble saturation measurements. Absorption saturation measurements are often performed by monitoring emission intensity as a function of excitation intensity. A sub-linear relation is typically interpreted as a saturation of the absorbing state. In light of these single nanocrystallite experiments, however, these results are more appropriately interpreted as saturation of the emitting state. Figure 4.4a plots the emission time trace for a single nanocrystallite where the excitation is doubled approximately every 30 seconds following a short period of non-illumination. As can be seen, the peak emission intensity increases with increasing excitation intensity. At the same time, the average "on-time" decreases with intensity. A plot of the average peak emission intensity during an "on-time" versus excitation intensity shows a linear relation, consistent with absorption at a non-saturation rate (figure 4.4b). A plot of the average total emission

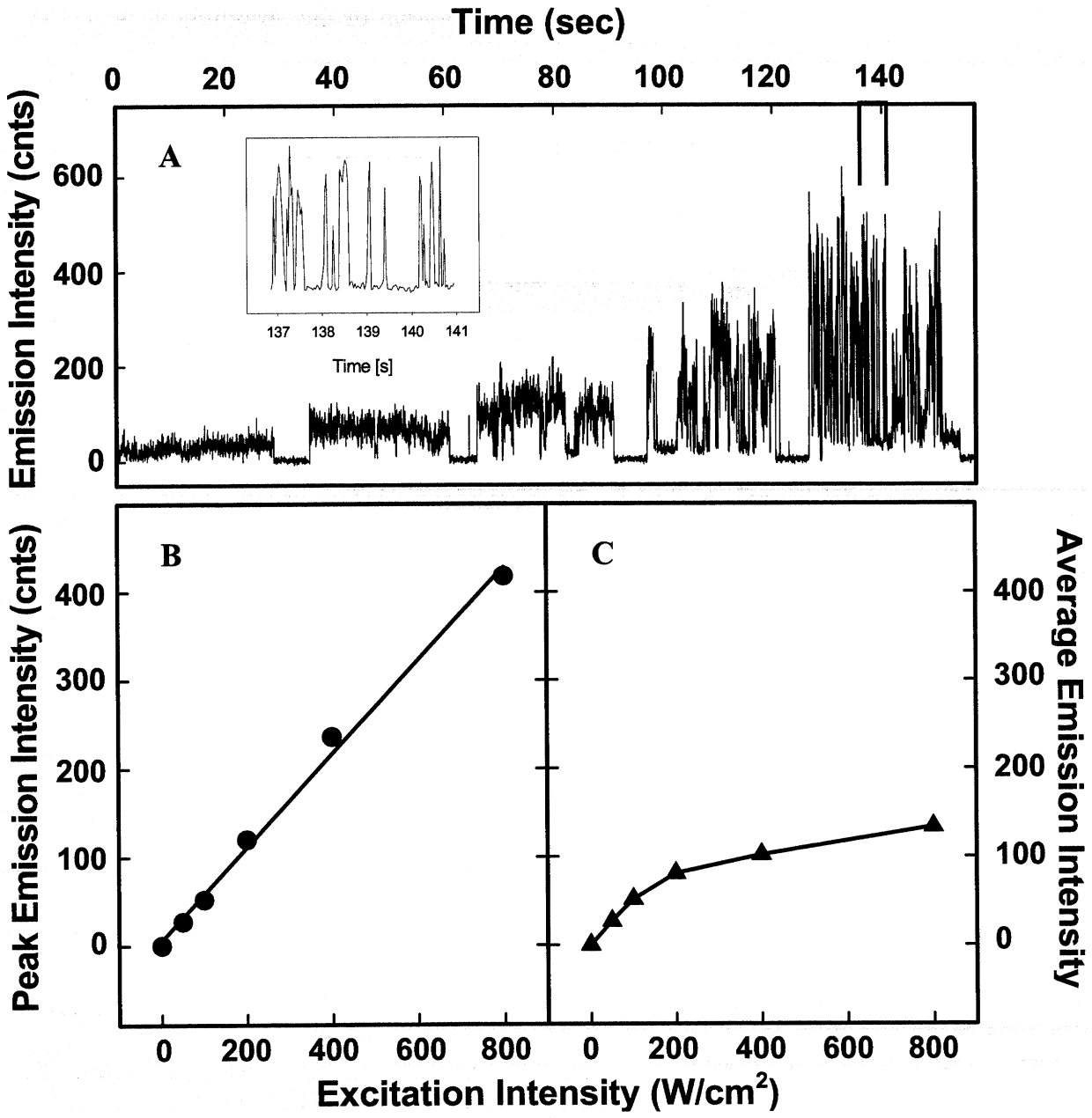

Figure 4.4: Emission saturation. (A) Intensity time trace for a single nanocrystallite where the excitation intensity is doubled approximately every 30 seconds. Between increases in excitation intensity, there is a brief period during which the excitation intensity is turned off. (Inset) Blowup of seconds 137-141 from (A), which are marked with vertical lines. (B) Plot of peak emission intensity during an "on-time" vs excitation intensity. (C) Plot of average emission intensity vs excitation intensity, revealing an effective saturation of the emitting state.

intensity over all times (both "on" and "off") versus excitation intensity, however, reveals a sub-linear relation (figure 4.4c). This is not saturation of the absorbing state, but is actually the result of the excitation intensity dependent the "on-times". Identical results are expected when averaged over an ensemble, suggesting that ensemble saturation measurements may provide more information about the emitting state that the absorbing state. This represents an entirely new perspective on a classic experiment which can only be correctly interpreted on the single nanocrystallite level. This type of insight exemplifies the power of single nanocrystallite detection.

4.5 Conclusion

Several conclusions can be drawn from the data presented in this chapter, the most significant of which is that detection of single nanocrystallites at both room and cryogenic temperatures is possible. By imaging single nanocrystallites, it is possible to uncover dynamic effects that were never expected on the basis of ensemble experiments. Fluorescence intermittency, which is hidden in ensemble measurements due to ensemble averaging, reveals a dynamic interaction between each nanocrystallite and its environment. Data suggests that fluorescence intermittency is the result of ionization and neutralization of the nanocrystallite. Neutralization occurs either through the return of the ionized charge, or through a second ionization event that removes the remaining charge from the CdSe core. In addition to revealing fascinating new physics, fluorescence intermittency may also represent a limitation on the maximum emission intensity observed in ensemble samples. By adding a ZnS overcoating, it is possible to adjust the frequency of fluorescence intermittency by decreasing the rate of ionization.

This provides us with some physical control over the dynamics of this system, and may improve ensemble results. In fact, at 10K, an overcoating of 10-14Å can reduce intermittency to a timescale of minutes. In this case, images of single nanocrystallites appear relatively stable over time. By stabilizing intermittency, we can begin to focus on changes in emission intensity as a function of experimental parameters such as the polarization of the absorbed or emitted light. This will be the topic of the next chapter.

4.6 References

[1] M. Danek et al., J. Cryst. Growth **145**, 714 (1994).
[2] M. Danek et al., Chem. Mater. **8**(1), 173 (1996).
[3] M. Nirmal, B.O. Dabbousi, M.G. Bawendi, J.J. Macklin, J.K. Trautman, T.D. Harris and L.E. Brus, Nature **383**, 802 (1996).
[4] D.I. Chepic, et al. J. Lumin. **47**, 113 (1990).
[5] U. Banin, M. Bruchez, A.P. Alivisatos, T. Ha, S. Weiss, and D.S. Chemla, J. Chem. Phys. **110**(2), 1195 (1999).

Chapter 5: Polarization Dependence

5.1 Introduction

Polarization spectroscopy has long been used to gain insight into the orientation and physical nature of excitation and emission transition dipole moments in ensemble molecular and solid state systems[1]. In many systems, however, there is no order to the orientation of individual chromophores within the ensemble, causing polarization information to be lost. In single chromophore spectroscopy, individual transition dipoles can be measured one at a time. As a result, information can be obtained regarding the orientation of individual transition dipoles even within an amorphous matrix[2,3]. Since no ensemble analogue exists, this type of experiment exemplifies the power of single chromophore spectroscopy.

Near-field scanning optical microscopy, which has both a spatially varying longitudinal and transverse polarized electromagnetic field, can actually be used to determine the three dimensional (3D) orientation of individual transition dipoles[4]. Far-field microscopy (both wide-field and confocal) lacks a significant longitudinal electromagnetic field and, in general, can only provide information about the 2D orientation of single chromophores within the sample plane[2,3,5-7]. This information is still useful, however, and for most single molecule applications, the convenience and flexibility of far-field microscopy outweighs the additional orientation information of near-field microscopy. In single nanocrystallite experiments, information about the orientation of individual nanocrystallites can be extremely valuable, since many theoretical predictions regarding the effects of directional perturbations, such as electric[8] and magnetic fields[9,10], depend on the relative orientation of the nanocrystallite's unique c-axis.

5.2 Experimental

Emission polarization was studied in single nanocrystallites by observing changes in the detected emission intensity collected through a linear polarizer (analyzer). Polarization data was taken using the experimental apparatus described in chapter 3 (in image mode), with an analyzer in front of the CCD detector that was rotated in 15 degree increments between consecutive images. In chapters 6 and 9, polarization data was taken in spectral mode. In these cases, a wedge depolarizer was added after the analyzer so that no polarization selectivity from the diffraction grating would contribute to the observed results. Since wedge depolarizers works by rotating light to different degrees depending on the spatial position across the optic, the analyzer/depolarizer assembly was placed away from the image plane of the microscope in order to maximize the depolarization of each individual point within the spectrum.

In order to verify that the experimental apparatus had no intrinsic polarization selectivity which might affect the single nanocrystallite data, two non-polarized samples were studied: Amorphous ensemble nanocrystallite films and 1μm latex spheres filled with an ensemble of randomly oriented dye molecules (Nile Red). Both of these samples should be intrinsically non-polarized due to the randomly oriented nature of the individual chromophores within each ensemble system. While these non-polarized emitting sources should be a good test for the presence of polarization selectivity in our detection system, careful consideration must be made in exciting these samples to avoid creating a polarization anisotropy through selective excitation. For instance, if dye-spheres are excited with linear polarized light, the individual molecules of the ensemble that are oriented parallel to the excitation polarization will be selectively excited. The

polarization radiation pattern of this sample will then reflect this selective excitation, resulting in polarized emission.

Circularly polarized light is made up of equal components of two orthogonal linear polarized beams that are out of phase with each other by 90°. In many cases, excitation with circularly polarized light will avoid selective excitation of a particular orientation within the ensemble. When excited with circularly polarized light, no emission polarization was observed in either the dye spheres or ensemble nanocrystallite samples, confirming that the experimental apparatus was free from polarization selectivity.

5.3 Results

The inset of figure 5.1 shows images of two single nanocrystallites as a function of analyzer angle. The emission intensity of the two nanocrystallites can be seen oscillating out of phase with each other as the analyzer is rotated. Also plotted in figure 5.1 are the normalized emission intensities as a function of angle for these two nanocrystallites. The intensities can be clearly seen oscillating with a high degree of polarization [$(I_{max}-I_{min})/I_{max}$ = 81% and 93%] as a sine-squared function of the analyzer angle with a 180 degree period. The high degree of polarization suggests the existence of a highly oriented transition dipole. Rotation of the *excitation* polarization by 90 degrees had no observable effect on the degree of *emission* polarization or phase. This indicates that the observed *emission* polarization is not the result of a polarization memory, but is instead consistent with an intrinsic, oriented transition dipole.

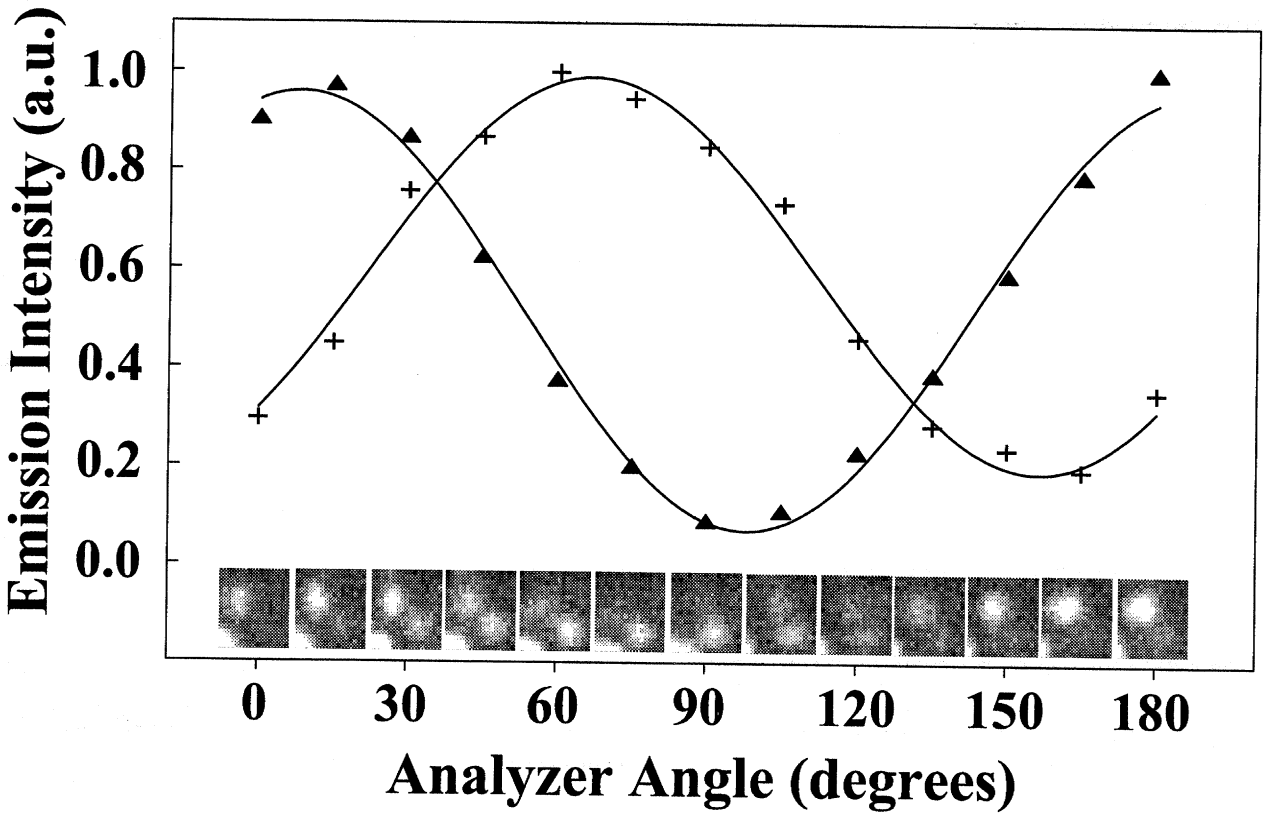

Figure 5.1: Single nanocrystallite polarization spectroscopy. Normalized emission intensity of two single 52Å overcoated nanocrystallites as a function of analyzer angle. The solid lines correspond to the fit to a sine-squared function of analyzer angle with a 180 degree period. Data is the average of 2 complete 180 degree rotations. (Inset) Images of the two nanocrystallites in figure 5.1 as a function of analyzer angle (angle can be read directly off the x-axis below each image). Data was taken with a 5 second integration time, 60W/cm^2 excitation intensity and 0 degree excitation polarization.

While the nearly spherical shape of these nanocrystallites may at first seem incompatible with a highly oriented transition dipole, the prolate shape and unidirectional nature of the wurtzite crystal structure provide a unique axis along which a dipole could be oriented. What is more surprising is that the degree of polarization is strongly dependent on the particular nanocrystallite. Figure 5.2 plots the emission intensity of three single nanocrystallites as a function of analyzer angle. As can be seen, even within the same sample, different nanocrystallites display different degrees of polarization.

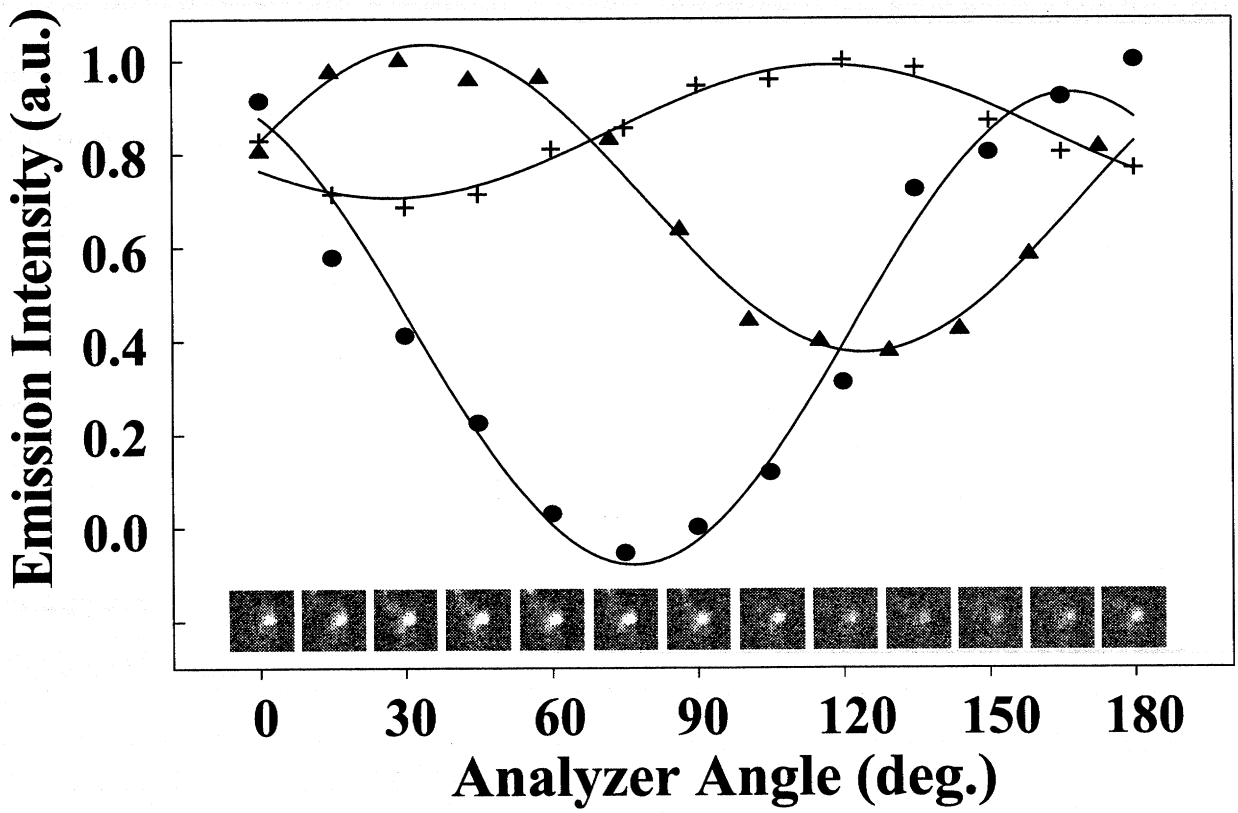

Figure 5.2: Single nanocrystallite polarization spectroscopy. Normalized emission intensity of three single 52Å overcoated nanocrystallites as a function of analyzer angle. The solid lines correspond to the fit to a sine-squared function of analyzer angle with a 180 degree period. Data is the average of 6 complete 180 degree rotations. (Inset) Image of one nanocrystallite from figure 5.2 (triangles) as a function of analyzer angle (angle can be read directly off the x-axis below each image). All data was taken with 5 second integration time, 60W/cm^2 excitation intensity and 0 degree excitation polarization.

5.4 Discussion

5.4.1 "Bright axis" Transition Dipoles

The data in figure 5.2 is quite different from what is typically observed in other single chromophore systems. Polarized electromagnetic waves in the far-field have a strong electromagnetic field in 1 dimension, providing information about the orientation of the projection of a single transition dipole within the sample plane (the plane normal to the

propagation direction of the light)[2,3,5-7]. The strength of a transition is proportional to $|\vec{\mu} \cdot \vec{E}|^2$, where $\vec{\mu}$ is the transition dipole vector and $\vec{E}$ is the polarization of the absorbed or emitted light. Transition dipoles in the single chromophores studied to date have generally been unidirectional, creating a single "bright axis" along which the absorbed or emitted electromagnetic field is coupled. The intensity of the detected signal is then proportional to $\cos^2(\theta)\cos^2(\phi)$ where θ is the angle between the emission polarization and the projection of μ onto the sample plane, and ϕ is the tilt angle between μ and the sample plane (out-of-plane angle) (see figure 5.3 for details). When a polarizer is rotated in the emission pathway, the detected intensity oscillates between $I_{min}= 0$ and $I_{max}= |\mu|^2 \cdot \cos^2(\phi)$. The result is 100%

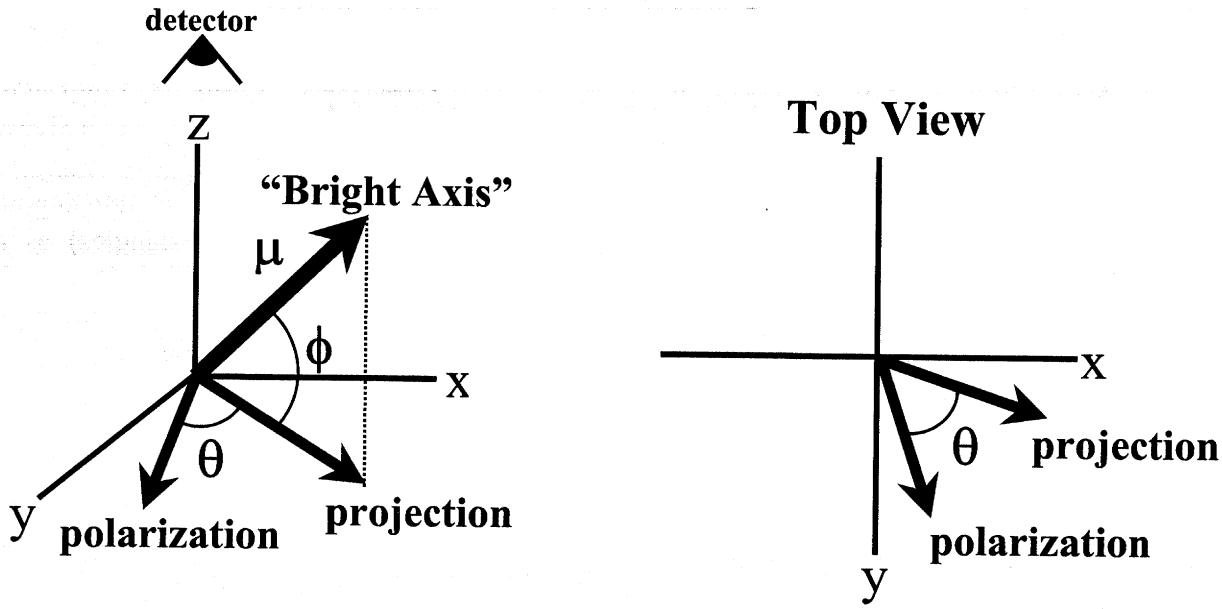

Figure 5.3: Coordinate system and definition of angles used in the calculation of the polarization dependence of "bright axis" chromophores. In this system, light propagates along the z-axis, and the x-y plane corresponds to the sample plane

polarized emission regardless of the orientation of the molecule*, with the phase corresponding to the in-plane angle of the transition dipole. Since local inhomogeneities generally make it impossible to know the absolute value of $\vec{\mu}$, the out-of-plane angle (ϕ) cannot be determined. As a result, for systems with a "bright axis", standard far-field polarization spectroscopy can only provide information about the orientation of the projection of a single transition dipole within the sample plane (this corresponds to the in-plane orientation)[2,3]. This is not consistent, however, with the data in figure 5.2.

While the majority of the single molecules studied so far are predicted to have a "bright axis", there are some cases where a range of polarizations have still been observed. Less than 100% polarization was observed in single pentacene molecules in p-terphenyl. In this case, however, the loss of polarization was the result of birefringence of the crystalline p-terphenyl matrix turning the linear polarized emission into elliptical light[6,7].

The different degrees of polarization observed in figure 5.2 are not an artifact of the experimental or sample preparation procedure such as those described in refs. 6 and 7. To verify this, single DiI molecules were studied. Previous single molecule experiments have shown that single DiI molecules in PMMA show very high degrees of polarization, as expected for a chromophore with a "bright axis"[2,3]. In our experimental apparatus, the average degree of polarization for the 10 single DiI molecules studied was also found to be ~100%, consistent with a "bright axis" transition. In addition, results nearly identical to

* This result is only strictly true for a radiating dipole in free space, observed with an infinitely small collection angle. In reality, the large collection angle of the microscope objective allows the detection of some light emitted parallel to the collection axis. It is therefore possible to have some "bright axis" transitions which do not show 100% polarization. In practice, these dipoles are rarely seen since they also emit the least light in the direction of the detector. As a result, virtually all single chromophores with a "bright axis" show 100% polarization. Later in this chapter, and in Appendix 2 we will address the effects of collection angle and the radiation pattern of a dipole on a dielectric surface.

those seen in figure 5.2 (and figure 5.6 below) have also been obtained for nanocrystallites that were deposited onto the substrate surface, in hexane, with no surrounding matrix. The data in figure 5.2 is actually consistent with a different type of transition dipole, predicted to exist in CdSe nanocrystallites: A "dark axis" transition dipole.

5.4.2 Band Edge States in CdSe Nanocrystallites

Within the simple "particle-in-a-sphere" model, the lowest excited state, is 8-fold degenerate. This degeneracy is lifted, however, by intrinsic asymmetries within the nanocrystallite. These include the exchange interaction between electron and hole, the unidirectional nature of the wurtzite crystal structure, and the prolate shape of the nanocrystallite[9]. These effects split the band edge state into a series of 5 states defined in

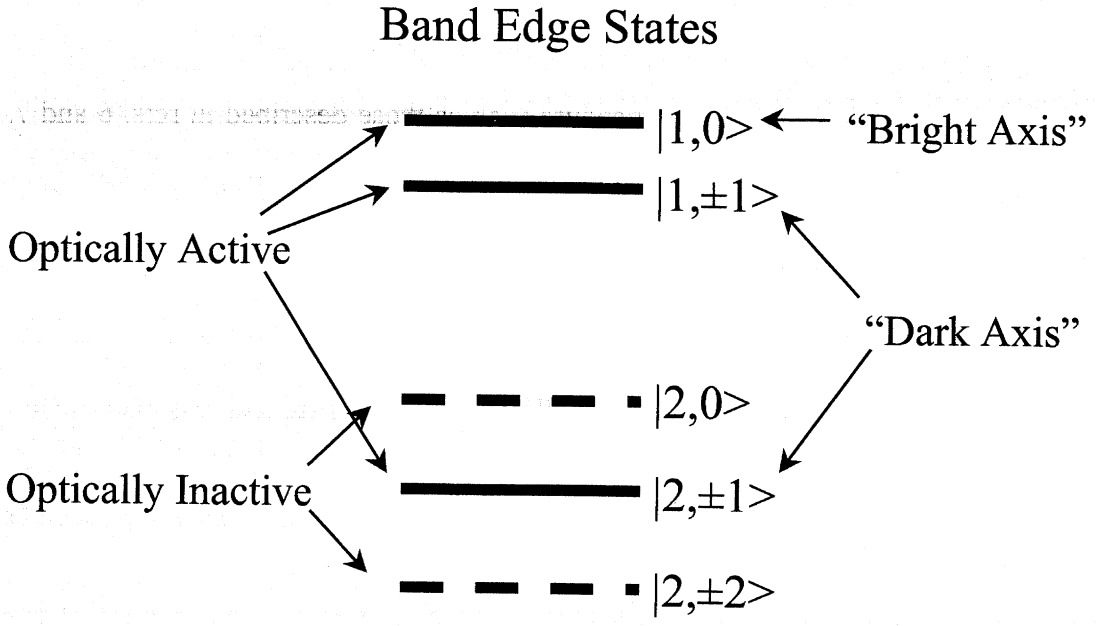

Figure 5.4: The five energy levels that make up the band edge states in CdSe nanocrystallites. The ordering of the states is qualitatively displayed, with the lowest energy states at the bottom. Solid and dashed lines indicate optically active and optically inactive states as indicated. Also indicated are the "bright" or "dark" axis nature of the transition dipole for each optically active state.

terms of the projection of their angular momentum, as shown in figure 5.4. Both Effective Mass Approximation[9] and Pseudopotential [11] calculations predict a similar ladder of states, with emission from the lowest of these states being a highly spin forbidden transition. As a result, emission from this state is thought to proceed either through a virtual transition or mixing with a nearby optically active state[12]. Tight-Binding Approximation calculations also predict mixing of the lowest excited state with higher-lying optically active states[13].

5.4.3 Polarization Selection Rules

The polarization selection rules for the band edge states can be determined by calculating the transition probability matrix between the ground and excited states. In the basis of single particle (electron and hole) states, the transition probability can be written as

$$P = \left| \left\langle \psi_h \left| \vec{e} \cdot \mu \right| \psi_e \right\rangle \right|^2 \qquad [5.1]$$

where μ is the momentum operator, $\vec{e}$ is the polarization of the light, and ψ_e and ψ_h are the electron and hole wavefunctions respectively. This can be expanded in terms of the Bloch functions for the electron and hole so that

$$P = \left| \left\langle \varphi_h u_h \left| \vec{e} \cdot \mu \right| \varphi_e u_e \right\rangle \right|^2 \qquad [5.2]$$

where $\varphi_{e(h)}$ and $u_{e(h)}$ are the envelope and unit cell wavefunctions for the electron (hole). Since the momentum operator acts *only* on the unit cell wavefunction, and the envelope function is essentially constant on this length scale, this equation can be further simplified by separating the envelope wavefunctions from the transition dipole matrix.

$$P = \left| \left\langle \varphi_h \left| \varphi_e \right\rangle \left\langle u_h \left| \vec{e} \cdot \mu \right| u_e \right\rangle \right|^2 . \qquad [5.3]$$

The transition dipole orientations for emission from the band edge states can be determined by calculating the non-zero matrix values ($\left|\langle u_h|\vec{e}\cdot\mu|u_e\rangle\right|^2$) for all orientations of $\vec{e}$. In the basis set of atomic orbitals, the matrix values for the 5 band edge states are as follows:

$$|2,\pm2\rangle \rightarrow \left|\langle \sqrt{2}/2\,(X \mp iY)\downarrow(\uparrow)|\vec{e}\cdot\mu|S\uparrow(\downarrow)\rangle\right|^2$$

$$|2,\pm1\rangle \rightarrow \left|C^+/\sqrt{2}\,\langle (X \mp iY)\downarrow(\uparrow)|\vec{e}\cdot\mu|S\downarrow(\uparrow)\rangle - \frac{C^-}{\sqrt{6}}\langle [(X \mp iY)\uparrow(\downarrow) \mp 2Z\downarrow(\uparrow)]|\vec{e}\cdot\mu|S\uparrow(\downarrow)\rangle\right|^2$$

$$|2,0\rangle \rightarrow \left|i\sqrt{3}/6\,\langle [(X+iY)\downarrow +2Z\uparrow]|\vec{e}\cdot\mu|S\uparrow\rangle + i\sqrt{3}/6\,\langle [(X-iY)\uparrow -2Z\downarrow]|\vec{e}\cdot\mu|S\downarrow\rangle\right|^2 \qquad [5.4]$$

$$|1,\pm1\rangle \rightarrow \left|C^+/\sqrt{6}\,\langle [(X \mp iY)\uparrow(\downarrow) \mp 2Z\downarrow(\uparrow)]|\vec{e}\cdot\mu|S\uparrow(\downarrow)\rangle + C^-/\sqrt{2}\,\langle (X \mp iY)\downarrow(\uparrow)|\vec{e}\cdot\mu|S\downarrow(\uparrow)\rangle\right|^2$$

$$|1,0\rangle \rightarrow \left|i\sqrt{3}/6\,\langle [(X+iY)\downarrow +2Z\uparrow]|\vec{e}\cdot\mu|S\uparrow\rangle - i\sqrt{3}/6\,\langle (X-iY)\uparrow -2Z\downarrow|\vec{e}\cdot\mu|S\downarrow\rangle\right|^2$$

where X, Y and Z are the selenium 4p atomic orbitals, S is the cadmium 5s orbital, the arrows represent spin states, and C^+ and C^- are size dependent coefficients defined in ref. 9. In these equations, the Z orbital is oriented parallel to the unique axis of the wurtzite crystal structure (c-axis). Spins indicated in parentheses correspond to the spin of the negative angular momentum state (e.g. the electron spin state for the $|2,-2\rangle$ state is down while its spin in the $|2,2\rangle$ state is up).

Since the momentum operator cannot act on the spin state of a wavefunction, the non-zero elements of these transition matrices due to symmetry considerations are:

$$|2,\pm 2\rangle \rightarrow 0$$

$$|2,\pm 1\rangle \rightarrow \left|\pm \tfrac{C^{+}}{\sqrt{2}}\langle (X \mp iY)\downarrow(\uparrow)|\vec{e}\cdot\mu_{xy}|S\downarrow(\uparrow)\rangle \mp \tfrac{C^{-}}{\sqrt{6}}\langle (X \mp iY)\uparrow(\downarrow)|\vec{e}\cdot\mu_{xy}|S\uparrow(\downarrow)\rangle\right|^{2}$$

$$|2,0\rangle \rightarrow \left|\tfrac{i\sqrt{3}}{6}\langle 2Z\uparrow|\vec{e}\cdot\mu_{z}|S\uparrow\rangle - \tfrac{i\sqrt{3}}{6}\langle 2Z\downarrow|\vec{e}\cdot\mu_{z}|S\downarrow\rangle\right|^{2} = \left(\tfrac{i\sqrt{3}}{3} - \tfrac{i\sqrt{3}}{3}\right)\cdot\langle Z|\vec{e}\cdot\mu_{z}|S\rangle = 0 \quad [5.5]$$

$$|1,\pm 1\rangle \rightarrow \left|\tfrac{C^{+}}{\sqrt{6}}\langle (X \mp iY)\uparrow(\downarrow)|\vec{e}\cdot\mu_{xy}|S\uparrow(\downarrow)\rangle + \tfrac{C^{-}}{\sqrt{2}}\langle (X \mp iY)\downarrow(\uparrow)|\vec{e}\cdot\mu_{xy}|S\downarrow(\uparrow)\rangle\right|^{2}$$

$$|1,0\rangle \rightarrow \left|\tfrac{i\sqrt{3}}{6}\langle 2Z\uparrow]|\vec{e}\cdot\mu_{z}|S\uparrow\rangle + \tfrac{i\sqrt{3}}{6}\langle 2Z\downarrow|\vec{e}\cdot\mu_{z}|S\downarrow\rangle\right|^{2}$$

where $\mu_{xy} = \mu_x \pm i\mu_y$. As mentioned in section 5.4.2, transitions between the ground and lowest excited state ($|2,\pm 2\rangle$) are optically spin forbidden since a photon cannot carry an angular momentum of 2. Similarly, while not spin forbidden, an evaluation of the integral for the $|2,0\rangle$ state reveals that the transition probability for emission from this state is also identically zero.

Of the remaining 3 optically active states, 2 distinct transition dipole orientations exist. The $|1,0\rangle$ state has a "bright axis" transition dipole oriented along the c-axis of the nanocrystallite. The $|2,\pm 1\rangle$ and $|1,\pm 1\rangle$ states both have a degenerate transition dipole, oriented isotropically in the x-y plane. In this case, what remains is a unique, unidirectional "dark axis", which is the only axis along which no light is emitted. This unique "dark axis" is oriented parallel to the c-axis. Pseudopotential calculations also predict similar dipole orientations [14]. While the orientation of the transition dipoles for these states are known, theoretical and experimental results have not determined which of these states will contribute to the relaxation of the lowest excited state, which is formally inactive. As a result, we have no way, a priori, to know what the orientation of the emission dipole will be.

5.4.4 "Dark Axis" Transition Dipoles

For transitions involving states with a "dark axis", the detected emission intensity is proportional to $(1-\cos^2(\theta)\cos^2(\phi))$ where θ and ϕ are defined as in section 5.4.1, relative to the "dark axis" orientation (figure 5.5a). In this case, as the emission analyzer is rotated, the strength of the transition oscillates between $I_{max}=|\mu|^2$ and $I_{min}=|\mu|^2\cdot\cos^2(\phi)$. As a result, the degree of polarization will vary from 0 to 100% depending on the out-of-plane angle (figure 5.6b). The data in figure 5.2 is consistent with emission from a "dark axis" transition dipole.

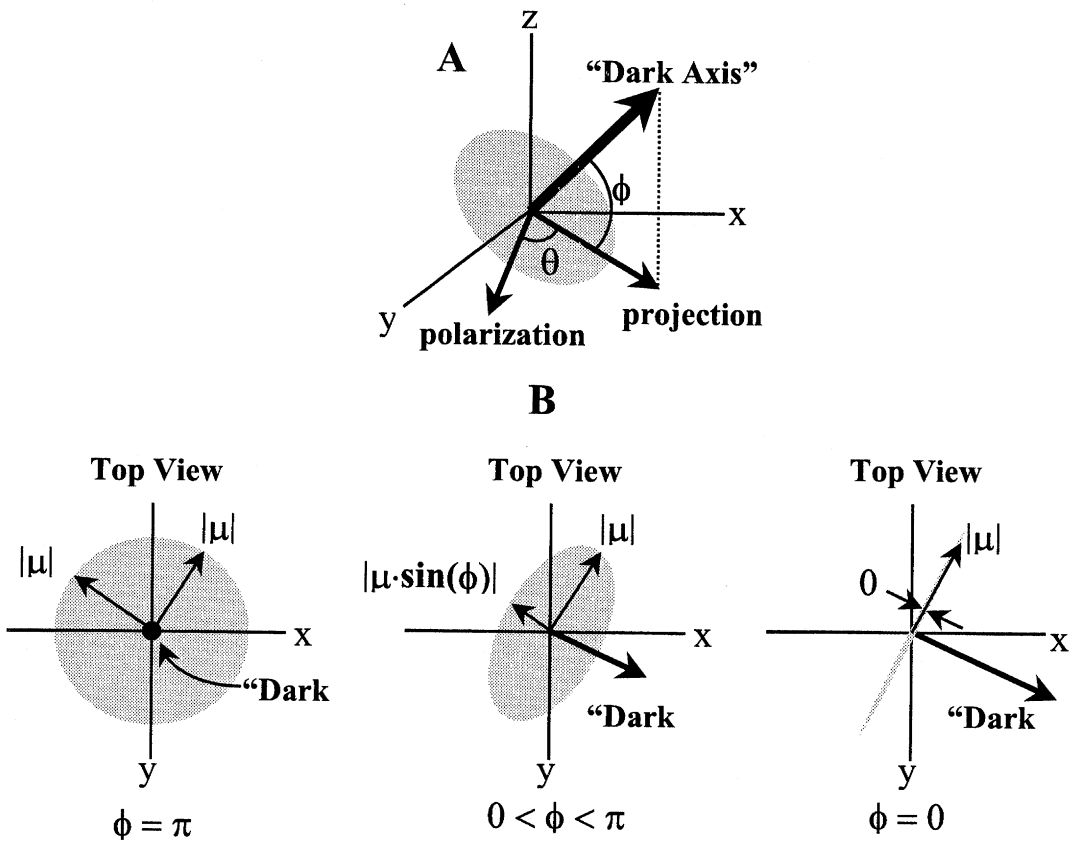

Figure 5.5: "Dark axis" coordinate system with light propagation along the z-axis. (A) The shaded disk represents the planar, degenerate transition dipole oriented normal to the "dark axis". (B) Top views depict the projection of the dipole onto the sample (x-y) plane at three different values of ϕ. This projection (squared) corresponds to the polarization modulation measured by the detection system. Also included are the magnitudes of two orthogonal dipole projections, as well as the projection of the "dark axis" onto the sample plane at each angle.

An interesting characteristic of "dark axis" transition dipoles is that, since the absolute value of μ can be measured directly ($I_{max}=|\mu|^2$), the out of plane angle (ϕ) can be calculated based on the degree of polarization observed. As a result, it is, in principle, possible to use far-field polarization spectroscopy to directly measure the 3 dimensional orientation of individual nanocrystallites from the phase (in-plane angle) and degree of polarization (out-of-plane angle) of each. Note, however, that there is no way to distinguish between angles into (ϕ) and out of ($-\phi$) the sample plane.

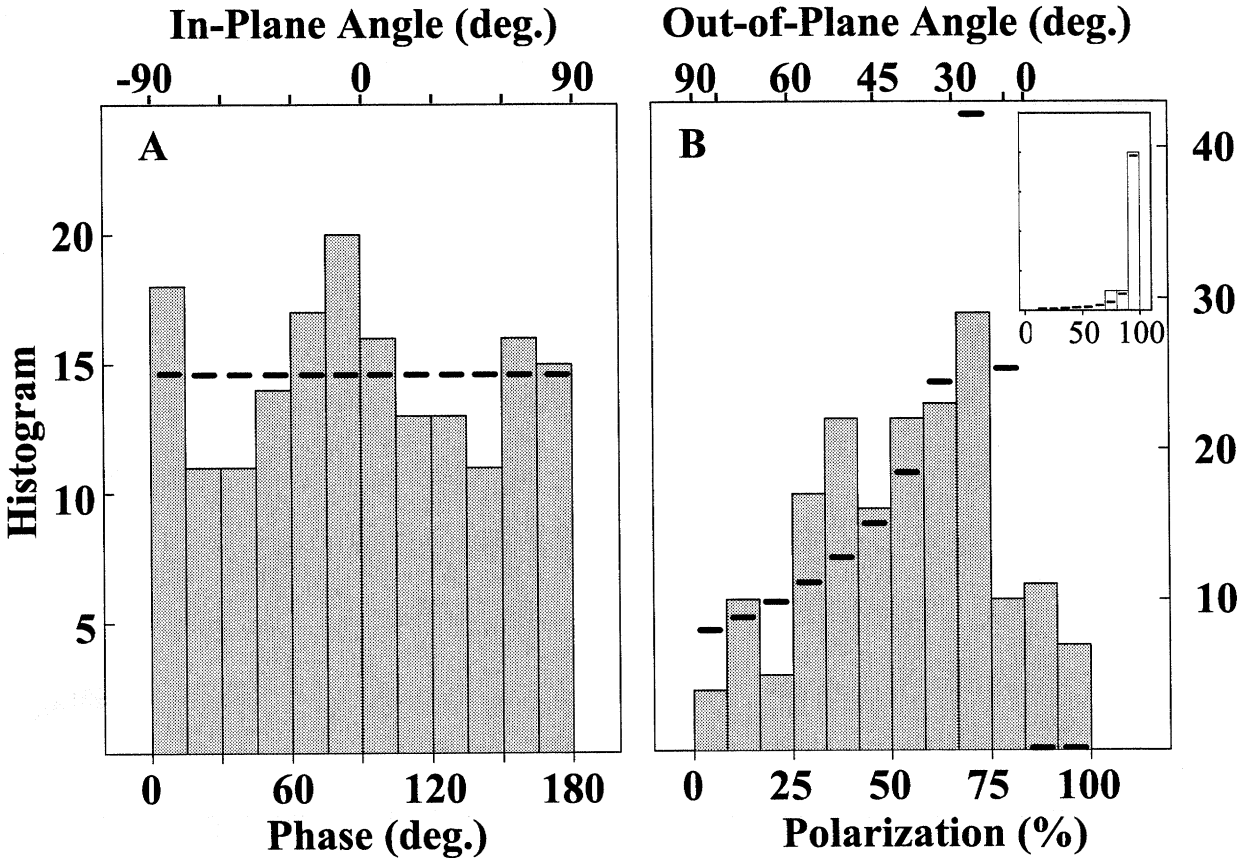

Figure 5.6: Polarization statistics. (A) Histogram of polarization phase angles for 176 single nanocrystallites, with the corresponding in-plane orientation of the c-axis (top axis). (B) Histogram of degrees of polarization with the corresponding out-of-plane angle for the same 176 nanocrystallites. (Inset) Histogram of degrees of polarization of 10 single DiI molecules. Solid lines in the main and inset figure correspond to the calculated probability histogram for an isotropic distribution of "dark" and "bright" axis orientations respectively.

Figure 5.6 displays data from 176 single nanocrystallites showing the phase and degree of polarization for each. As can be seen, a broad distribution of parameters is observed which covers the entire range of phase angles and degrees of polarization. While emission is characterized by a broad range of polarizations, the polarization dependence of the excitation was found to be significantly weaker (average = 23%, σ=14%). While strong absorption polarization has been reported for single CdS nanocrystallites[15], the weak excitation polarization observed in the present experiment is not unexpected since the nanocrystallites were excited in a region with a relatively high density of electronic states. While individual states should have distinct transition dipole orientations[9,12], it is likely that multiple, overlapping states are excited simultaneously, decreasing the degree of polarization in excitation.

5.4.5 Effect of Prolate Shape

An additional effect which could potentially contribute to the observed polarization dependence is the prolate shape of the nanocrystallites. In porous silicon, differential screening of the electromagnetic field along the major and minor axes of a dielectric ellipsoid has been shown to result in stronger emission and absorption along the major axis[16]. For a prolate ellipsoid with an intrinsically isotropic transition dipole, the relative emission intensity of light with a polarization $\vec{e}$ is

$$I(\omega_e) = 1 + \kappa(\omega_e)(\hat{c} \cdot \vec{e})^2, \qquad [5.6]$$

where $\hat{c}$ is a unit vector oriented along the major axis of the ellipsoid, ω_e is the emission frequency, and $\kappa(\omega_e)$ is a factor which depends on both the shape of the ellipsoid and the emission frequency such that

$$\kappa(\omega_e) = \frac{\delta(\omega_e)(1-3n^{(z)})[4+\delta(\omega_e)(1+n^{(z)})]}{4[1+\delta(\omega_e)n^{(z)}]^2}, \qquad [5.7]$$

where $\delta(\omega_e) = \frac{\varepsilon_i(\omega)}{\varepsilon_o(\omega)} - 1$, $\varepsilon_i(\omega)$ and $\varepsilon_o(\omega)$ are the dielectric constants of the ellipsoid and the surrounding medium respectively, and $n^{(z)}$ is the shape dependent depolarization factor defined as:

$$n^{(z)} = \frac{1-e^2}{2e^3}(\ln\frac{1+e}{1-e} - 2e), \qquad [5.8]$$

where $e = \sqrt{\left|1 - {}^{a^2}\!/_{c^2}\right|}$, and a and c are the dimensions of the minor and major axes of the ellipsoid.

If we assume that the emission is intrinsically isotropic, then for CdSe nanocrystallites with aspect ratio (c/a) of 1.15 and a dielectric constant of 10 in a surrounding medium of PMMA ($\varepsilon_o(\omega) \approx 2.5$), this depolarization effect would result in a ~15% degree of polarization. This cannot explain the large degree of polarization observed in these experiments, consistent with the conclusion that the observed polarization dependence is the result of an oriented electronic transition dipole. In addition, since the c-axis is oriented parallel to the major axis of the nanocrystallite, differential screening due to shape should not contribute to the polarization dependence of either "bright" or "dark" axis transitions, since emission from these states occurs either along the major or minor axes but not both. Shape may play a more significant role in excitation polarization where the strong electronic orientation effects are reduced.

5.4.6 Dipole Radiation Pattern and Microscope Collection Angle

There are two additional effects which contribute to the predicted polarization dependence of both "bright" and "dark" axis transitions and therefore affect the shape of the expected probability distribution in figure 5.6b. First, we have only considered the radiation pattern from an isolated dipole in free space. The pattern of radiation from a dipole embedded in a thin film on a dielectric interface, however, has been found both theoretically[17-19] and experimentally[20] to be significantly different than that of a free dipole. Second, we have so far assumed an infinitely small collection angle in our detection optics. This is not a good assumption, since the large numerical aperture of the microscope objective used in these experiments allows the detection of photons emitted with an angle of as much as ~45 degrees from normal. The result is that some photons are detected with a polarization that is perpendicular to the sample plane. In the simple discussion of the polarization dependence of "bright" and "dark" axis states, these additional contributions have been neglected. The sum of these effects slightly alters the expected polarization dependence of both "bright" and "dark" axis transitions (although the general conclusions remain the same). A complete discussion of the calculations used to account for the surface effect and finite collection angle is included in Appendix 2. The solid lines in figure 5.6 and 5.6(inset) represent the calculated probability histogram, including the theoretical contribution of the surface and collection angle, for an isotropic distribution of "dark" and "bright" axis orientations respectively. The data in figure 5.6 is consistent with emission from a "dark axis" state with an isotropic distribution of orientations within the ensemble, while the data for DiI (inset) is representative of a distribution of "bright axis" orientations.

An additional consequence of the large collection angle used in these experiments is that the degree of polarization for "bright axis" transitions should be strongly correlated with the maximum emission intensity. For "bright axis" transitions, the lowest degrees of polarization result from dipoles oriented out of the sample plane. These dipoles, however, also emit the fewest photons in the direction of the detector. "Dark axis" transitions should have no such correlation since, in theory, the angular dependence of I_{max} is negligible (see Appendix 2 for details). Examination of 85 single nanocrystallites revealed no correlation between maximum emission intensity and the degree of polarization, consistent with emission from a "dark axis" state (figure 5.7).

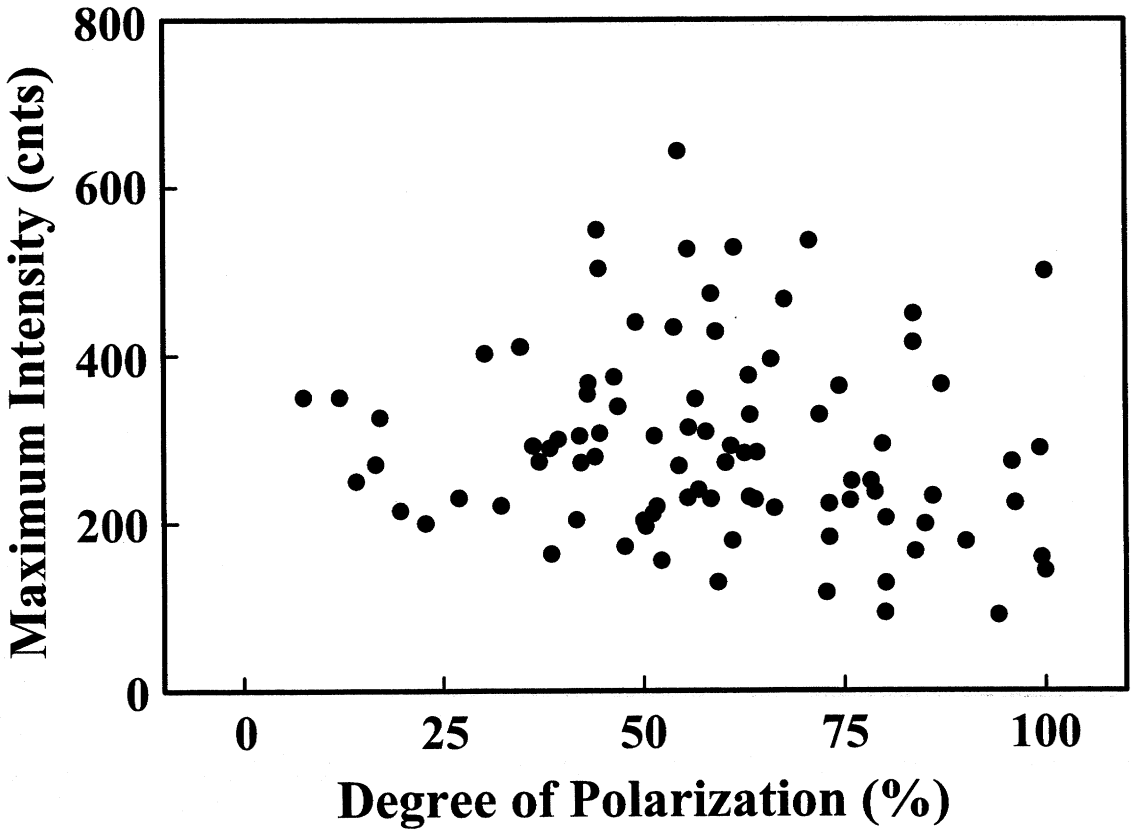

Figure 5.7: Plot of maximum emission intensity vs degree of polarization for 85 single nanocrystallites. Maximum intensity is taken from a sine-squared fit to the polarization data for each nanocrystallite. No correlation between intensity and polarization is found.

5.4.7 3-Dimenstional Orientation of Single Nanocrystallites

The data presented so far suggest that at 10K, emission from the band edge of CdSe nanocrystallites involves a "dark axis" transition dipole. If we include the effect of surface and collection angle, it is possible to estimate both the in-plane and out-of-plane angles for each nanocrystallite. It is therefore possible to use the highly parallel and flexible detection of far-field microscopy to directly measure the 3D orientation of each nanocrystallite within the sample. From the data in figure 5.6a and 5.6b, the in-plane and out-of-plane orientation of each nanocrystallite c-axis can be calculated. The top axes of figure 5.6 have been added to indicate the corresponding angles.

Knowing the orientation of single nanocrystallites relative to the experimental frame of reference can be extremely valuable in interpreting single nanocrystallite experiments. Many theoretical predictions, which can easily be studied on the single nanocrystallite level, rely on a precise knowledge of the orientation of the c-axis relative to applied perturbations such as electric [8] and magnetic fields[9,10]. In addition, changes in the orientation of the transition dipole over time can indicate either rotation of the nanocrystallite within the sample or significant changes in the electronic structure. For instance, this information can be useful in studying effects such as fluorescence intermittency.

Figure 5.8 plots the total emission intensity as a function of analyzer angle for a single nanocrystallite. A relatively constant phase and degree of polarization are observed over several full rotations of the analyzer. At ~720 degrees, however, the emission from this single nanocrystallite turns off. The nanocrystallite remains dark for more than 2 minutes (~5 seconds/15 degree rotation). At ~1260 degrees, emission

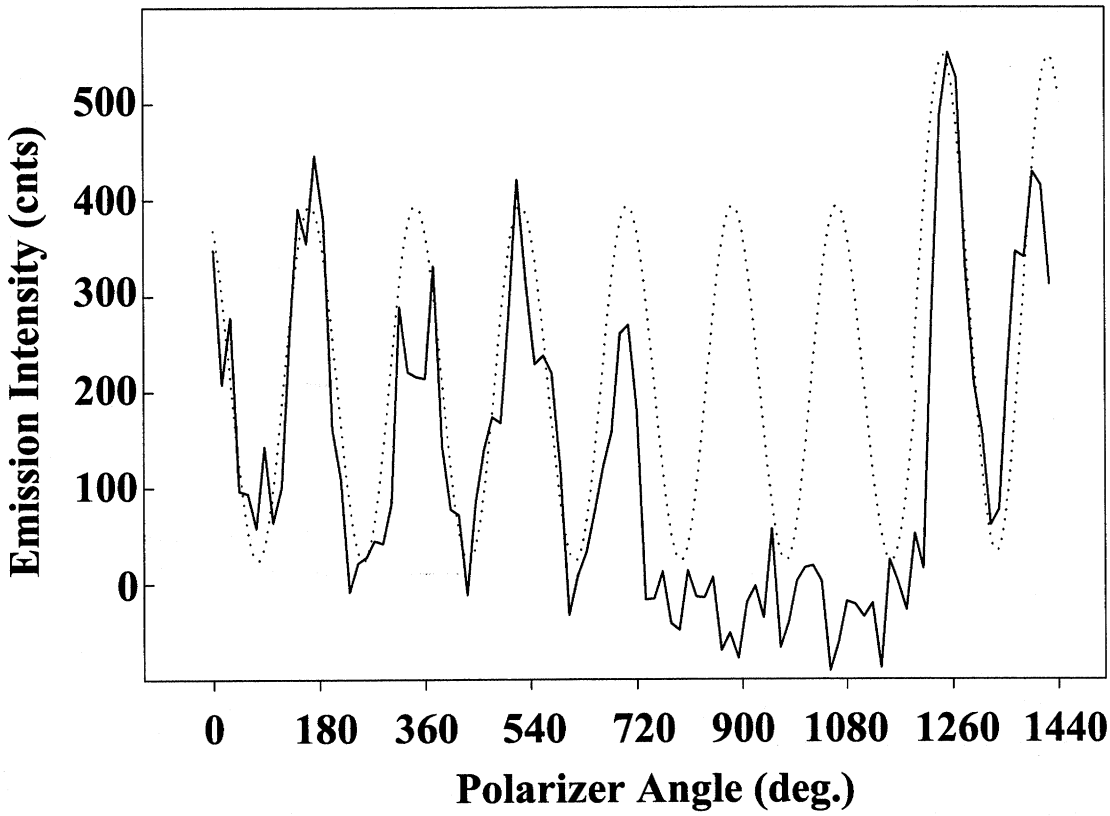

Figure 5.8: Polarization and fluorescence intermittency. Plot of intensity from a single 52Å overcoated nanocrystallite over several full rotations of the analyzer. A dark period occurs between the angles of ~720-1260 degrees. After the dark period, fluorescence resumes with the same phase and degree of polarization but with a higher intensity. The dotted line represents a fit to the data before the dark period. Note that there is a break in the fit line at ~1150 degrees where the total intensity has been increased but the phase and degree of polarization remain the same.

resumes at a higher intensity than before, but with the same phase and relative degree of polarization. This result, which was found in all cases studied, suggests that the changes causing fluorescence intermittency do not effect the relative orientation of the transition dipole moment. This indicates that the "catastrophic" change that causes the nanocrystallite to be dark for such an extended period of time does not significantly affect the electronic structure. This is consistent with the proposed ionization mechanism for intermittency described in chapter 4.

5.4.8 Room Temperature Polarization

While the experiments described above were done at cryogenic temperatures, measurements of single 38Å nanocrystallites at room temperature also revealed strong emission polarization. The data in figure 5.9 was taken by removing the linear polarizer and replacing it with a polarizing beam-displacing cube. The displacing-cube separates the image into two orthogonal polarizations that are projected onto different regions of the CCD. This allows both polarizations to be monitored simultaneously.

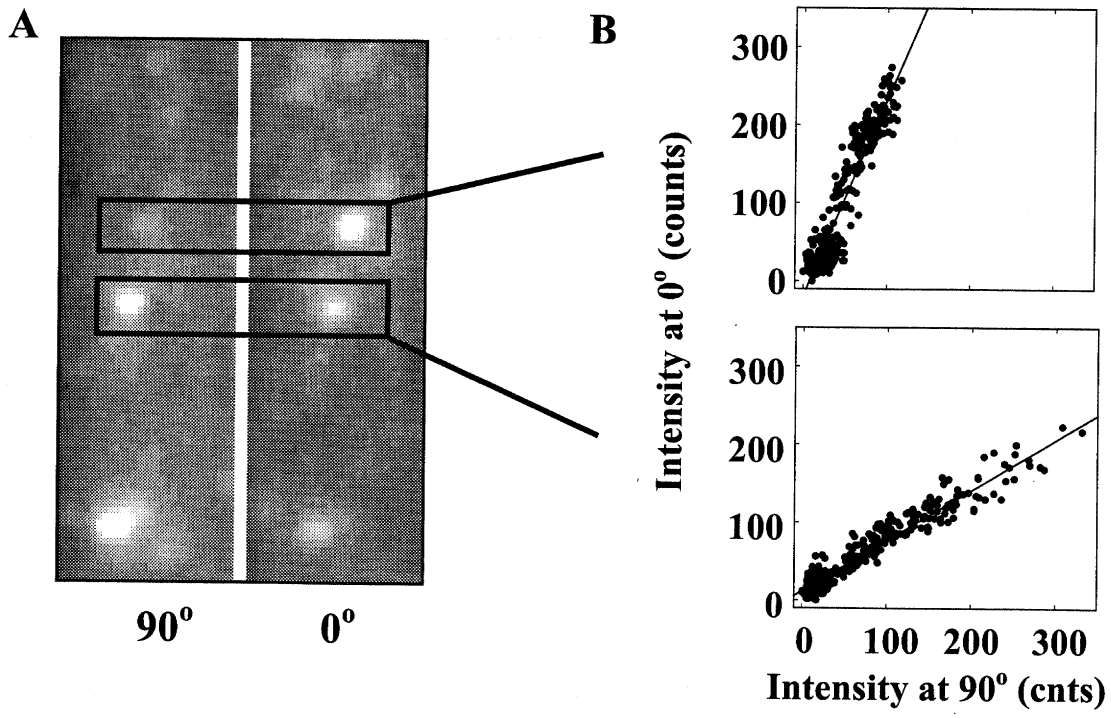

Figure 5.9: Polarized emission at room temperature. (A) Two images of the same single nanocrystallites taken by projecting the 0° (right) and 90° (left) components of the emission polarization simultaneously onto different areas of the CCD detector. (B) Scatter plots for two nanocrystallites in which the intensity of emission polarized along the 0° axis is plotted against the intensity along the 90° axis. Data in figure 5.9 was taken with a 0.5 second integration time and an excitation intensity of 200W/cm^2.

Nanocrystallites which appear brighter on the right side have a transition dipole oriented more strongly along the 0° axis. The opposite is true for nanocrystallites oriented along the 90° axis. This type of data collection was necessary to avoid complications arising from fast fluorescence intermittency at room temperature which caused the total emission intensity to change dramatically over time. Figure 5.9b, demonstrates that, while the total fluorescence from each nanocrystallite varies strongly from frame to frame, the ratio of the intensities along the two polarization axes remains the same. Differences in the slope of the two data sets represent differences in the polarization dependence from each nanocrystallite. While it is somewhat surprising that polarization dependence is observed at room temperature, where emission is thought to arise from multiple excited states, the effect of the prolate shape described in section 5.4.5 may contribute. In addition, the order of the excited states seen in figure 5.4 indicates that the only "bright axis" state in the band edge is farthest from the lowest excited state. This may also contribute to the room temperature polarization dependence by favoring emission from the "dark axis" states.

5.5 Conclusion

By using polarization spectroscopy to study emission in single CdSe nanocrystallites we were able to obtain new information about the nature of the emitting state that could not be obtained in ensemble experiments. The observed polarization dependence suggests that emission results from a degenerate electronic transition dipole oriented isotropically in the x-y plane of the nanocrystallite. While theoretical calculations have predicted the presence of such dipoles, these experiments represent the first experimental evidence confirming their existence. In addition, while theoretical

predictions have indicated the presence of both "bright" and "dark axis" states near the band-edge, there is no theoretical evidence indicating which dipoles are involved in the emission pathway. By uncovering this information experimentally, new insight is provided about the mechanism of relaxation from the lowest excited state.

In addition to contributing to our understanding of the electronic structure of the emitting state, the 2D nature of a "dark axis" transition dipole allows the determination of not only the in-plane angle but also the out-of-plane tilt of the nanocrystallite c-axis. This allows us to directly measure the 3D orientation of individual nanocrystallites using standard far-field optics. The ability to measure 3D orientation creates a significant advantage in the study of single nanocrystallites over other single chromophores. Many theoretical predictions that can be studied on the single nanocrystallite level rely on a knowledge of the c-axis orientation relative to applied perturbations such as pressure, electric and magnetic fields. Studies of coupling or energy transfer between nanocrystallites or a surface may also benefit from an understanding of relative orientations. The ability to measure the 3D orientation of single nanocrystallites has greatly increased the potential power of our single nanocrystallite experiments and will be used throughout the remainder of this thesis. As an example, we have demonstrated that fluorescence intermittency does not involve a significant change in the electronic structure of the nanocrystallites, consistent with the proposed ionization mechanism.

5.6 References

[1] E. W. Thulstrup and J. Michl, J. Am. Chem. Soc. **104**, 5594 (1982).
[2] J.J. Macklin et al., Science **272**, 255 (1993).
[3] Ruiter, A.G.T. et al., J. Phys. Chem. A **101**, 7318 (1997).
[4] E. Betzig and R.J. Chichester, Science **262**, 1422 (1993).
[5] T. Ha, et al, Phys. Rev. Lett. **80**(10), 2093 (1998).
[6] F. Guttler et al., J. Lumin. **56**, 29 (1993).
[7] F. Guttler, et al., Chem. Phys. **211**, 421 (1996).
[8] S.A. Blanton, R.L. Leheny, M.A. Hines, and P. Guyot-Sionnest, Phys. Rev. Lett. **79**, 865 (1997).
[9] Al.L. Efros et al., Phys. Rev. B, **54**(7), 1 (1996).
[10] M. Kuno, et al., J. Chem. Phys. **108**(10), 4242 (1998).
[11] A. Franceschetti, H. Fu, L.W. Wang and A. Zunger, "Many-body pseudopotential theory of excitons in InP and CdSe QDs" Phys. Rev. B, (in press).
[12] Al.L. Efros, Phys. Rev. B **46**(12), 7448 (1992).
[13] K. Leung, S. Pokrant and K.B. Whaley, Phys. Rev. B **57**(19), 12291 (1998).
[14] A. Zunger, personal communication.
[15] Tittel, J., et al., Ber. Bunsenges. Phys. Chem. **101**, 1626-1630 (1997).
[16] E. Kovalev et al., Phys. Rev. Lett. **77**(10), 2089 (1996).
[17] W. Lukosz, J. Opt. Soc. Am., **71**(6), 744 (1981).
[18] W. Lukosz, J. Opt. Soc. Am., **69**(11), 1495 (1979).
[19] W. Lukosz, Phys. Rev. B, **22**(6), 3030 (1980).
[20] Ch. Fattinger and W. Lukosz, J. Lumin., **31&32**, 933 (1984).

Chapter 6: Spectroscopy of Single Nanocrystallites

6.1 Introduction

In chapters 4 and 5, we uncovered new and unexpected physical phenomena which provided significant insight into the physics and dynamics of CdSe nanocrystallites. There is a limit, however, to what can be learned from these imaging experiments. In order to truly explore the physics of quantum confinement and the unique optical and electronic properties of CdSe nanocrystallites, it is necessary to do spectroscopy on single nanocrystallites.

6.2 Experimental

The experimental apparatus used to collect emission spectra from single nanocrystallites is the same as that used to obtain images (see chapter 3 for details). In image mode, the emission signal passes through a spectrometer that has had the diffraction grating replaced by a mirror. The dark edges in images such as figure 6.1a actually correspond to the edges of the entrance slit on the spectrometer. In order to take spectra from single nanocrystallites, the entrance slit is partially closed, spatially isolating a subset of the nanocrystallites along a vertical stripe of the image (figure 6.1b). It is usually possible to align many nanocrystallites at different vertical positions within the narrowed entrance slit. If the diffraction grating is replaced in the spectrometer, the light from each vertical position is dispersed onto the CCD resulting in spectra from single nanocrystallites (figure 6.1c). What results is an image in which single nanocrystallite spectra are dispersed along the x-axis and are vertically separated from each other along the y-axis depending on their spatial position within the entrance slit.

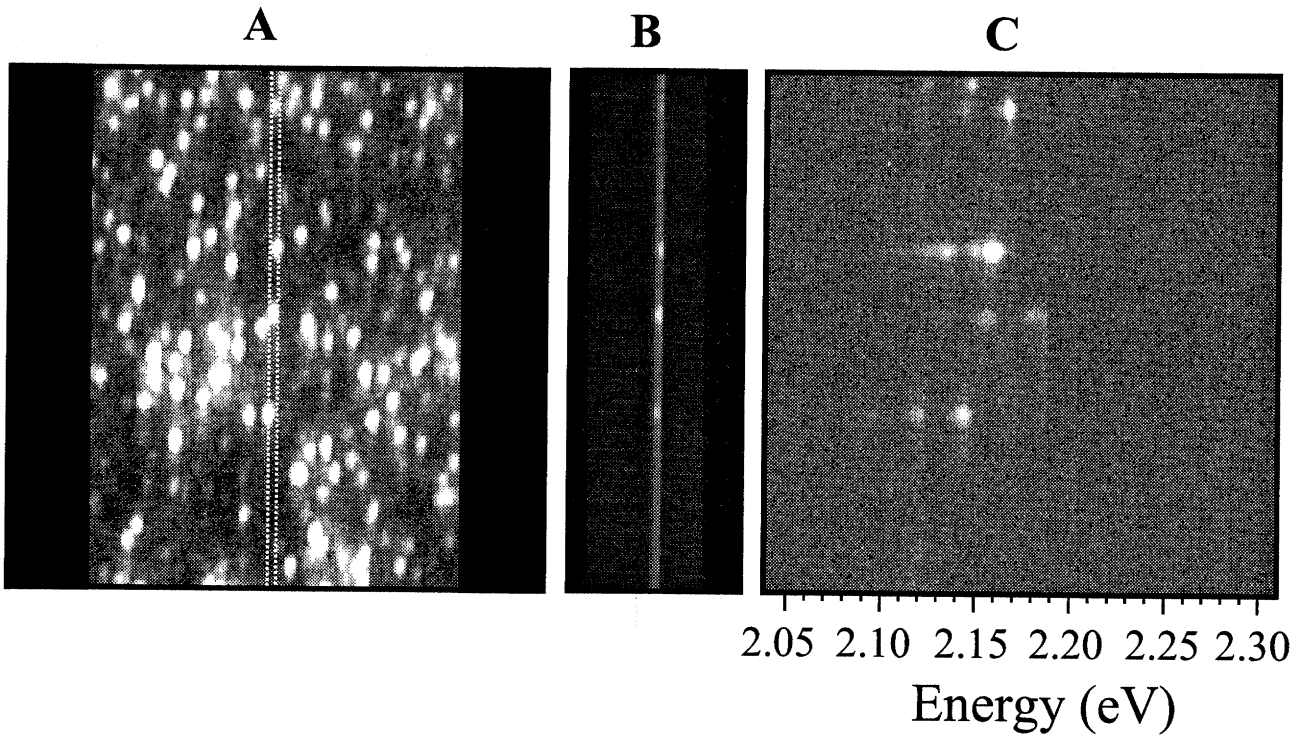

Figure 6.1: Single nanocrystallite imaging and spectroscopy. (A) Image of single 45Å nanocrystallites at 10K with the entrance slit open to 7mm. White dotted lines represent the center of the entrance slit. (B) Image of the same region as in (A) with the entrance slit closed to 0.125mm. Several bright spots can still be seen between the narrowed slits. (C) Spectrally dispersed image of the entrance slit in (B). This image consists of several single nanocrystallite spectra plotted along the x-axis, each separated along the y-axis according to their vertical position between the entrance slit. For each single nanocrystallite image in (B), there is a corresponding single nanocrystallite spectrum in (C).

Using this procedure, it is possible to collect spectra from many single nanocrystallites simultaneously. In addition to spatial separation, it is also possible to use spectral resolution to distinguish the emission from single nanocrystallites (an example can be seen later in figure 6.5). Using this technique and the proper concentration, it is typically possible to collect spectra from more than 100 single nanocrystallites at once.

6.3 Results and Discussion

6.3.1 Single Nanocrystallite Spectra

Traditional emission spectra can be extracted from images such as figure 6.1c by taking a cross section. Figure 6.2 compares the spectrum of a single non-overcoated nanocrystallite to a fluorescence line narrowed spectrum from a similarly sized ensemble sample. As can be seen, the spectrum from an individual nanocrystallite shows a greatly reduced linewidth over what is obtained using fluorescence line narrowing[1]. In addition, the longitudinal-optical (LO) phonon structure of the single nanocrystallite

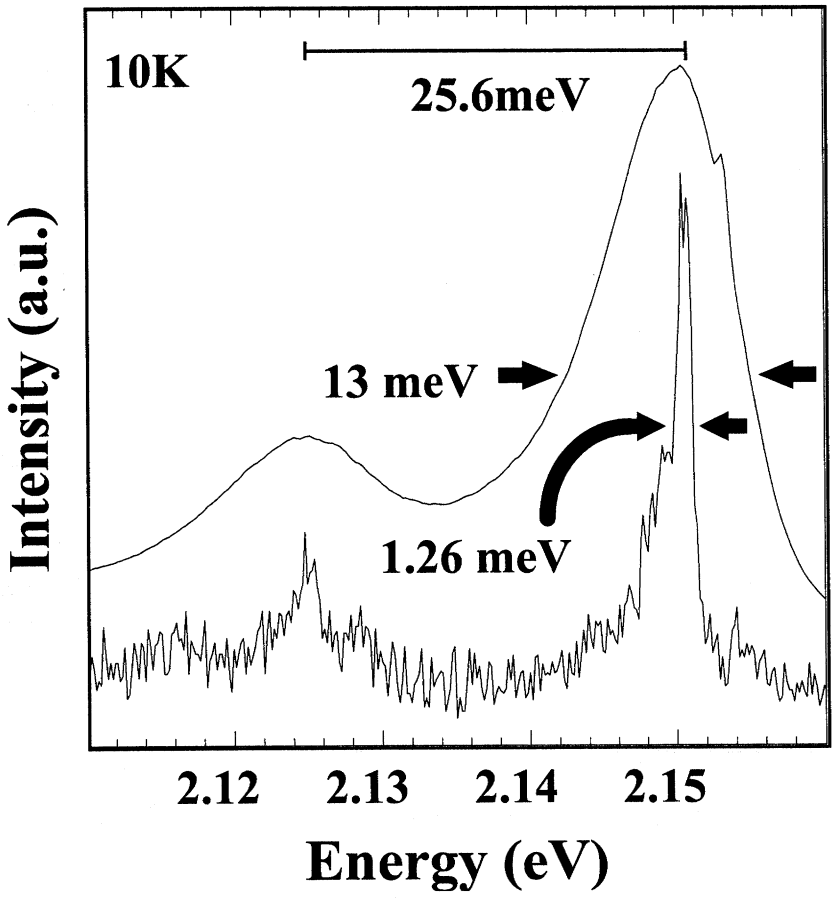

Figure 6.2: Ensemble vs Single nanocrystallite spectrum. Comparison of a single 45Å nanocrystallite spectrum (bottom) and a fluorescence line narrowed spectrum of a 45Å ensemble sample (top).

spectrum is clearly resolved, and has a peak spacing that is comparable to the bulk LO phonon frequency and the phonon frequency measured in ensemble samples.

Figures 6.3a and b show a comparison between a representative sample of single nanocrystallite spectra and the corresponding ensemble spectra from those samples. Note that figures 6.3a and b show data from 2 different size samples, and that the energy of both the ensemble and single nanocrystallite spectra are shifted relative to each other as a result of quantum confinement.

As expected, the ensemble emission spectrum can be reproduced by a convolution of the average single nanocrystallite lineshape with the distribution of zero-phonon energies measured within the sample. Figure 6.4 displays a histogram of emission energies from ~500 single nanocrystallites compared to the ensemble spectrum obtained from the same sample.

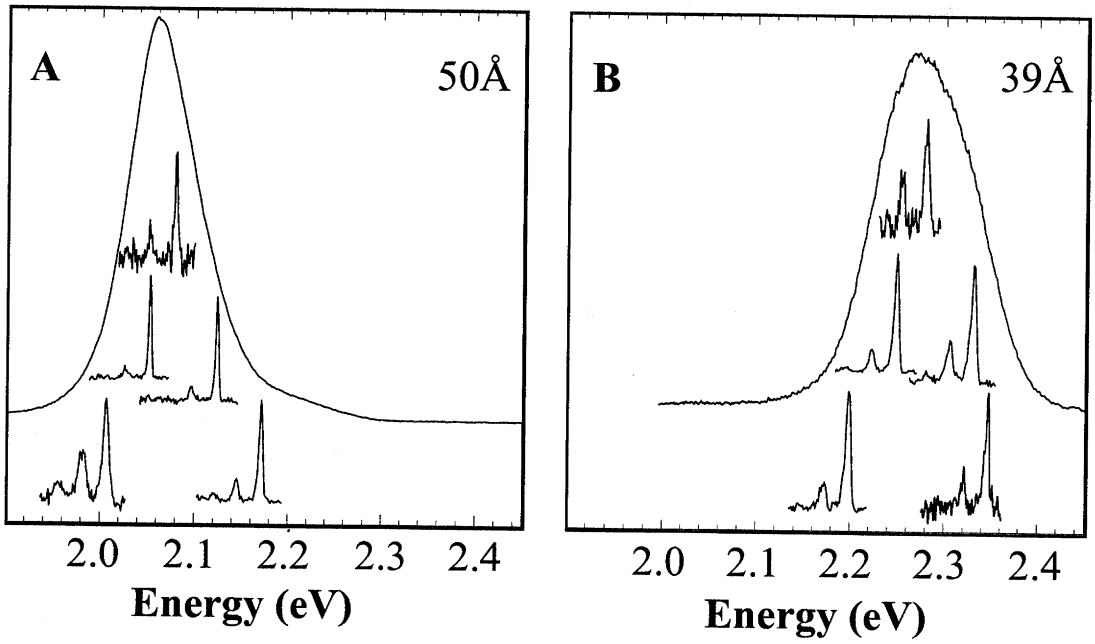

Figure 6.3: Ensemble vs single nanocrystallite spectra. Ensemble spectra of two different size nanocrystallite samples, with a representative set of single nanocrystallite spectra obtained from each sample. All single nanocrystallite spectra were taken with a 60 sec integration time and an excitation intensity of 200W/cm^2.

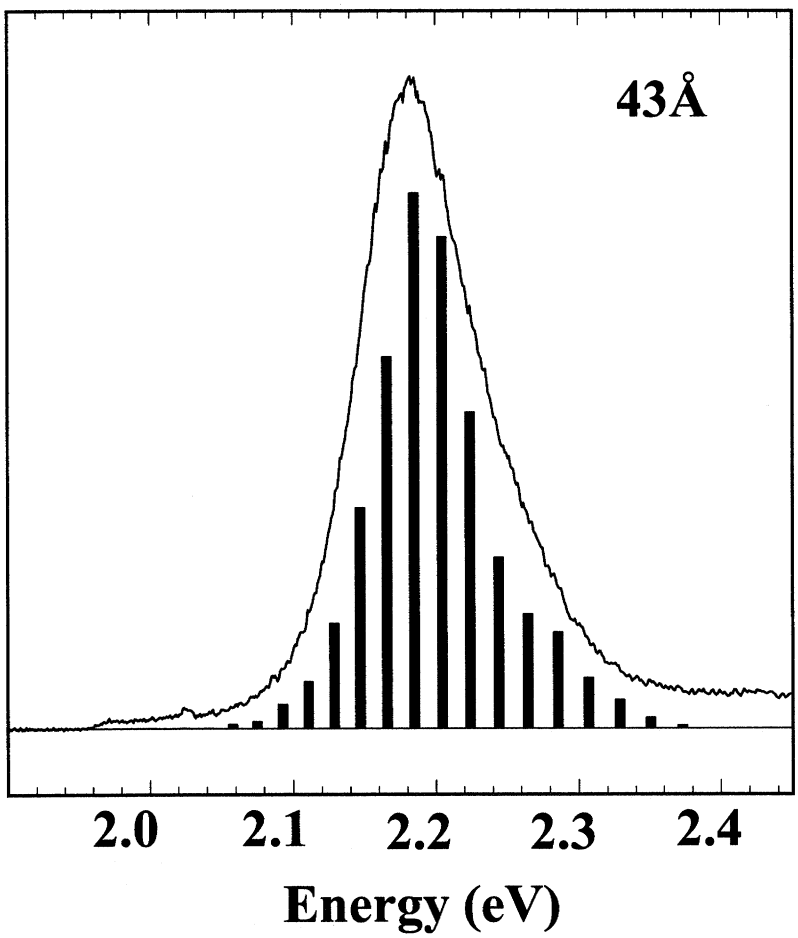

Figure 6.4: Ensemble vs single nanocrystallite spectra. Ensemble spectrum with histogram of energies of 513 single nanocrystallite spectra obtained from that sample. The histogram includes the scaled contribution of zero, one and two phonon lines from each nanocrystallite.

Comparisons such as figure 6.4 are essential to the study of single chromophores and are made possible by the highly parallel detection scheme used in these experiments. By comparing what is observed on the single nanocrystallite level with ensemble results, we can draw several important conclusions. First, by showing that the distribution of single nanocrystallite spectra matches what is expected from ensemble measurements, we confirm that the spectra collected in these experiments actually originate from single nanocrystallites

and not some other impurity molecule*. Second, by comparing single nanocrystallite results to ensemble results, we confirm that the nanocrystallites being observed are representative of those in the ensemble distribution. (i.e. the single nanocrystallites measured in these experiments are not an anomalous subset of the nanocrystallite population). Third, these types of comparisons can uncover whether experimental conditions, such as the high excitation intensities used to detect single nanocrystallites (10-1000W/cm^2), somehow change the fundamental nature of the nanocrystallites being studied. Finally, by building ensemble characteristics from single nanocrystallite data, it is often possible to gain a better understanding of how different effects contribute to ensemble measured results.

Throughout this thesis, several comparisons between ensemble and single nanocrystallite data will be made. In general, the conclusions drawn from these comparisons are the same as that for figure 6.4: The data obtained from single CdSe nanocrystallites is representative of that collected in ensemble experiments. This suggests that the results of these experiments are useful in understanding the physics of nanocrystallites and interpreting the results of ensemble studies.

6.3.2 Additional Evidence for Single Nanocrystallite Detection

Figures 6.2-6.4 provide additional evidence that the data collected in these experiments results from single CdSe nanocrystallites. First, single nanocrystallite spectra are very narrow* and are easily separated, even when they are spatially overlapped within an image. As an example, figure 6.5 shows the spectrum arising from two nanocrystallites that

* Qualitative comparisons such as figure 6.2 provide similar confirmation.
* As will be shown in chapter 7, under certain conditions, single nanocrystallite linewidths can be significantly narrower than what is observed in figures 6.2 and 6.3.

reside within the same resolution limited area of the sample. The spectrum consists of 2 distinct phonon progressions that are easily separated and identified as single nanocrystallite spectra. Second, all single nanocrystallite spectra have qualitatively similar spectral characteristics, with the exception of absolute emission energy (see figure 6.3). This also suggests that we are detecting single nanocrystallites, since spectra originating from multiple sources would have highly variable lineshapes, dependent on the distribution of single nanocrystallites within each.

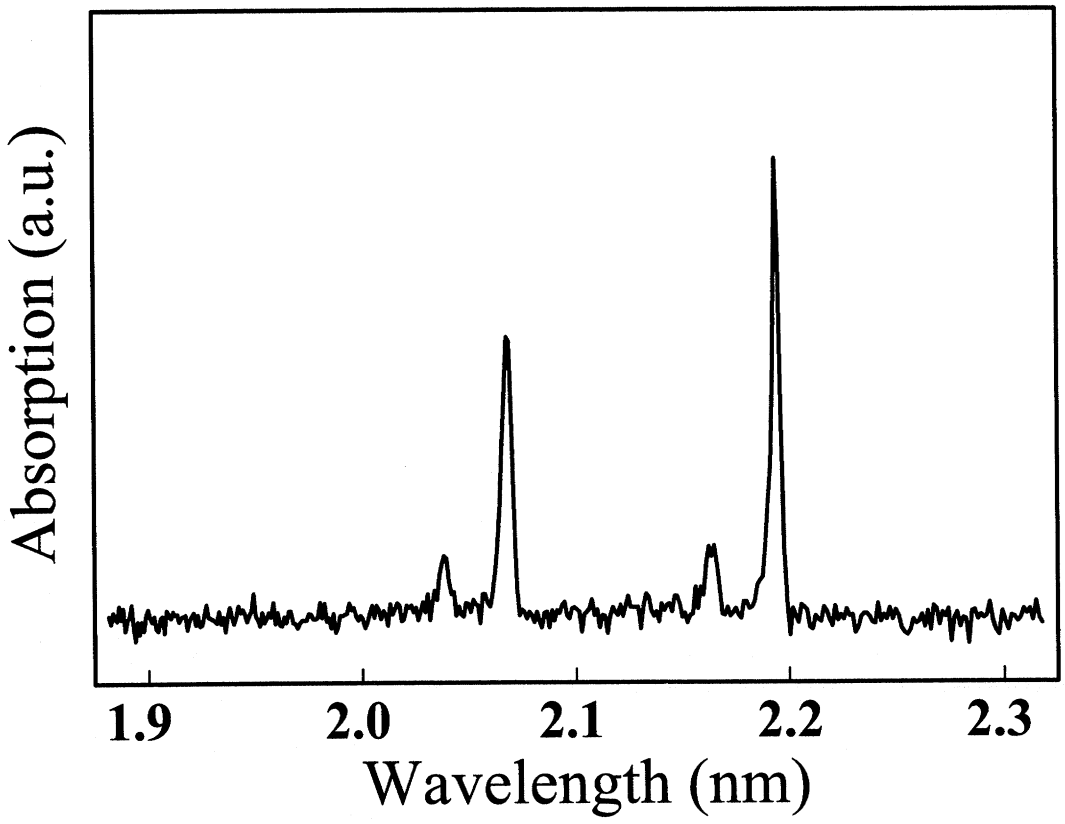

Figure 6.5: Emission spectrum of two single nanocrystallites located within the same resolution limited region of the sample.

6.3.3 Phonon Coupling

Within a given sample a wide range of phonon couplings is observed between single nanocrystallite spectra (see figure 6.3). For instance, in a 43Å overcoated sample, phonon coupling constants, which are measured as the ratio of the integrated intensities of the zero LO phonon line to the one LO phonon line, ranged from 0.06 to 1.3 with an average of value of 0.488. This number is consistent with the average value measured by fluorescence line narrowing over a range of nanocrystallite sizes[1].

The variation in phonon coupling observed is quite surprising given the structural uniformity measured in these nanocrystallite samples. Phonon coupling is a very sensitive measure of the overlap between the electron and hole wavefunctions within the nanocrystallite core (figure 6.6). A separation between the electron and hole results in a temporary electric field within the nanocrystallite. This field tends to distort the ionic crystal lattice by pulling the positively charged Cd^{2+} ions toward the electron and the negatively charged Se^{2-} ions toward the hole (figure 6.6b). When the exciton recombines, the temporary field is removed and the distorted crystal lattice relaxes to its equilibrium state, producing vibrations (figure 6.6c). The result is enhanced coupling of the emitted photon to optical phonons. This interaction is called Fröhlich coupling[2-6], and the degree of coupling is related to the amount of separation between the electron and hole wavefunctions.

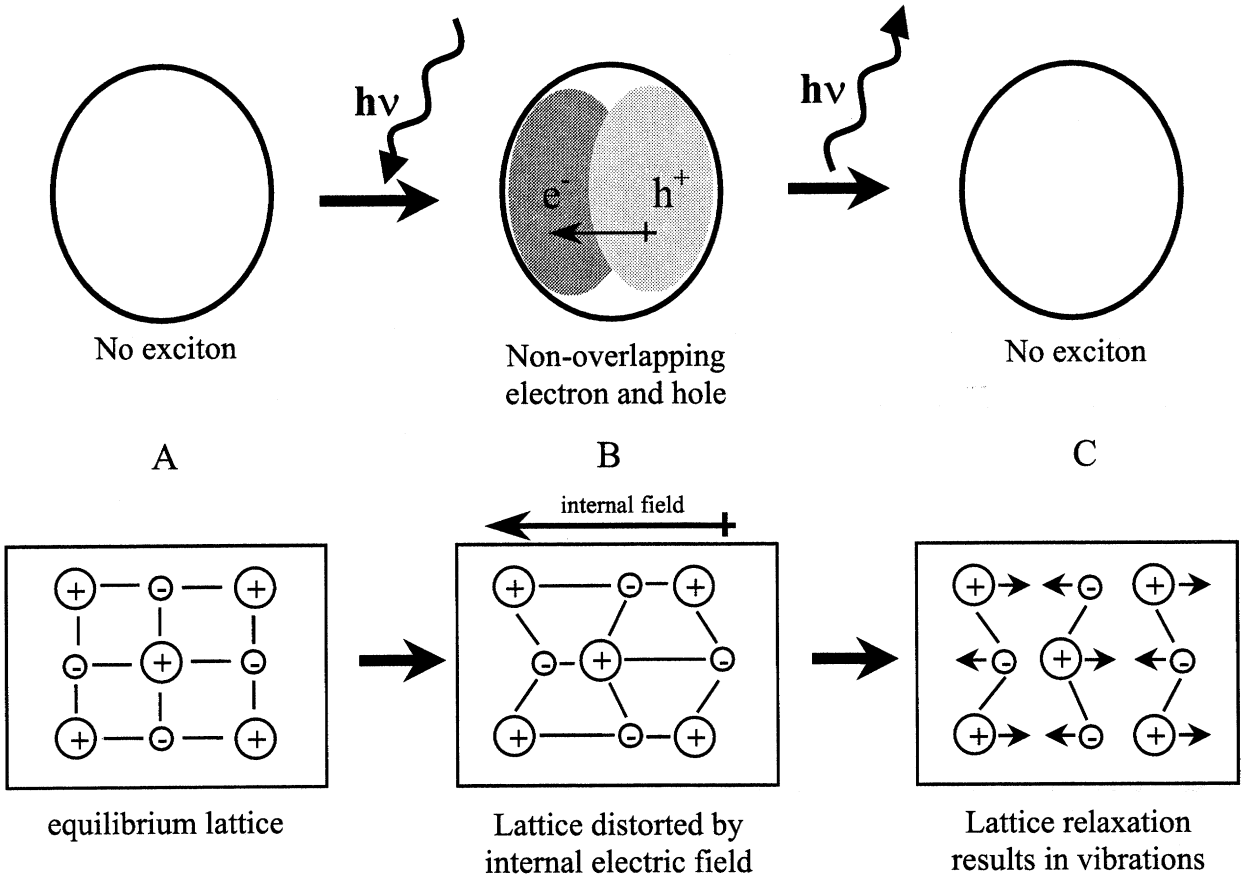

Figure 6.6: Frolich coupling to optical phonons. (A) In the absence of an exciton, the CdSe crystal lattice sits at an equilibrium position. (B) An exciton with a separation between the electron and hole wavefunction creates a temporary internal electric field which distorts the ionic crystal lattice. (C) When the exciton recombines, the internal field vanishes and the atoms relax to their equilibrium positions, creating lattice vibrations.

The presence of an electric field can strongly affect the overlap of the electron and hole wavefunctions in CdSe nanocrystallites, affecting the measured phonon coupling[6,7]. While this effect will not be discussed in detail until chapter 8, the differences in phonon coupling described above may indicate differences in the local electric field around each nanocrystallite.

6.3.4 Polarization Spectroscopy

Polarization spectroscopy reveals that the polarization dependence of both the zero and one LO phonon transitions are the same. Figure 6.7 plots the polarization dependence of each peak for a single nanocrystallite. Identical degrees of polarization and phase indicate that there is no difference in the polarization selection rules for these 2 transitions. This suggests two possible mechanisms for relaxation of the lowest excited state: 1) The formally spin forbidden lowest excited state is mixed with a higher lying

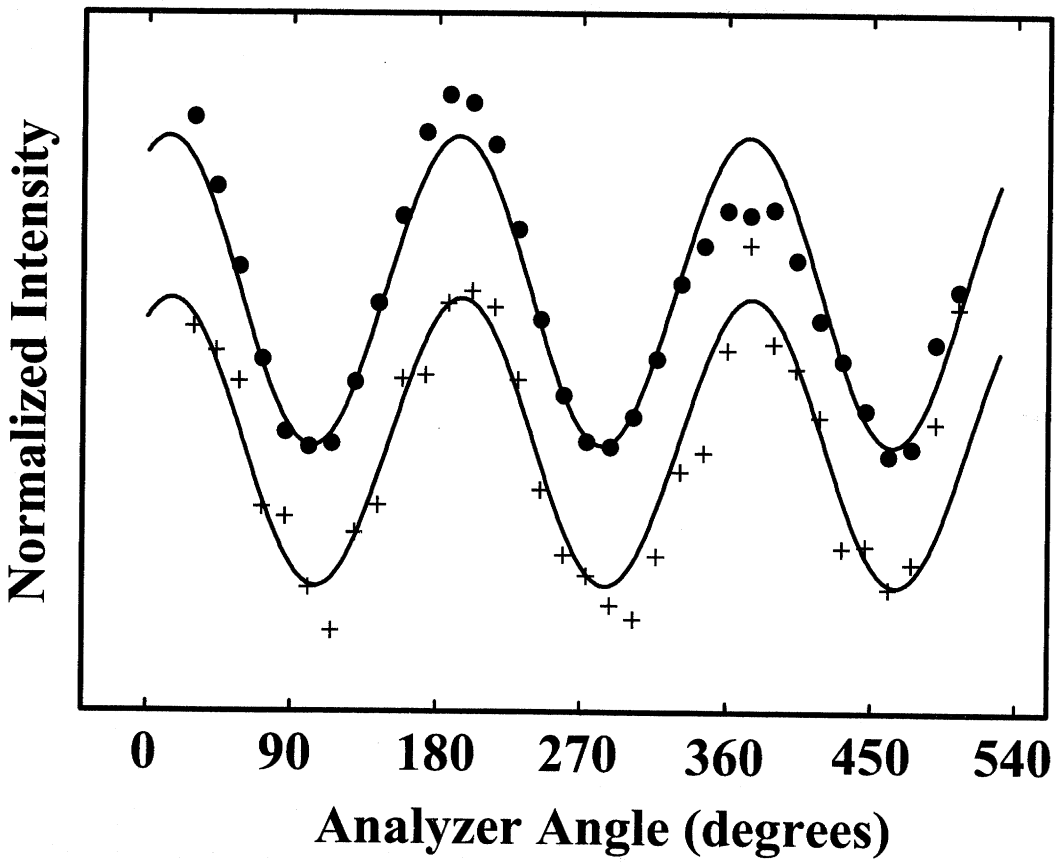

Figure 6.7: Polarization spectroscopy of a single nanocrystallite spectrum. Emission intensity of the zero phonon line (circles) and one phonon line (crosses) of a single 52Å overcoated nanocrystallite as a function of analyzer angle with fits. The data has been normalized and offset for clarity, so that a direct comparison between the phase and degree of polarization can be made. The data in figure 6.7 was taken with an integration time of 30 seconds, excitation intensity of 60W/cm^2 and excitation polarization at 0 degrees.

optically active state that has a "dark axis" transition dipole (either $|2,\pm1\rangle$ or $|1,\pm1\rangle$). In this case, the selection rules for both transitions would be defined by those of the optically active state. 2) Zero phonon emission from the lowest excited state proceeds through a virtual transition, in which non-resonant excitation into a higher lying optically active state occurs after absorption of a low energy acoustic phonon, followed by non-resonant emission from this state[8]. In this type of transition, only the total energy is conserved, similar to Raman scattering. The selection rules for the ZPL in this case would be those of the optically active virtual state (either $|2,\pm1\rangle$ or $|1,\pm1\rangle$) while the selection rules for the 1PL would be defined by the lowest excited state. The nature of the $|2,\pm2\rangle$ state wavefunction (equation 5.4) suggest that LO phonon assisted emission directly from this state may also have a "dark axis" transition dipole, consistent with this mechanism.

6.3.5 Excited State Emission/Phonon Bottleneck

Another feature which is common to all single nanocrystallite spectra is the *lack* of emission from higher excited states, such as bi-exciton emission or hot-band emission. This is true even under high excitation intensities (greater than 3000W/cm^2). The absence of bi-exciton emission is no surprise since non-radiative Auger recombination should quench emission from this state[9,10] (see chapter 4 for details). The lack of hot-band emission is more surprising. In these experiments, excitation occurs into a highly excited state, followed by non-radiative relaxation to the emitting state. Hot-band emission is emission that occurs before the exciton reaches the lowest excited state. Theoretical calculations predict that the reduced density of phonon states in quantum

confined structures should greatly decrease the rate of non-radiative relaxation[11,12]. This phenomenon, referred to as the "phonon bottleneck", should enhance hot-band emission in nanocrystallites due to the relatively short radiative lifetimes of many higher excited states. While potentially hidden in ensemble spectra, the elimination of inhomogeneous broadening in single nanocrystallite spectra should easily uncover evidence of hot-band emission. Our results, however, do not support the presence of a phonon bottleneck in CdSe nanocrystallites. This is consistent with alternative theoretical predictions suggesting that rapid Auger scattering of the excited carriers is responsible for relaxation through the ladder of states, supplementing phonon mediated relaxation[13-16].

6.4 Conclusion

In this chapter, we have shown that it is possible to collect spectra from single CdSe nanocrystallites. Single nanocrystallite spectroscopy has confirmed that the images collected in chapters 4 and 5 do, in fact, result from single nanocrystallites. It has also confirmed that the physical nature of the nanocrystallites detected in these experiments is representative of the ensemble distribution. Several new physical characteristics were observed in single nanocrystallite spectra that can not be seen in ensemble experiments. A range of phonon couplings was measured between individual spectra, potentially corresponding to differences in the local environment around individual nanocrystallite. Polarization dependence of the zero and one LO phonon transitions indicates that both transition involve a "dark axis" transition dipole, providing insight into the nature of the emission pathway from the lowest excited state. Finally, the absence of emission from

higher excited states, indicates the lack of a phonon bottleneck in CdSe nanocrystallites, consistent with proposed Auger mechanisms for relaxation of the exciton to the lowest excited state.

6.5 References

[1] D.J. Norris and M.G. Bawendi, Phys. Rev. B **53**, 16347 (1996).
[2] J.J. Shiang, A.N. Goldstein, and A.P. Alivisatos, J. Chem. Phys **92**, 3232 (1990).
[3] J.J. Shiang, S.H. Bisbud, and A.P. Alivisatos, J. Chem. Phys. **98**, 8432 (1993).
[4] A.P. Alivisatos et al., J. Chem. Phys. **90**, 3463 (1989).
[5] M.C. Klein, F. Hache, D. Richard, and C. Flytzanis, Phys. Rev. B **42**, 11123 (1990).
[6] S. Nomura and T. Kobayashi, Phys. Rev. B **45**, 1305 (1992).
[7] Efros, Al. L., *Phonons in Semiconductor Nanostructures*, (Kluwer Academic Publishers, Boston, 1993), p 299.
[8] Efros, Al.L., Phys. Rev. B **46**(12), 7448-7458 (1992).
[9] D.I. Chepic et al, J. Lumin. **47**, 113 (1990).
[10] M. Nirmal et al, Nature **383**, 802 (1996).
[11] U. Bockelmann and G. Bastard, Phys. Rev. B **42**(14), 8947 (1990).
[12] H. Benisty, C.M. Sotomayor-Torres, and C. Weisbuch, Phys. Rev. B **44**(19), 10945 (1991).
[13] U. Bockelmann and T. Egeler, Phys. Rev. B **46**(23), 15574 (1992).
[14] Al. L. Efros, V.A. Kharchenko, and M. Rosen, Solid State Commun. **93**(4), 281 (1995).
[15] V.I. Klimov and D.W. McBranch, Phys. Rev. B. **55**, 13173 (1997).
[16] U. Woggon, H. Giessen, F. Gindele, O. Wind, B. Fleugel, and N. Peyghambarian, Phys. Rev. B **54**, 17681 (1996).

Chapter 7: Spectral Diffusion

7.1 Introduction

One area of particular interest that can, in principle, be addressed on the single nanocrystallite level, is the nature of the homogeneous lineshape of CdSe nanocrystallites. While theory predicts that nanocrystallites should have atomic-like spectral transitions due to long excited state lifetimes and weak coupling to acoustic phonons [1], previous ensemble experiments have suggested that linewidths in both excitation[2-4] and emission[5-7] are quite broad. For example, "homogeneous" linewidths extracted from fluorescence line narrowing experiments in CdSe nanocrystallites are reported to be ~5meV[8].

Initially, it was expected that single nanocrystallite spectroscopy would uncover the true "homogeneous" line shape of these samples. However, while the linewidths presented in chapter 6 are significantly narrower than what is measured in ensemble experiments, many single nanocrystallites reveal linewidths that are much broader than predicted, with non-Lorentzian lineshapes that are strongly dependent on the particular nanocrystallite (figure 7.1). In fact, published results from our lab[9-11], as well as others[12-15], have revealed a range of single nanocrystallite linewidths over 2 orders of magnitude. It has therefore been difficult to use single nanocrystallite lineshapes to learn about the intrinsic physics of this system.

In this chapter, we carefully examine single nanocrystallite spectra and uncover a new spectral phenomenon: Spectral diffusion. This discovery can help explain the variations in linewidth observed in these experiments, and demonstrates that the these nanocrystallites are far more dynamic than was originally expected based on ensemble experiments.

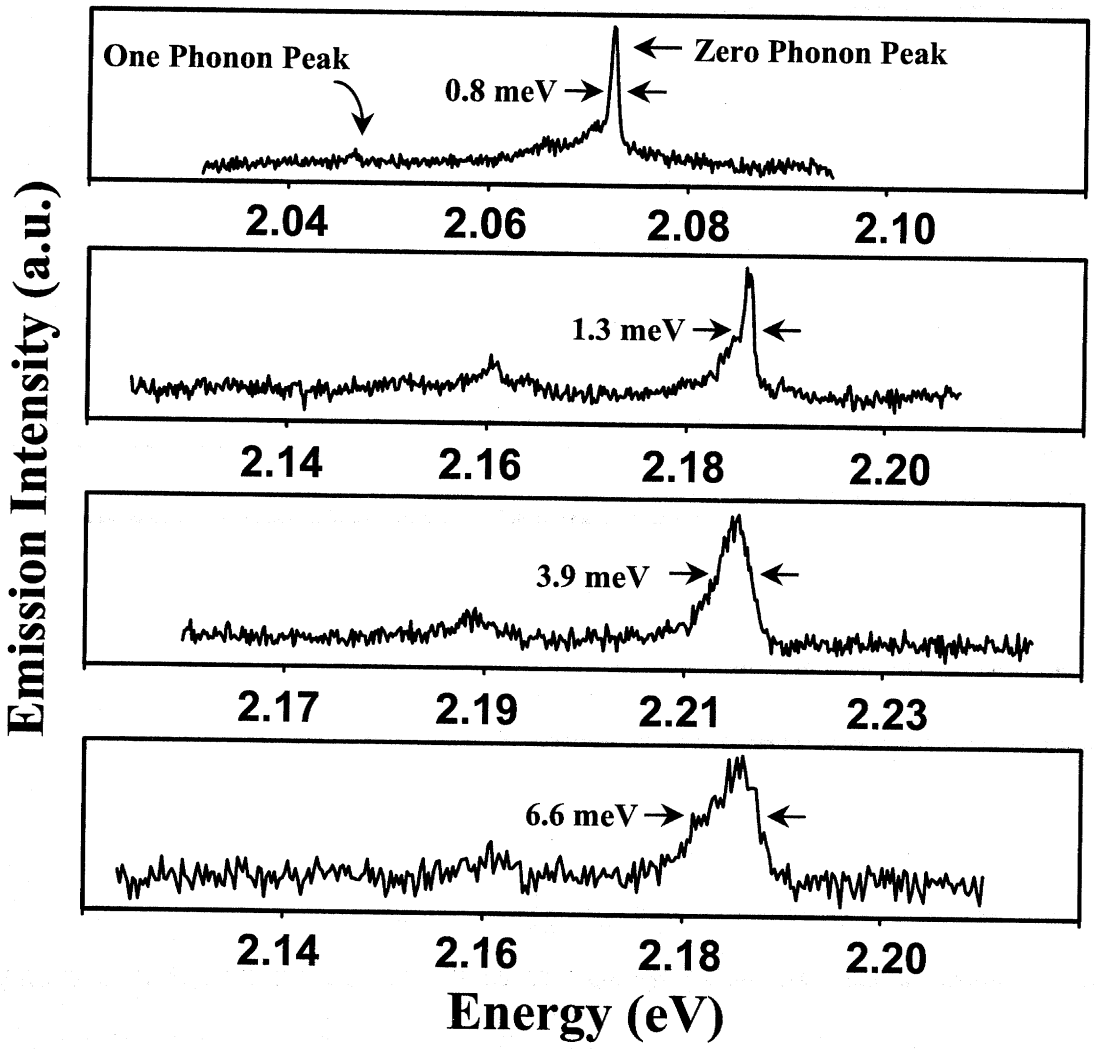

Figure 7.1: Emission spectra from 4 different single nanocrystallites revealing a range of emission line shapes and widths. Note that while the x-axis is different for each of the spectra, the relative scales remain the same.

7.2 Experimental

Single nanocrystallite spectra were acquired as described in chapter 6. The high speed data described in section 7.3.2 was taken with the Pentamax intensified CCD camera. The readout time between frames for this data was negligible, allowing the acquisition of ~10 spectra/second with an integration time of 0.1 seconds. All other spectra were taken using the standard liquid nitrogen cooled CCD.

7.3 Results and Discussion

A representative selection of single nanocrystallite spectra are displayed in figure 7.1, revealing a range of linewidths that is typical for a given sample. These differences are quite surprising since the physical structure of the nanocrystallites is so uniform throughout the ensemble (recall figure 1.4). What is even more surprising is that the lineshape *within* a single nanocrystallite appears to be strongly dependent on the experimental conditions. Figure 7.2 shows 3 spectra from the same nanocrystallite taken with three different excitation intensities. This broadening as a function of excitation intensity exists even though excitation occurs far from the emitting state so that traditional power or saturation broadening should be insignificant[16]. There is also a strong lineshape dependence on integration time (figure 7.3). These results were unexpected based on previous ensemble measurements in which these effects were completely hidden by ensemble averaging.

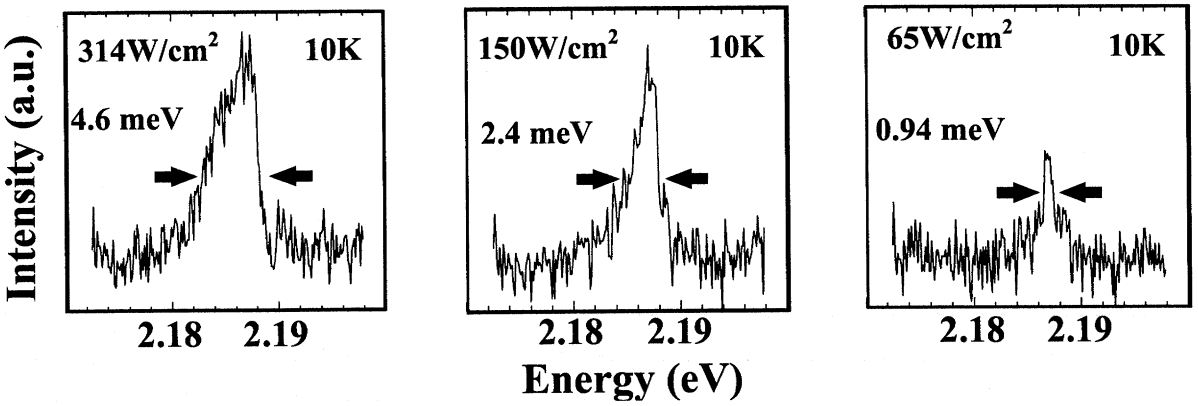

Figure 7.2: Three spectra from the same single 45Å non-overcoated nanocrystallite, taken with different excitation intensities and an integration time of 1 minute.

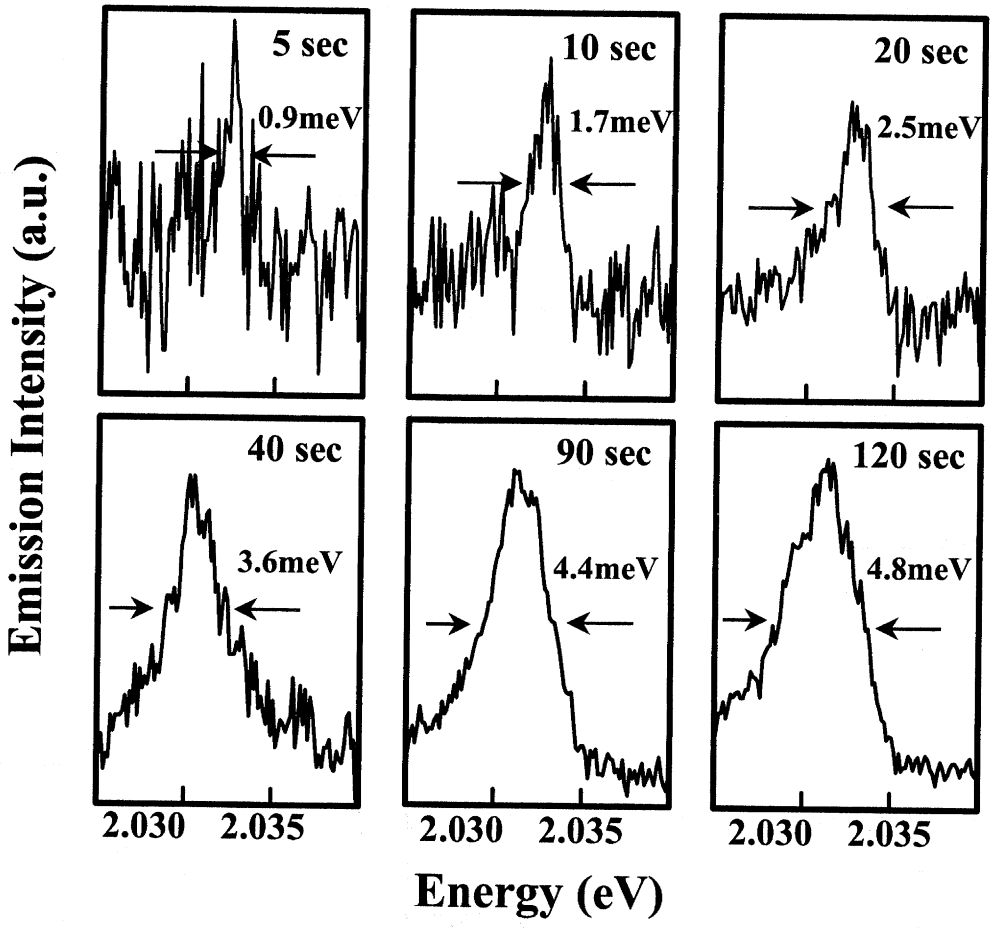

Figure 7.3: Six spectra from the same single 56.5Å non-overcoated nanocrystallite, taken with different integration times and an excitation intensity of 85W/cm^2.

7.3.1 Spectral Diffusion in Single Molecules

Results similar to those in figure 7.3 have also been reported in single molecule spectroscopy and low temperature spectral hole-burning, where linewidths are found to be dependent on acquisition time[17-22]. In these cases, lineshapes are thought to arise from rapid shifting of the emission energy on a timescale that is fast relative to the acquisition time of the experiment. This shifting is referred to as spectral diffusion. Spectral diffusion in single molecules result from changes in the local environment which perturb the single molecule energy states[19-22].

7.3.2 Spectral Diffusion in Single Nanocrystallites – Small Shifts

Figure 7.4 demonstrates that single nanocrystallite lineshapes are also dominated by spectral diffusion. A typical single nanocrystallite spectrum from a 52Å overcoated sample, taken with a 10s integration time, can be seen in figure 7.4a (typical integration times used in our lab to acquire single nanocrystallite spectra are ~ 30 to 60 seconds; other labs have reported integration times as long as 10 minutes[14]). The observed peak, which corresponds to the zero phonon transition, has a FWHM of ~2meV and appears to have some additional structure which is blue shifted by ~3meV from the main peak. While it may be tempting to interpret the lineshape of this spectrum in terms of intrinsic nanocrystallite physics, figure 7.4b indicates that this would not be appropriate. Spectra of the same nanocrystallite taken with 100 times shorter integration time (0.1s) reveal a single peak with no side-band, which is much narrower than the spectrum in figure 7.4a. In 150 of these fast spectra taken in rapid succession, this resolution limited peak can be seen shifting in energy over the entire 10s spectrum (figure 7.4b). Shifting below our resolution limit may also be occurring and multi-peak spectra such as frame 6 of figure 7.4b indicate spectral shifting on a sub 0.1s timescale. Peaks in figure 1b (frames 1-5) represent ~20 collected photons, indicating that changes in emission energy are not statistical fluctuations in single photon energies.

Figure 7.4c shows a histogram of peak positions for the 150 spectra described above. As can be seen, the 10s intensity distribution is well reproduced, including the relative emission intensity. In this way, we can directly relate the effects of spectral diffusion to the observed lineshape of a single nanocrystallite. Even the apparent side-band in figure 7.4a is found to be an artifact of spectral diffusion. A wide variety of different single nanocrystallite spectra including multiplet lineshapes as well as peaks as broad as 10meV

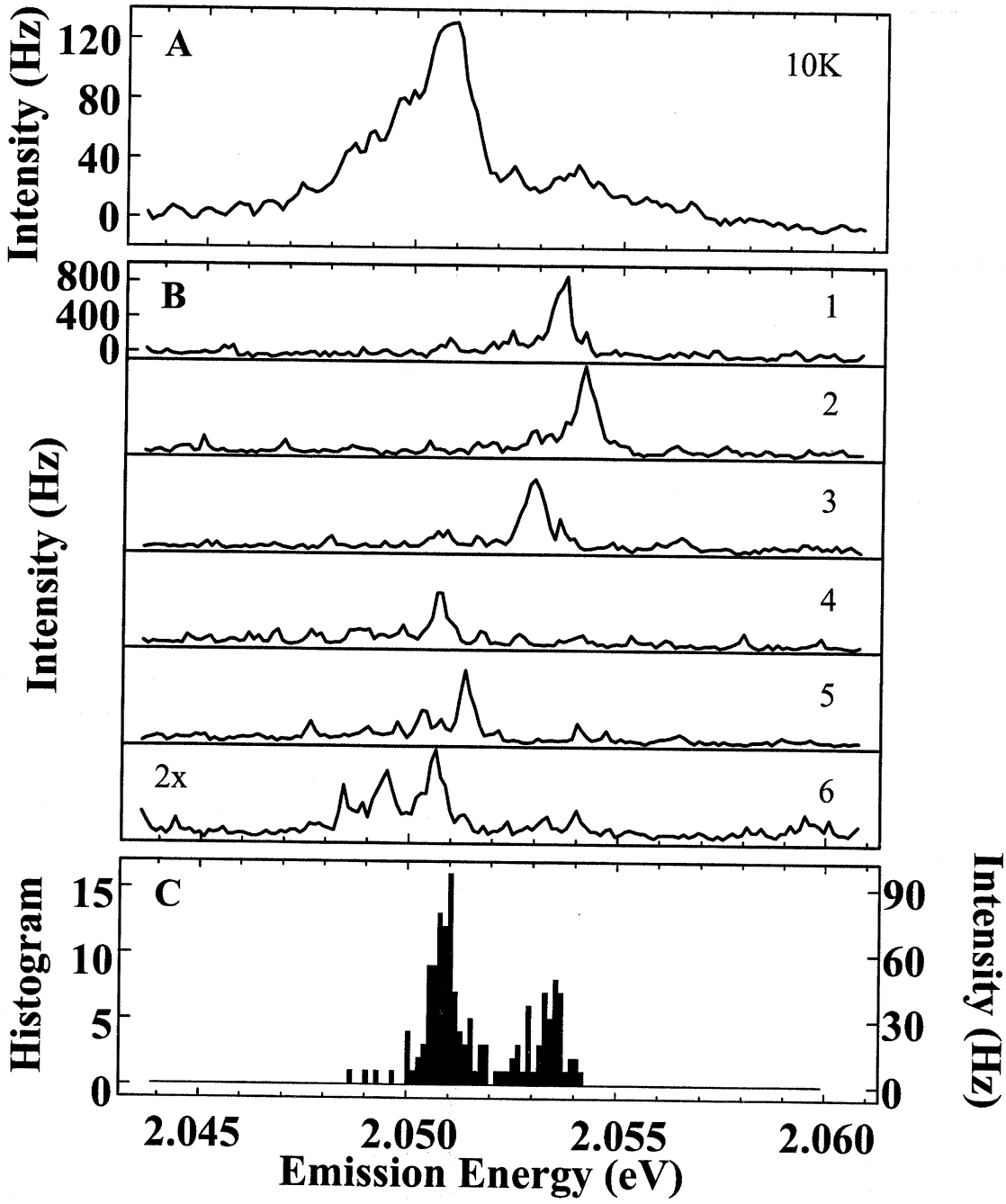

Figure 7.4: Contribution of spectral diffusion to single nanocrystallite lineshapes. (A) Spectrum of a single 56.5Å overcoated nanocrystallite with a 10 second integration time at 10K. (B) A representative sample of 6 spectra from the same nanocrystallite as in (A), with a 0.1 second integration time. Of the 150 spectra taken in rapid succession, frames 1-6 indicate spectrum number 1, 16, 35, 59, 84 and 150 respectively. (C) Histogram of peak positions from each of the 150 spectra described in (B) including the equivalent emission intensity assuming ~90 counts were collected in each 100ms bin. Excitation intensity for all spectra in figure 7.4 was 200W/cm^2.

have been analyzed in this same manner. This data suggests that on the time scale of several seconds, the primary contribution to single nanocrystallite lineshapes is spectral diffusion.

In molecular systems, spectral diffusion results from changes in the local environment that interact with single molecules through short range strain fields[19-22]. The observation of a similar effect in single nanocrystallites is actually quite surprising. While single molecules are exquisitely sensitive to changes in their surrounding environment[23-28], the electronic structure of the delocalized exciton in CdSe nanocrystallites does not appear to be sensitive to the chemical nature of the nanocrystallite surface[29]. As such, the energy of a single nanocrystallite spectrum should be relatively unaffected by small changes in the surrounding environment. This implies that the perturbing force required to produce the observed spectral shifts must be quite large.

There are two main implications of the data in figure 7.4. First, it is clear that the lineshape of a single nanocrystallite contains information about changes in the nanocrystallite or the surrounding environment and not the intrinsic physics of the nanocrystallite. Second, changes in the lineshape of a single nanocrystallite spectrum resulting from different experimental conditions are likely to be the result of changes in spectral diffusion(figure 7.2 and 7.3) . This is clearly true for broadening as a function of integration time. This is also the case for broadening as a function of excitation intensity, and in some instances this effect can be observed directly. Figure 7.5a shows five consecutive spectra of the zero LO phonon line of a single 43Å overcoated nanocrystallite taken with an excitation intensity of 65W/cm^2. A narrow peak can be seen abruptly shifting in energy over a range of ~2meV, usually appearing at several discrete positions

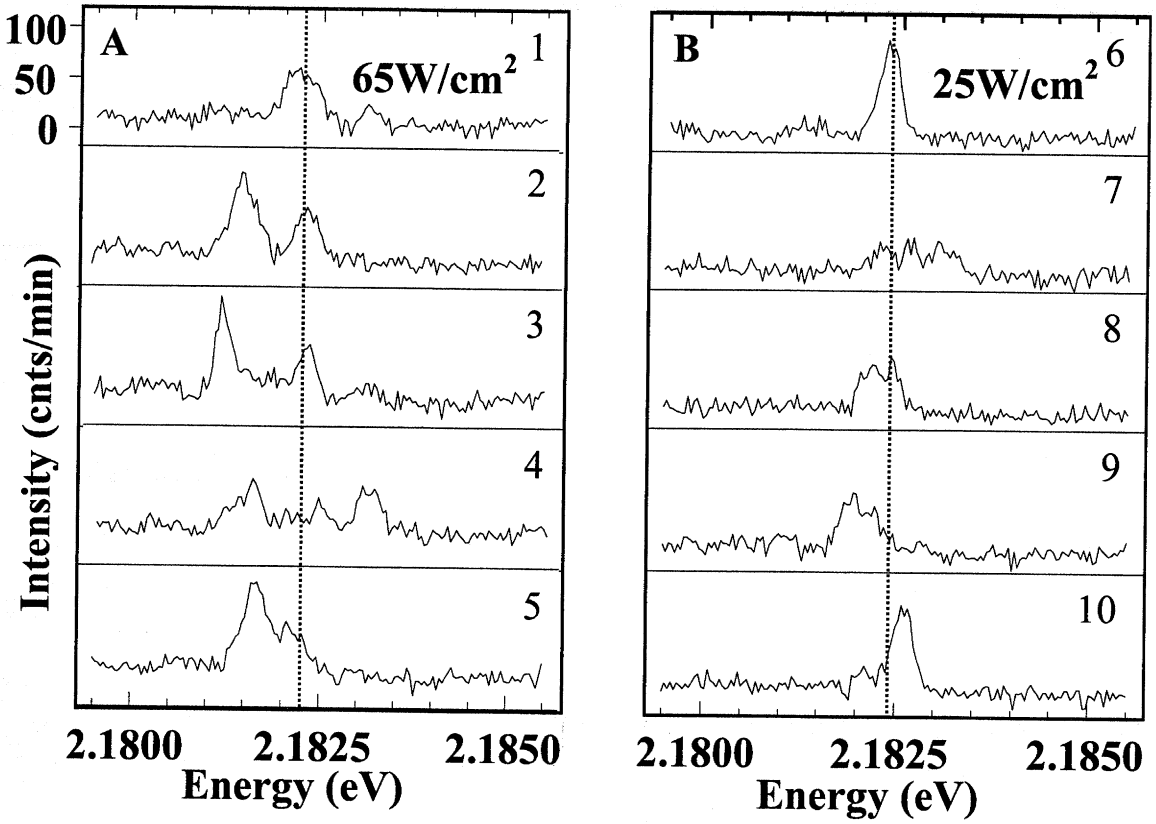

Figure 7.5: The effect of excitation intensity on small spectral shifts. (A) Five consecutive 60 second spectra of a single 43Å overcoated nanocrystallite at 65W/cm^2 excitation intensity. (B) The next five consecutive spectra of the same nanocrystallite at 25W/cm^2, showing a decrease in the number and magnitude of the small spectral shifts observed.

within a single spectrum. When the excitation intensity is reduced to 25W/cm^2, the frequency and range of the spectral shifting decreases (figure 7.5b).

By decreasing the excitation intensity, it is possible to reduce spectral diffusion in some nanocrystallites to the point where shifts that are observable above our resolution limit occur on a timescale of many seconds to minutes. At these intensities, resolution limited linewidths as narrow as 120μeV have been observed (figure 7.6). These peaks are ~600 times narrower than the full ensemble spectrum and 50 times narrower than linewidths extracted from fluorescence line narrowing experiments. Such narrow

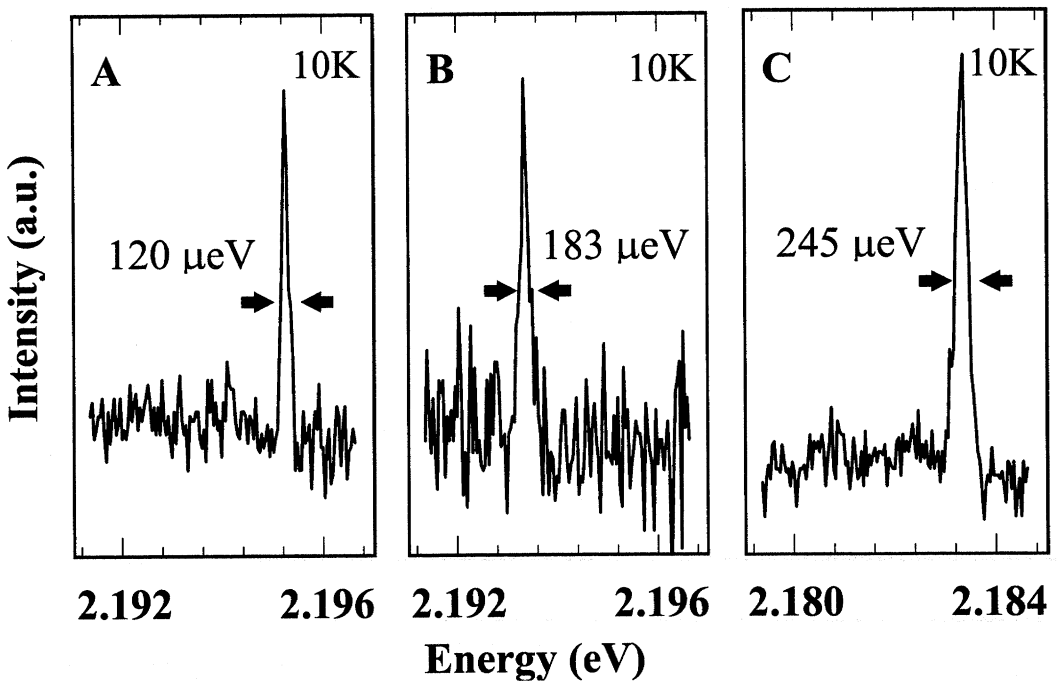

Figure 7.6: Single nanocrystallite spectra. (A)-(C) High resolution spectra of ultra-narrow zero phonon lines from 3 different single 43Å overcoated nanocrystallites. Spectra were taken with a 60 second integration time and an excitation intensity of 25W/cm^2.

linewidths suggest very weak coupling to low energy acoustic phonons. This finding is consistent with theoretical predictions and reinforces the description of these nanocrystallites as "artificial atoms".

7.3.3 Spectral Diffusion in Single Nanocrystallites – Large Shifts

While the small spectral shifts described above occur on a very fast time scale, a second type of spectral shifting is also observed. These shifts result in much larger changes in the emission energy and occur on a time scale from seconds to many minutes, even under high excitation intensities. Figure 7.7 shows 16 consecutive low resolution spectra of a single nanocrystallite which reversibly shifts in energy more than 80meV over time. As the spectrum shifts to lower energy, there is a corresponding decrease in emission

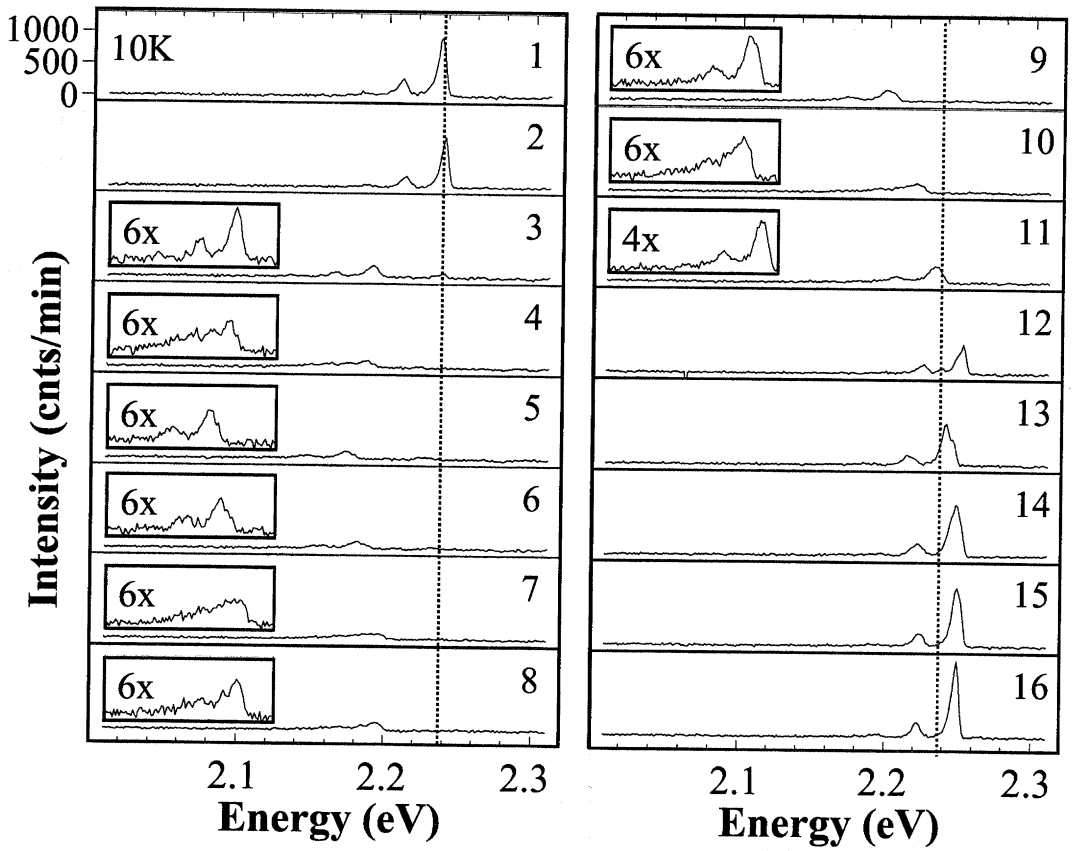

Figure 7.7: Large spectral diffusion shifts. Sixteen consecutive 60 second spectra of the same single 39Å nanocrystallite with an excitation intensity of 2.5kW/cm^2. Insets show magnification of the y-axis by the indicated amounts.

intensity and an increase in phonon coupling. These changes, however, are reversible when the spectrum shifts back to higher energies. The magnitude of the large spectral diffusion shifts seen in single nanocrystallites is enormous relative to those observed in molecular systems (the largest reported molecular shifts are <1meV). Once again this implies an extremely large perturbation of the single nanocrystallite electronic structure.

The large decrease in emission intensity seen in figure 7.7 is likely to result, in part, from the absorbing state shifting out of resonance with the exciting laser. The ensemble absorption spectrum for 39Å nanocrystallites is shown in figure 7.8. The bold arrow indicates excitation at 514nm. The thin arrow indicates the relative excitation energy if the

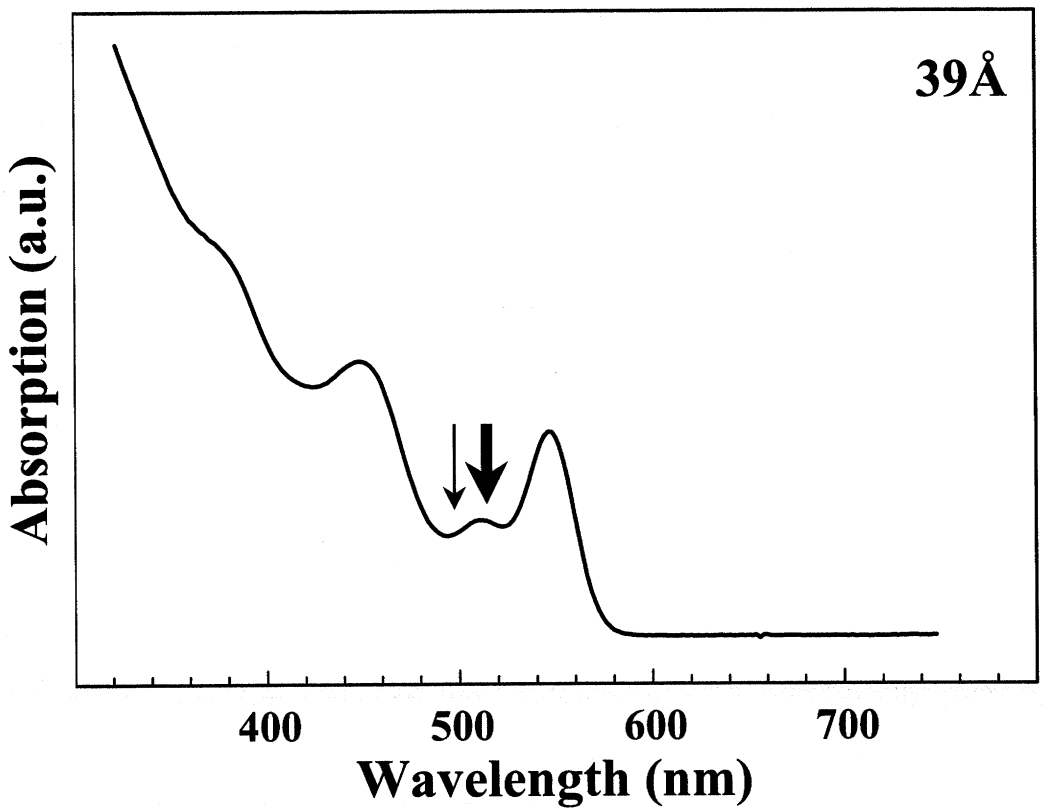

Figure 7.8: Ensemble absorption spectrum of a 39Å non-overcoated sample. Bold arrow indicates excitation at 514nm. The thin arrow indicates excitation ~80meV to the blue, approximating the change in absorption upon an 80meV red shift of the spectrum.

spectrum is shifted by 80meV. Even in ensemble samples, a shift of the magnitude observed in figure 7.7 would be sufficient to move the absorption spectrum out of resonance with the excitation laser. Preliminary studies of the excited state spectrum of single CdSe nanocrystallites have indicated that the line width of this state is somewhat narrower than what is measured on the ensemble level (~25meV FWHM). As such, it is not surprising that the emission intensity decreases dramatically upon shifts of this magnitude. This conclusion, however, assumes that the absorbing states shift comparably

in magnitude to the emitting state. While it is logical to assume that the absorbing states shift, there is currently no direct evidence of spectral diffusion in the absorbing states.

The most interesting feature of figure 7.7 is the increase in LO phonon coupling as the spectrum shifts to lower energy. As discussed in section 6.3.3, phonon coupling is a sensitive measure of the overlap between the electron and hole wavefunction. Changes in phonon coupling such as those observe in figure 7.7 can indicate the presence of a changing local electric field, which polarizes the exciton state, separating the charges. In fact, the spectral characteristics of figure 7.7 are similar to what is observed in low temperature ensemble Stark experiments[30]: In the presence of an applied electric field, ensemble emission spectra shift to lower energies with a corresponding increase in phonon coupling and a decrease in emission intensity. Both phonon coupling and the Stark shift are found to have a quadratic dependence on electric field, yielding a linear relation

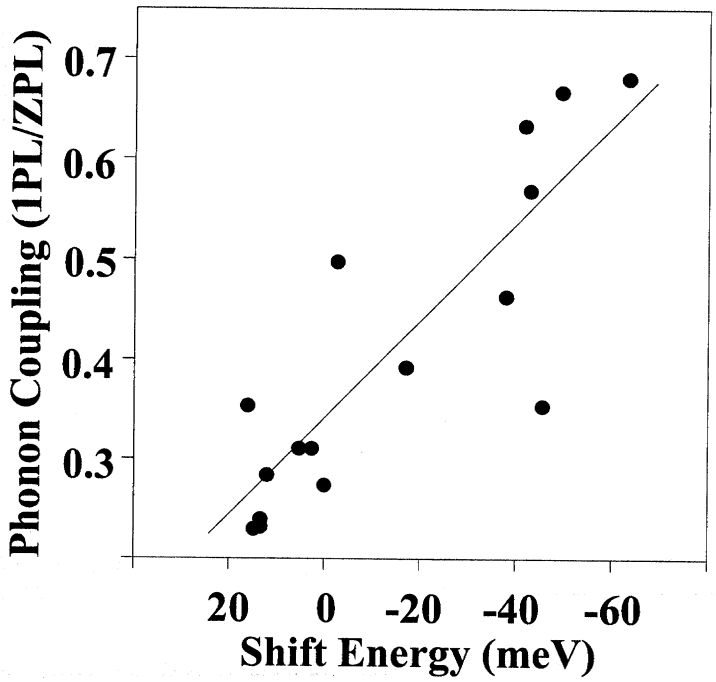

Figure 7.9: Changes in phonon coupling associated with spectral diffusion shifts. Phonon coupling vs the magnitude of the spectral diffusion shift for the single nanocrystallite in figure 7.7.

between these two parameters. Consistent with this, figure 7.9 reveals that the measured phonon coupling for spectra such as those in figure 7.7 change linearly with the magnitude of the spectral diffusions shift. The decrease in emission intensity observed in ensemble Stark measurements also results from a separation of the electron and hole wavefunctions, which increases the emitting state lifetime, decreasing the measured quantum yield. A similar effect may also contribute to the decrease in emission intensity accompanying large spectral diffusion shifts.

7.3.4 Additional Evidence for Single Nanocrystallite Detection

Spectral diffusion provides additional evidence of single nanocrystallite detection. Individual spectra collected simultaneously are seen to shift independently of each other, even when they fall within the same diffraction limited detection area. This is not surprising since local environmental fluctuations will tend to be relatively inhomogeneous, and nanocrystallites within a diffraction limited area can still be relatively far apart. As a result, spectra arising from multiple nanocrystallites with the same absolute emission energy, should split over time as the individual spectra shift independently. This in not observed, indicating that the spectra collected in these experiments arise from single nanocrystallites.

7.4 Conclusion

In this chapter, we discovered a new spectral phenomenon, referred to as spectral diffusion, revealing the dynamic nature of CdSe nanocrystallites. Once again, this effect can not be observed in ensemble measurements and was completely unexpected based on

previous results. Spectral diffusion is found to occur over a wide range of time and energy scales. While qualitatively similar to spectral diffusion in single molecules, the shifts observed in nanocrystallites are orders of magnitude larger than what is seen in molecular systems. Careful examination of single nanocrystallite spectra suggests that measured line shapes are primarily the result of spectral diffusion occurring on a timescale that is fast relative to the acquisition time of a typical spectrum. An excitation intensity dependence to the frequency of spectral diffusion shifts results in single nanocrystallite line shapes that are strongly dependent on experimental conditions such as excitation intensity and integration time.

From these results, it seems clear that under normal conditions, the shape of a single nanocrystallite spectrum contains information about the dynamics of the local environment and not the inherent physics of the nanocrystallite. As such, it seems inappropriate to attempt to define a "homogeneous" lineshape or width for these nanocrystallites on the timescale of fluorescence measurements. Instead, single nanocrystallite linewidths serve only as an upper bound for the true intrinsic width. At low excitation intensities, this upper bound is found to be ~120μeV and is currently limited by the spectral resolution of our experimental apparatus. Such extraordinarily narrow linewidths in a solid state system strongly reinforces the picture of these nanocrystallites as "artificial atoms".

In addition to small, relatively continuous spectral shifts, large discrete shifts are also observed and occur on a timescale of many seconds to minutes. The observed similarities between these large spectral diffusion shifts and ensemble Stark shifts suggest that changing local electric fields may play a role in spectral diffusion. In the next chapter,

we study Stark spectroscopy in single nanocrystallites in order to further investigate the role of local electric fields in spectral diffusion.

7.5 References

[1] D. Gammon, E.S. Snow, B.V. Shanabrook, D.S. Katzer, D. Park, Science **273**(5271), 87 (1996).

[2] U. Woggon, S. Gaponenko, W. Langbein, A. Uhrig, and C. Klingshirn, Phys. Rev. B **47**, 3684 (1993).

[3] D.M. Mittleman, R.W. Schoenlein, J.J. Shiang, V.L. Colvin, A.P. Alivisatos, and C.V. Shank, Phys. Rev. B **49**(20), 14435 (1994).

[4] D.J. Norris and M.G. Bawendi, J. Chem. Phys. **103**(13), 5260 (1995).

[5] A.P. Alivisatos, A.L. Harris, N.J. Levinos, M.L. Steigerwald, and L.E. Brus, J. Chem. Phys. **89**(7), 4001 (1988).

[6] V. Jungnickel, F. Henneberger, J. Lumin. **70**, 238 (1996).

[7] M. Nirmal, D.J. Norris, M. Kuno, and M.G. Bawendi, Phys. Rev. Lett. **75**, 3728 (1996).

[8] D.J. Norris and M.G. Bawendi, Phys. Rev. B **53**(24), 16338 (1996).

[9] S.A. Empedocles, D.J. Norris and M.G. Bawendi, Phy. Rev. Lett. **77**(18), 3873 (1996).

[10] S. Empedocles and M. Bawendi, Science **278**, 2114 (1997).

[11] S. Empedocles and M.G. Bawendi, J Phys. Chem. **103**, 1826 (1999).

[12] S.A. Blanton, M.A. Hines and P. Guyot-Sionnest, Appl. Phys. Lett. **69**(25), 3905 (1996).

[13] S.A. Blanton, A. Dehestani, P.C. Lin and P. Guyot-Sionnest, Chem. Phys. Lett. **229**, 317 (1994).

[14] J. Tittel W. Gohde, F. Koberling, Th. Basche, A. Kornowski, H. Weller, and A. Eychmuller, J. Phys. Chem. B **101**(16), 3013 (1997).

[15] U. Banin, M. Bruchez, A.P. Alivisatos, T. Ha, W. Weiss, and D.S. Chemla, J. Chem. Phys. **110**(2), 1195 (1999).

[16] W. Demtroder, *Laser Spectroscopy: Basic Concepts and Instrumentation, 2nd Enlarged Edition (Springer, 1996).*

[17] Berg, M. et al, Chem. Phys. Lett. **139**(1), 66 (1987).

[18] Trautman, J.K.; Macklin, J.J.; Brus, L.E.; Betzig, E. Nature **369**, 40 (1994).

[19] Koedijk, J.; Wannemacher, R.; Silbey, R.; Volker, S. J. Phys. Chem **100**(51), 19945 (1996).

[20] Geva, E.; Skinner, J.L. J. Phys. Chem. B **101**(44), 8920 (1997).

[21] Pfluegl, W.; Brown, F.L.H.; Silbey, R.J. J. Chem. Phys. **108**(16) 6876 (1998).

[22] E. Geva and J.L. Skinner, J. Phys. Chem. B **101**(44), 8920 (1997).

[23] W.E. Moerner, Science **265**, 46 (1994) and references therein.

[24] W.P. Ambrose and W.E. Moerner, Nature **349**, 225 (1991).

[25] Th. Basche, W.P. Ambrose, and W.E. Moerner, J. Opt. Soc. Am. BB9B, 829 (1992).

[26] Th. Basche and W.E. Moerner, Nature **355**, 335 (1992).

[27] M. Orrit, J. Bernard, A. Zumbusch and R.I. Personov, Chem. Phys. Lett. **196**, 595 (1992).

[28] L. Fleury, A. Zumbusch, M. Orrit, R. Brown, and J. Bernard, J. Lumin. **56**, 15 (1993).

[29] Kuno, M.; Lee, J.K.; Dabbousi, B.O.; Mikulec, F.V.; Bawendi, M.G. J. Chem. Phys. **106**(23), 9869 (1997).

[30] Sacra, A. thesis, Massachusetts Institute of Technology (1996).

Chapter 8: Stark Spectroscopy

8.1 Introduction

The quantum-confined Stark effect in semiconductor nanocrystallites has often been used to probe the nature of the excited states in these systems[1-4]. For instance, delocalized states should be highly polarizable, while localized states should have a strong dipole character. Long radiative lifetimes measured in ensemble nanocrystallite samples have been explained by two conflicting theories which predict that emission originates from either localized surface trap states, or a long-lived, delocalized exciton state within the nanocrystallite core. These two types of states are easily distinguished by the application of an electric field, resulting in a linear or quadratic Stark shift respectively. In the past, however, inhomogeneous broadening and ensemble averaging have greatly complicated the interpretation of ensemble Stark measurements. For example, while the presence of an excited state dipole has been suggested in ensemble Stark absorption studies[1,2], nearly identical Stark data have also been interpreted without the need for a polar state[3,4]. By eliminating the effects of ensemble averaging, single nanocrystallite spectroscopy should allow us to conclusively determine the nature of the emitting state.

In addition to contributing to our understanding of the basic physics of nanocrystallites, the quantum-confined Stark effect also has important potential applications. For instance, the Stark effect in quantum wells has proven effective in some optical modulation applications[5]. Optical modulators are a key component in many optical computing and fiber-optic communication paradigms. In quantum wells, quantum confinement in one dimension allows the formation of excitonic states with electric field induced Stark shifts that are many times

greater than the electron-hole binding energy[5]*. As a result, the Stark effect in quantum wells is significantly enhanced relative to bulk materials. It is expected that nanocrystallites, with narrow linewidths and quantum confinement in all three dimensions, should produce electro-optic modulation devices with even higher efficiency.

8.2 Experimental

In order to examine the size dependence of the Stark effect in nanocrystallites, four samples were studied with average diameters of 44, 52, 58 and 75 Å. The 75 Å sample was further divided, and half of the sample was overcoated with a ~6 Å layer of ZnS[6,7].

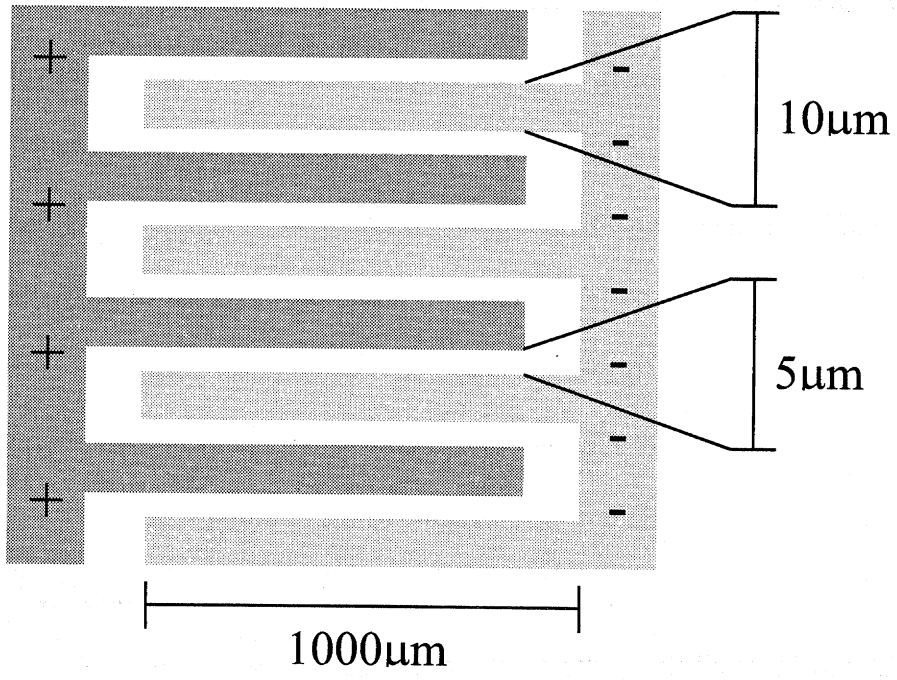

Figure 8.1: Electrodes. Graphic representation depicting the interdigitated electrodes used to apply electric fields to single nanocrystallite samples. A bias was applied between the two the electrodes producing an electric field between adjacent "fingers". Note that this figure is not drawn to scale.

* In bulk semiconductors, strong electric fields can pull the electron and hole apart, destroying the excitonic state and limiting the magnitude of the potential Stark shift. In quantum confined semiconductors, the edges of the material physically prevent the electron and hole from being pulled apart, allowing much larger fields to be applied. without destroying the state.

Electric fields were applied by using photolithographically patterned Ti/Au electrodes on a crystalline quartz substrate. The electrodes were patterned in an interdigitated design (figure 8.1) with an interelectrode spacing of 5 μm and a height of 1200 Å (1000Å Au over 200Å Ti). A dilute solution of nanocrystallites in hexane was placed over the electrodes and the hexane was immediately wicked from the surface, leaving a small number of nanocrystallites adsorbed to the substrate (figure 8.2a). Numerical calculations show that the electric field profile between the electrodes is relatively constant within the center 3 μm (figure 8.2b). Spectra were only taken from nanocrystallites in this region to ensure a uniform electric field. The configuration of the Stark electrodes allowed images and spectra to be obtained using the standard procedures described in chapters 3 and 6.

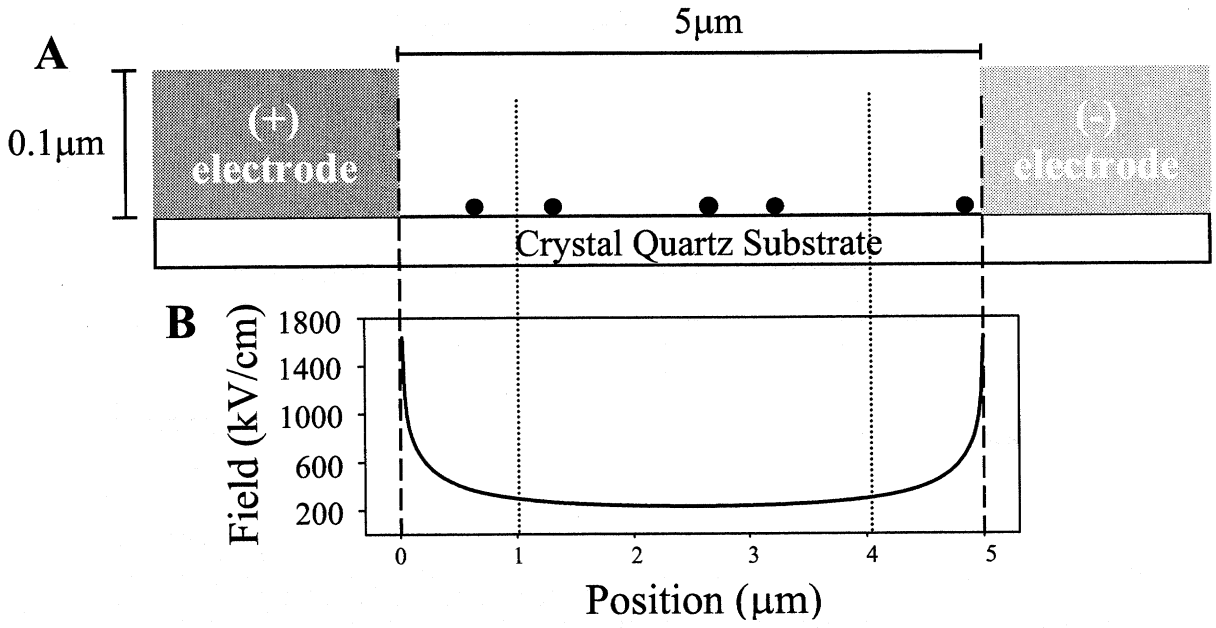

Figure 8.2: Electrodes. (A) Graphic representation of a cross section of the interdigitated electrodes described in figure 8.1. Circles represent a dilute dispersion of nanocrystallites between the electrodes. (B) Calculated electric field profile between adjacent electrodes. The position axis for (A) and (B) is the same. Dashed lines indicate the edges of the electrodes. Dotted lines indicate the region in which the electric field is sufficiently constant (σ=7%) for these experiments, corresponding to the center 3μm. Note that in this figure, the outer 2 nanocrystallites would not be studied due to a large uncertainty in the magnitude of the applied field.

8.3 Results

8.3.1 Single Nanocrystallite Stark Shifts

Figure 8.3a shows a series of emission spectra taken from the same single nanocrystallite with the applied electric field either on or off. A single peak corresponding to the zero phonon transition can be observed shifting between two distinct energies in response to the applied field. This shift is highly reproducible and results in a

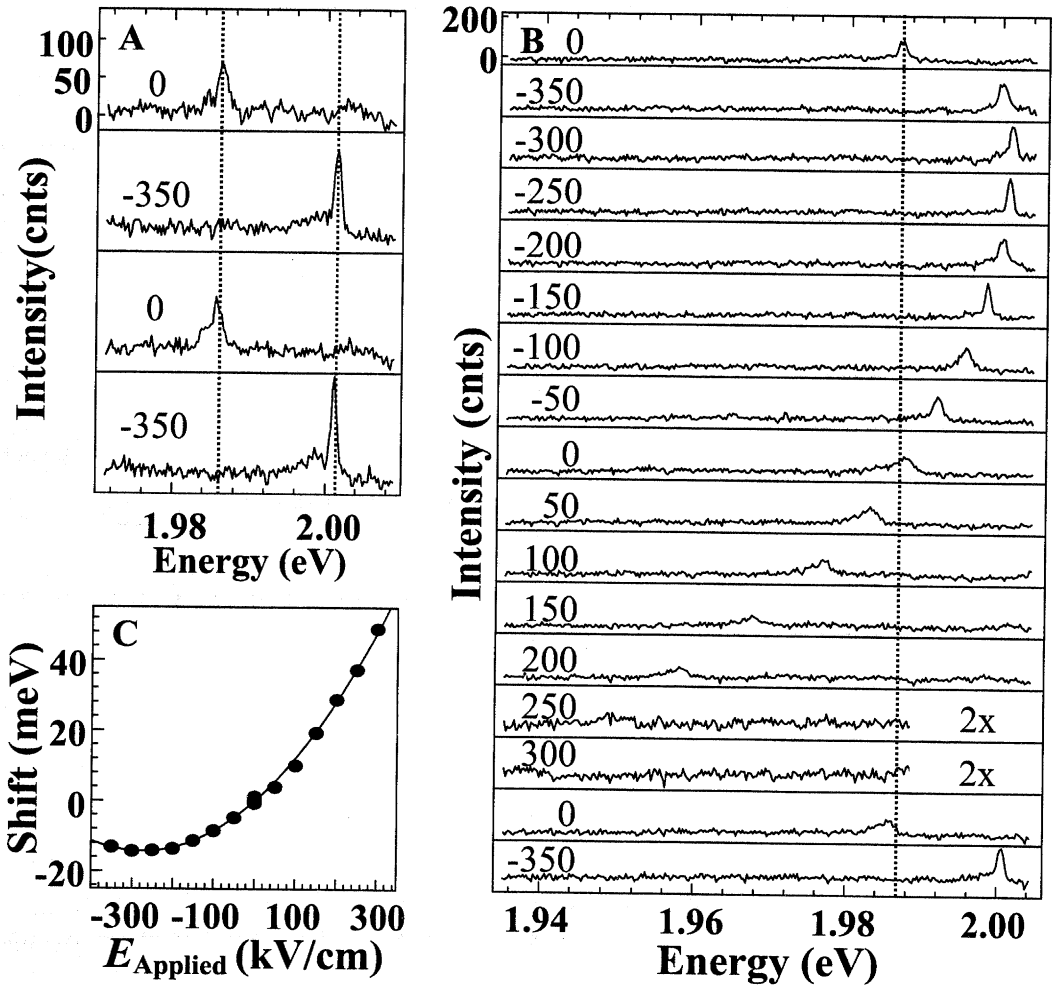

Figure 8.3: Single nanocrystallite Stark spectra. (A) Emission spectra of a single 75Å overcoated nanocrystallite under conditions of alternating electric field. Insets indicate the applied field in kilovolts per centimeter. (B) 17 spectra of the same single nanocrystallite under a range of electric fields. Insets indicate the applied field in kilovolts per centimeter and magnification of the y axis. (C) Plot of Stark shift versus electric field for spectra in (B). The line represents a fit to the sum of a linear and quadratic shift as a functions of field. All spectra were taken with an excitation intensity of 25 W/cm^2 and an integration time of 30 seconds.

change in energy that is 15 times greater than the observed, resolution-limited linewidth, and more than two orders of magnitude greater than the linewidths observed in chapter 7. Although the first absorbing state has not yet been characterized for single CdSe nanocrystallites, even conservative estimates based on ensemble measurements suggest that these shifts are approximately an order of magnitude greater than the width of this state[8], confirming the potential of these nanocrystallites for use in electro-optic modulation devices.

Figure 8.3b shows the same single nanocrystallite under a range of electric fields. The peak can be seen to shift continuously over more than 60 meV. The reproducibility of this shift is demonstrated in the final frames, which repeat the initial field sequence. The slight change in zero-field energy over the series is due to spectral diffusion. Shifts as large as 75 meV were observed in nanocrystallites from this sample. These shifts are comparable to room-temperature single nanocrystallite linewidths[9], suggesting the potential for use in non-cryogenic devices.

Figure 8.3c plots Stark shift as a function of field for the series in figure 8.3b. The data can be fit with the sum of a linear and quadratic function of the applied field, indicating the presence of both polar and polarizable character in the emitting state.

$$\Delta E = \mu\xi + 1/2\alpha\xi^2 + \ldots \qquad [8.1]$$

where E is the energy of the transition, ξ is the applied electric field, and μ and α are projections of the excited state dipole and polarizability along the applied field, respectively. Formally, what is measured in these experiments is actually the difference

between the excited and ground state dipole. For simplicity in discussion, however, we refer to this value as the excited state dipole. This is a reasonable assertion since, to a first approximation, any structural (ground state) dipole should be relatively unaffected by the presence of a delocalized excitation. The same argument holds true for the excited state polarizability.

8.3.2 Excited State Dipole and Polarizability

Within a given sample, a range of values for both the polarizability and the excited state dipole are measured. Variations in polarizability may be due to differences in size, shape, and orientation of individual nanocrystallites. Differences in the measured excited state dipole are largely due to a distribution of dipole orientations relative to the applied field. Figure 8.4a shows a representative sample of four single nanocrystallite

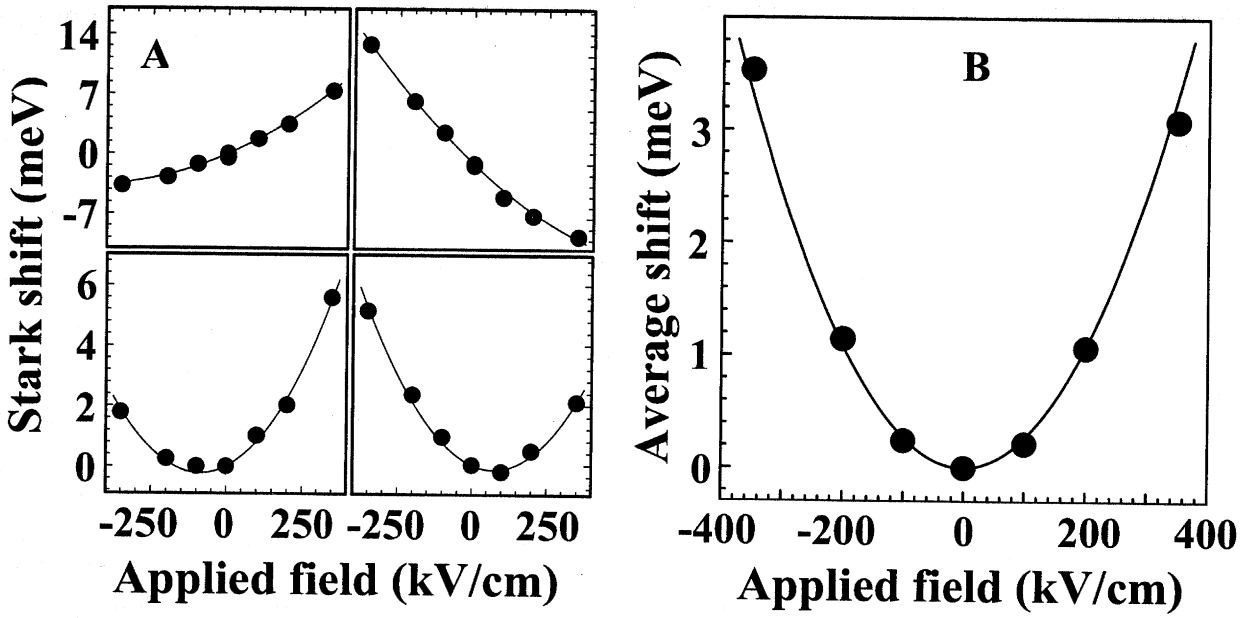

Figure 8.4: Spectral response to an applied electric field. (A) Stark shift of emission versus field for four different single nanocrystallites taken from the 58Å sample. Lines indicate fits to the sum of a linear and quadratic shift as a function of field. (B) Average shift versus field for 54 single nanocrystallites from the 58Å sample with the fit to a pure quadratic function of field.

Stark series from the 58 Å sample.

Although a polar component has been suggested in ensemble absorption studies[1,2], Stark shifts in ensemble emission spectra were previously found to be purely quadratic in the applied field[10]. In light of the current single nanocrystallite experiments, this result can be explained as the product of ensemble averaging. While individual nanocrystallites reveal a strong linear component in the Stark shift, the average dipole over the ensemble is zero (figure 8.4b). The result is that ensemble samples should have a quadratic shift of the peak emission as a function of field, with an additional broadening due to the linear contribution of individual nanocrystallites. Consistent with this, ensemble experiments reveal a broadening of the emission with increasing electric field. These studies, however, are further complicated by additional broadening due to changes in phonon coupling. In the past, ensemble emission broadening has been attributed entirely to changes in phonon coupling[10]. These single nanocrystallite results indicate, however, that a polar contribution must also be considered.

For the 58Å sample, an average polarizability of $2.38 \times 10^5 Å^3$ is obtained ($\sigma = 1.37 \times 10^5 Å^3$), which is comparable to the physical volume of the nanocrystallite ($\sim 10^5 Å^3$) and much larger than the polarizability of more traditional molecules (anthracene $\alpha \approx 25 Å^3$)*. The average magnitude of the excited state dipole (88.3 D) can also be extracted from this data. This dipole is extremely large; comparable to an electron and hole separated by 2/3 of the nanocrystallite radius.

* This is not surprising given the relatively large volume of a nanocrystallite compared to traditional molecules.

8.3.3 Local Electric Fields

The excited state dipole observed in these experiments is consistent with a highly polarizable excited state in the presence of a strong local electric field. The Stark shift measured is therefore a quadratic function of the total electric field ($\xi_{internal} + \xi_{applied}$), such that

$$\Delta E = 1/2\alpha(\xi_{total})^2 = 1/2\alpha(\xi_{internal} + \xi_{applied})^2$$

$$\Delta E = 1/2\alpha(\xi_{applied})^2 + \alpha\xi_{internal}\cdot\xi_{applied} + 1/2\alpha(\xi_{internal})^2 \qquad [8.2]$$

$$\Delta E = 1/2\alpha(\xi_{applied})^2 + \mu_{induced}\cdot\xi_{applied} + \text{constant}$$

where α is the same as in Eq. 8.1, $\xi_{internal}$ is the internal electric field resulting from any local fields, $\mu_{induced}$ is the excited state dipole induced by $\xi_{internal}$ such that $\mu_{induced} = \alpha\xi_{internal}$, and $1/2\alpha(\xi_{internal})^2$ is a constant. The average, unscreened, local electric field extracted from these single nanocrystallite measurements is extremely large (~10^6V/cm). This field magnitude is equivalent to that produced by a trapped charge on or near the surface of the nanocrystallites. This is consistent with the intermittency results of chapter 4 which concluded that, at cryogenic temperatures, the mechanism for intermittency could result in the presence of external charges around individual nanocrystallites.

While the data presented above are consistent with the presence of a local electric field, it is possible that the observed excited state dipole arises from some other (intrinsic) asymmetry in the exciton wavefunction. In fact, ensemble dielectric dispersion measurements have suggested the presence of a ground state dipole in CdSe nanocrystallites[11]. This dipole arises from the ionic nature of the crystal lattice, and could account for the observed excited state dipole in these experiments. Data presented in Chapter 9, however, confirms that the dipole observed in these experiments is largely the

result of an extrinsic electric field around individual nanocrystallites. As such, the remainder of this chapter will be described in terms of local electric fields. It should be noted, however, that the majority of the results described below do not depend on the source of the asymmetry in the excited state, but merely the presence of the dipole itself.

8.3.4 Implications of an Excited State Dipole

The presence of a large excited state dipole has several implications. First, the magnitude of the internal electric field extracted in all samples (~10^5 V/cm) implies extensive state mixing near the band edge, with potentially serious implications regarding our understanding of the electronic structure in these nanocrystallites, since current theoretical treatments have not considered this effect. This conclusion has also been reached using ensemble nonlinear optical techniques such as 2-photon excitation, where state mixing is observed directly[12]. At the same time, this state mixing may also help explain the anomalously large LO phonon couplings measured in these nanocrystallites[8]. According to current theory, emission occurs from a delocalized exciton state[13] which should only weakly couple to optical phonons[14,15]. An excited state dipole breaks the inversion symmetry of the exciton wavefunction, creating a separation of charge within the ionic crystal. This charge asymmetry should then increase exciton-LO phonon coupling through a Fröhlich interaction, as described in section 6.3.3. Previous theoretical calculations of LO phonon couplings have concluded that the experimentally observed ensemble values could be accounted for by the presence of a local electric field equivalent to an electron on the surface of the nanocrystallite[14,15]. This field magnitude is consistent with what has been observed here. In addition, different local electric fields

around individual nanocrystallites may also explain the wide range of phonon couplings seen in single nanocrystallite experiments (see figure 6.3).

8.3.5 Size Dependence

Stark measurements of different size samples reveal some general trends in the average polarizability, excited state dipole and calculated internal electric field as a function of size (figure 8.5). The data in figure 8.5 was obtained from (47) 75Å overcoated nanocrystallites, (57) 75Å, (83) 58Å, (74) 52Å and (16) 44Å non-overcoated nanocrystallites. The plotted values include screening by the CdSe core and ZnS shell as necessary. The increase in polarizability with size is consistent with ensemble measurements[10] and with the increase in volume of the nanocrystallites. The observed

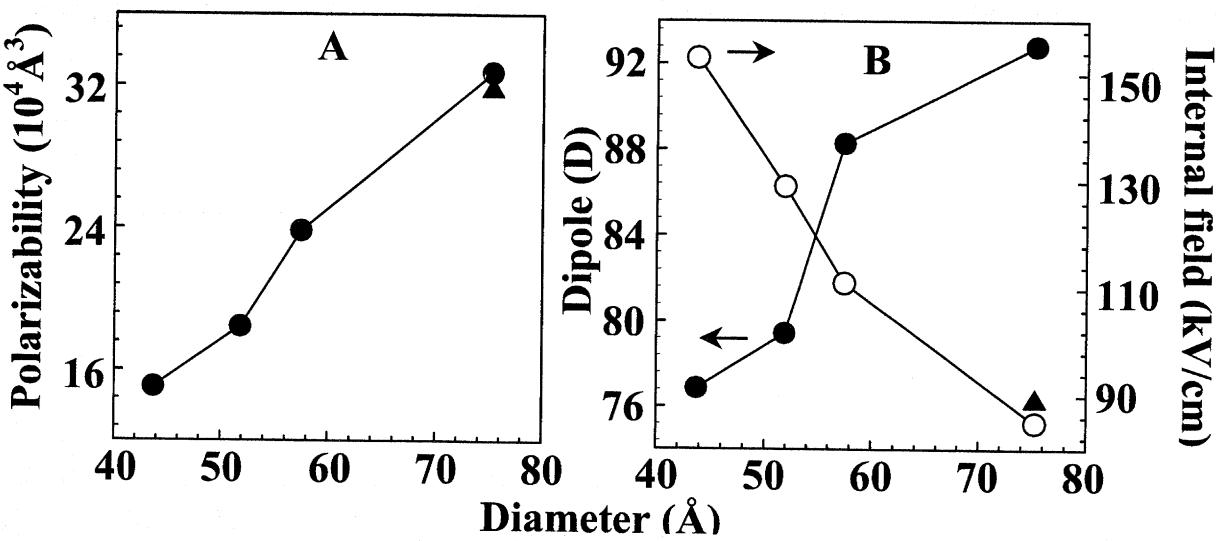

Figure 8.5: Spectral response to an applied electric field. (A) Measured average polarizability as a function of size for non-overcoated nanocrystallites (closed circles) and 75Å ZnS overcoated nanocrystallites (closed triangle). (B) Measured average excited state dipole and internal electric field (closed and open circles respectively) as a function of size for non-overcoated nanocrystallites. The closed triangle indicates the average excited state dipole for the 75Å ZnS overcoated nanocrystallites. The excitation intensity for all data presented was 250W/cm^2.

increase in excited state dipole with size is a result of the corresponding increase in polarizability, since the average internal electric field actually decreases with size. A decrease in the internal field with size is consistent with the existence of external electric fields. As the size of the nanocrystallite is increased, the average distance of an external charge from the center of the exciton wavefunction increases. The result is a decrease in the average internal electric field.

To reinforce this result, a ZnS overcoated sample with the same size CdSe core as one of the non-overcoated samples was also studied. The measured values of the polarizability for the overcoated and non-overcoated samples were found to be statistically identical, consistent with minimal delocalization of the exciton into the ZnS shell, as described in section 1.3.3. At the same time, however, a significant decrease in excited state dipole is observed. This is consistent with the ZnS shell forcing external charges to reside farther from the exciton wave function, while simultaneously screening external fields. The ZnS shell also acts as a barrier to ionization[9], potentially decreasing the number of charges around the nanocrystallite.

8.4 Conclusion

These electric field studies of single nanocrystallites have revealed both polar and polarizable character in the lowest excited state. These results are consistent with emission from a delocalized exciton state in the presence of a large local electric field. These local fields are thought to result from the presence of charge carriers on or near the surface of individual nanocrystallites which result from ionization of the nanocrystallites. The presence of strong local electric fields around individual nanocrystallites may help

explain the state mixing observed in previous two-photon absorption experiments, as well as the large LO phonon couplings measured in ensemble nanocrystallite experiments. It may also explain the wide distribution of phonon couplings measured in single nanocrystallite spectra. Once again, by eliminating the effects of ensemble averaging, we were able to uncover important new physical information, providing significant insight into the nature and physics of quantum confinement in these nanostructures.

8.5 References

[1] Colvin, V.L.; Alivisatos, A.P. J. Chem. Phys.**97**(1), 730 (1992).
[2] Colvin, V.L.; Cunningham, K.L.; Alivisatos, A.P J. Chem. Phys. **101**, 7122 (1994).
[3] Hache, F.; Richard, D.; Flytzanis, C. Appl. Phys. Lett. **55**, 1504 (1989).
[4] Sacra, A.; Norris, D.J.; Murray, C.B.; Bawendi, M.G. J. Chem. Phys. **103**(13), 5236 (1985).
[5] D.A. Miller, *Confined Excitons and Phonons* (Plenum, New York, 1995), p.675.
[6] M.A. Hines and P. Guyot-Sionnest, J. Phys. Chem. **100**, 468 (1996).
[7] B.O. Dabbousi et al., J. Phys. Chem. B. **101**, 9463 (1997).
[8] D. Norris, Al. Efros, M. Rosen and M. Bawendi, Phys. Rev. B, **53**, 16347 (1996).
[9] M. Nirmal, B.O. Dabbousi, M.G. Bawendi, J. Macklin, J. Trautman, T. Harris and L. Brus, Nature **383**(6603), 802 (1996).
[10] A. Sacra, thesis, MIT (1996).
[11] Blanton, S.A. et al., Phys. Rev. Lett. **79**(5), 865 (1997).
[12] M.E. Schmidt, S.A. Blanton, M.A. Hines and P. Guyot-Sionnest, J. Chem. Phys. **106**(12), 5254 (1997).
[13] Al. L. Efros, M. Rosen, M. Kuno, M. Nirmal, D.J. Norris and M.G. Bawendi, Phys. Rev. B **54**(7), 1 (1996).
[14] Nomura, S.; Kobayashi, T. Phys. Rev. B **45**(3), 1305 (1982).
[15] Efros, Al. L. *Phonons in Semiconductor Nanostructures*, (Kluwer Academic Publishers, Boston, 1993), p 299.

Chapter 9: Spectral Diffusion - Large Shifts

9.1 Introduction

In chapter 7, a surprising new effect was observed in single nanocrystallite spectra: Spectral diffusion. Spectral diffusion was divided into two categories, labeled "small" and "large" shifts. Small shifts occur on a relatively fast time scale (<1 second) and tend to be somewhat continuous within a relatively narrow energy range (order 1meV). Large shifts occur on a much longer timescale (minutes) and are relatively discontinuous in energy. As the name suggests, these shifts can be quite large (order 10 meV).

At the moment, the distinction between large and small spectral diffusion shifts is somewhat arbitrary. In fact, since small shifts occur on a variety of energy scales, and on a variety of timescales (as do large shifts), there is no reason to believe that these two effects are fundamentally different. As we will see in the next two chapters, however, while the origin of spectral diffusion appears to be the same for both small and large shifts, the mechanism for these shifts is quite different.

In chapter 7, we found that the spectral characteristics of large spectral diffusion shifts were very similar to those observed in low temperature ensemble Stark measurements. This motivated a hypothesis that local electric fields may play a role in the production of spectral diffusion by inducing Stark shifts in single nanocrystallite spectra. This hypothesis was further supported by the direct measurement of extremely large local electric fields around individual nanocrystallites in chapter 8. To further investigate the role of electric fields in spectral diffusion, this chapter will continue the investigation of the Stark effect in single nanocrystallites using the same procedures as described in chapter 8.

9.2 Results and Discussion

9.2.1 Spectral Diffusion vs Single Nanocrystallite Stark Shifts

In order to evaluate the hypothesis that spectral diffusion is the result of changing local electric fields, it is possible to compare spectral diffusion to single nanocrystallite Stark shifts. A direct comparison between the two effects (figure 9.1) reveals that the changes in a single nanocrystallite spectrum observed in spectral diffusion and those induced by the presence of an applied electric field are very similar. As a quantitative

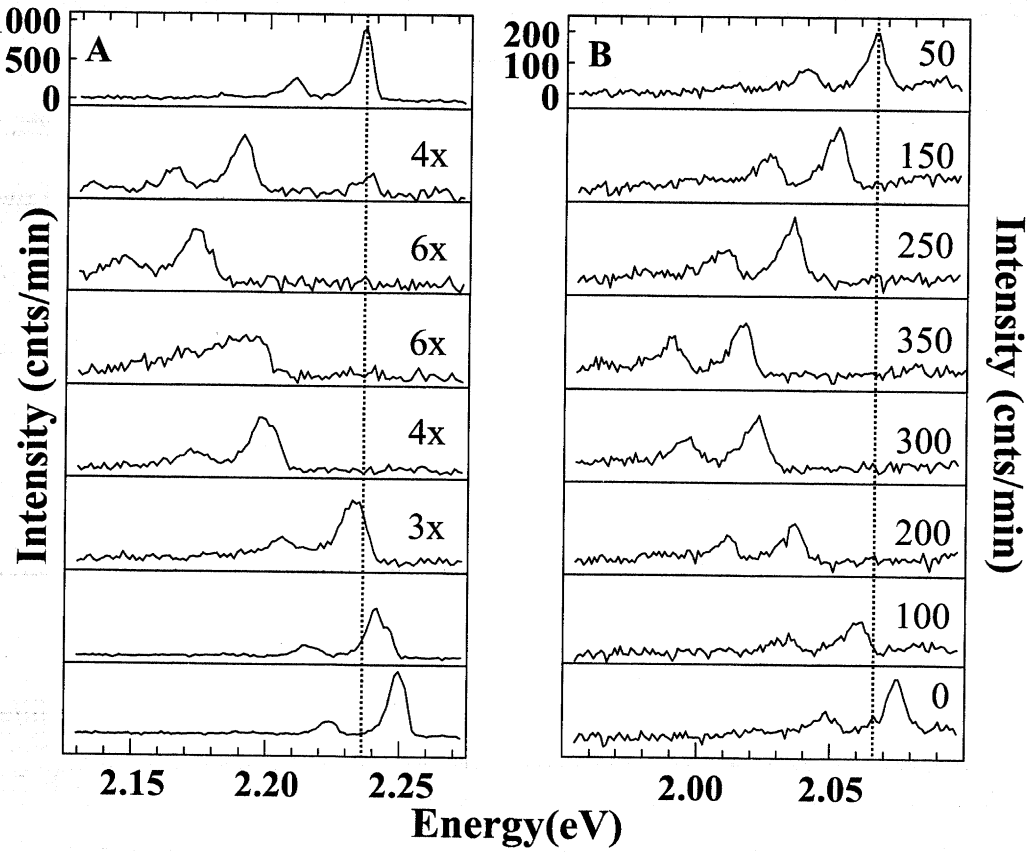

Figure 9.1: Stark shift versus spectral diffusion. (A) Eight sequential 1 minute emission spectra of a single nanocrystallite shifting due to spectral diffusion in the absence of an applied electric field. Insets indicate magnification of the y-axis. (B) Stark series for a single 24Å overcoated nanocrystallite. Insets indicate applied field in kilovolts per centimeter. Excitation intensity for data in (A) and (B) are 2500 and 285 W/cm^2 respectively.

comparison, figure 9.2 plots phonon coupling as a function of relative shift for spectral diffusion and the single nanocrystallite Stark series. As discussed in section 6.3.3, phonon coupling is a measure of the electron-hole overlap and should be sensitive to changes in the polarization of the exciton. An identical change in phonon coupling with shift characterizes both phenomena. The observed similarities strongly suggest that spectral diffusion is, in fact, the result of changing local electric fields.

One implication of changing local electric fields is that there should be a direct correlation between spectral diffusion shifts and changes in the magnitude of the induced excited state dipole measured for that nanocrystallite. Consistent with this prediction, distinct changes in the single nanocrystallite Stark shift can be seen accompanying spectral diffusion shifts. Figure 9.3a shows 11 consecutive spectra of the same single nanocrystallite under different field conditions. Following a spectral diffusion shift in the

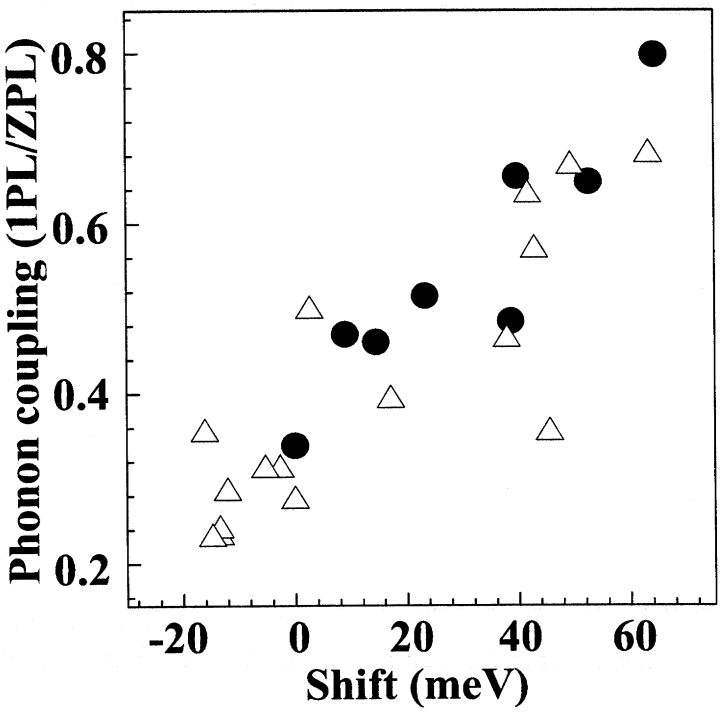

Figure 9.2: Phonon coupling versus shift for Stark data (closed circles) and spectral diffusion (open triangles). Phonon coupling is measured as the ratio of the integrated intensity of the one LO phonon line to the zero phonon line.

sixth frame, there is an increase in the magnitude of subsequent Stark shifts. Over 50 minutes, distinct changes in the zero-field energy are clearly observed (figure 9.3b). Accompanying each of these shifts is a corresponding change in the response to the applied field. During minutes 26-32, the Stark shifts become almost purely quadratic, indicating that the excited state dipole along the applied field has become very small.

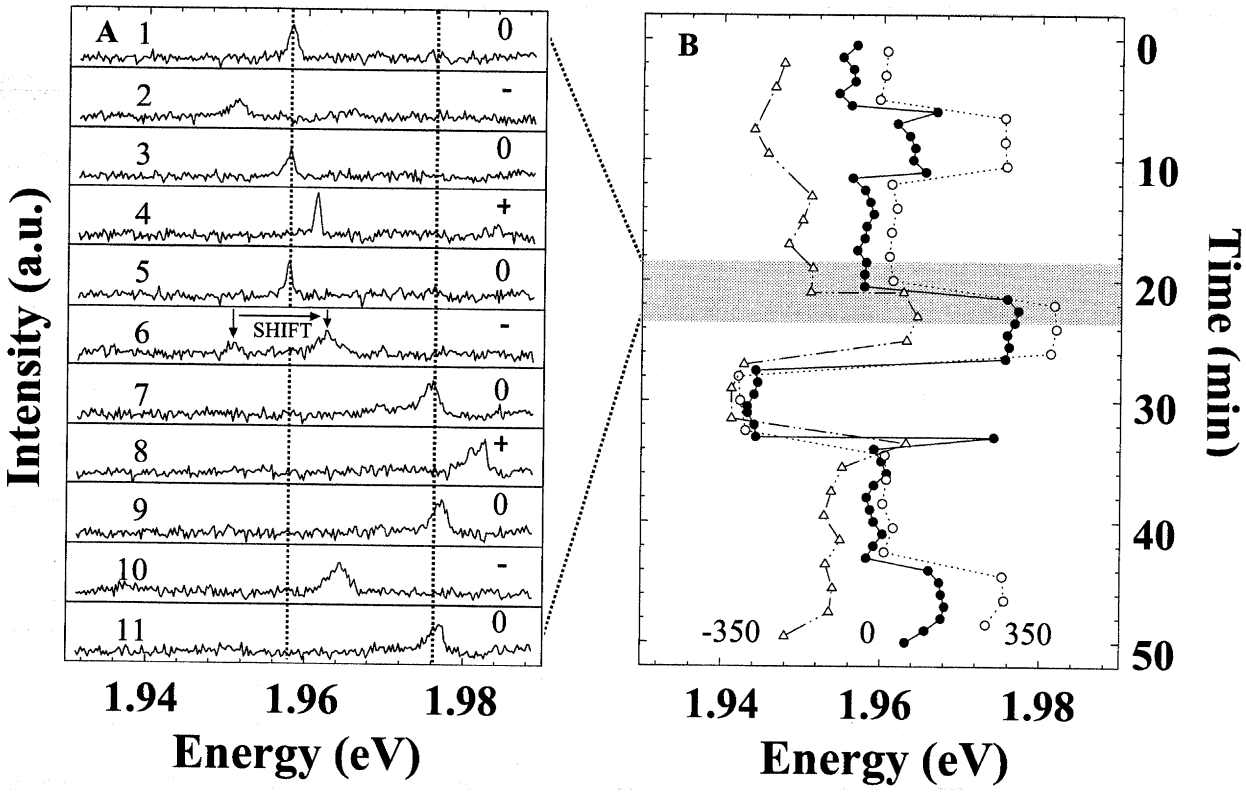

Figure 9.3: Influence of spectral diffusion on the Stark shift of a single nanocrystallite. (A) 11 consecutive 30 sec emission spectra of a single 75Å overcoated nanocrystallite under conditions of alternating zero-negative-zero-positive electric field. Insets indicate spectrum number and relative orientation of the field: (-) -350 kV/cm, (+) +350 kV/cm and (0) 0 V/cm. Dotted lines correspond to the zero-field energy before and after the spectral diffusion shift. (B) Summary of 100 consecutive 30 sec spectra of the same nanocrystallite under the field conditions described above. Data are plotted as a function of time, peak position and electric field. Closed circles indicate zero-field. Open triangles and open circles indicate fields of -350 and +350kV/cm, respectively. Excitation intensity for all spectra was 25 W/cm^2.

By measuring the complete Stark series for a single nanocrystallite before and after a spectral diffusion shift, it is possible to determine which of the Stark parameters is changing. Figure 9.4a shows a Stark series for a single 52Å overcoated nanocrystallite. Figure 9.4b show a Stark series for the same nanocrystallite after a spectral diffusion shift. A fit to the two curves reveals that, while the polarizability remains the same, the magnitude of the excited state dipole changes by a factor of 2.4. Analysis of the Stark parameters between the spectral diffusion shifts in figure 9.3 also reveal no change in the measured polarizability over the 50 minutes, however, the dipole contribution changes by almost a factor of 50. The correlation of spectral diffusion with changes in the magnitude of the induced excited state dipole is consistent with the Stark model of spectral diffusion.

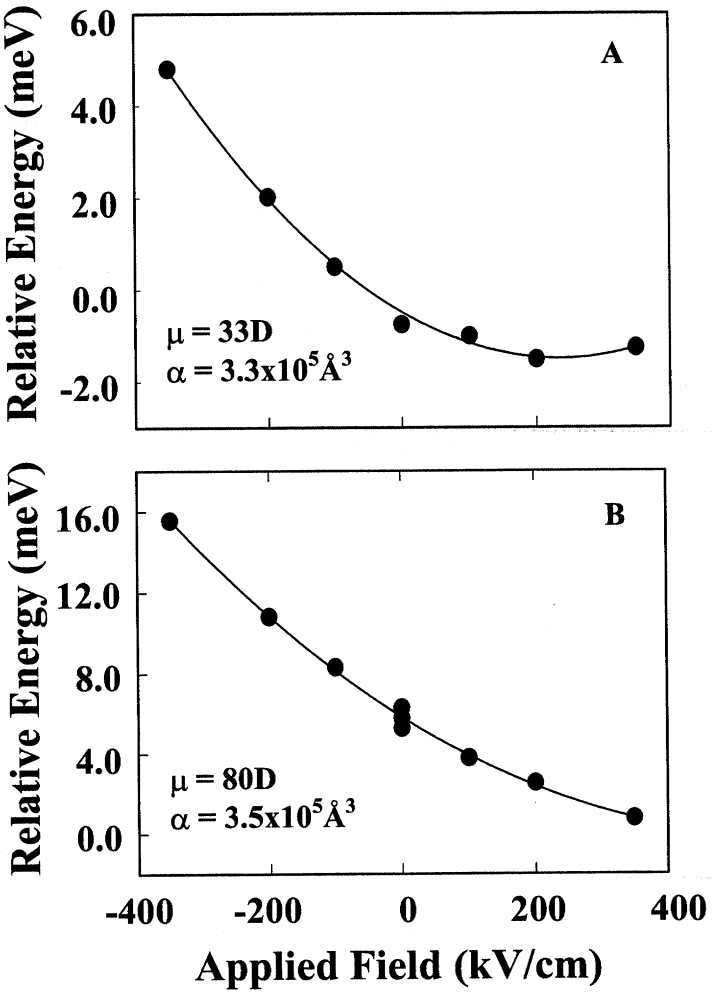

Figure 9.4: Effect of spectral diffusion on single nanocrystallite Stark shifts. (A) and (B) Stark series from a single 52Å overcoated nanocrystallite immediately before and after a spectral diffusion shift. Also included are the measured polarizability and excited state dipole for each series. Note that the offset of ~4meV between the zero-field energy of (A) and (B) represents the magnitude of the spectral diffusion shift.

Although an increase in the local electric field should result in a lower emission energy, there need not be a correlation between the direction of a spectral diffusion shift and the change in measured dipole along the applied field. For example, in figure 9.3b, the spectrum at 30 min is red shifted from that at 22 min, suggesting a large local field and therefore a larger total induced dipole. The component of the dipole measured along the applied field, however, is nearly nonexistent.

9.2.2 Nanocrystallite Rotation

An alternative interpretation of the data in figures 9.3 and 9.4 is that individual nanocrystallites are rotating within a static electric field, rather than remaining fixed within a fluctuating field. While reorientation of the nanocrystallites at 10K is unlikely, this is a very important distinction to make, since it addresses the nature of the dynamics in this system (i.e. is the local field changing relative to the nanocrystallite or is the nanocrystallite reorienting relative to the local field?).

The orientation of single nanocrystallites can be monitored through the use of polarization spectroscopy as described in chapter 5. It is important to note that the excited state dipole measured in these Stark experiments is completely unrelated to the transition dipole moment measured in polarization experiments. This is because the dynamic transition dipole is primarily a function of the electron and hole unit cell wavefunctions[1], while the static excited state dipole is primarily a function of the envelope wavefunction[2,3]. As discussed in section 5.4.3, the envelope wavefunction can be separated from the transition dipole matrix and does not contribute to the orientation of the transition dipole. Prior to employing polarization spectroscopy to study spectral diffusion,

however, we must confirm that the separation of the envelope and unit cell wavefunctions is valid, and that local electric fields do not influence the orientation of the transition dipole. To verify this, the polarization dependence of single nanocrystallites was studied in the presence and absence of an applied electric field ($2.5x10^5$V/cm). In all nanocrystallites studied, no change in the phase or degree of polarization was observed (figure 9.5). It should therefore be possible to use polarization spectroscopy to monitor changes in nanocrystallite orientation as a function of time.

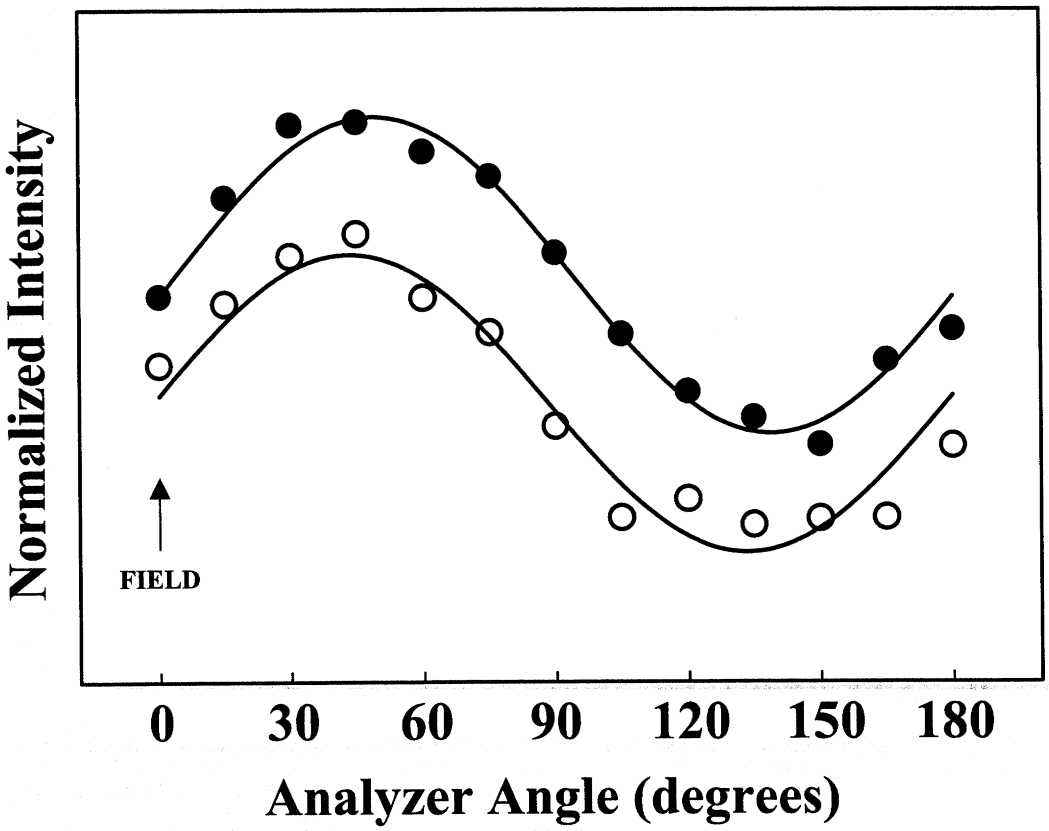

Figure 9.5: Polarization dependence in an applied electric field. Emission intensity of a single nanocrystallite as a function of analyzer angle is plotted in the presence and absence of a $2.5x10^5$V/cm electric field (open and closed circles respectively). The field is applied along the direction parallel to both the sample plane and the zero degree line of the polarizer. The data has been normalized and offset for clarity, so that a direct comparison between the phase and degree of polarization can be made.

Figure 9.6a plots the total emission intensity as a function of analyzer angle for a single nanocrystallite. Figure 9.6b show the simultaneous emission energy of the zero phonon line, plotted as a spectral trajectory over time. Over 40 minutes, many large spectral diffusion shifts can be seen, however, no change in the degree of polarization or phase is observed. Since the transition dipole is not affected by electric fields, the data in figure 9.6 confirms that spectral diffusion is the result of a dynamic local electric field and not reorientation of the nanocrystallite within a static field.

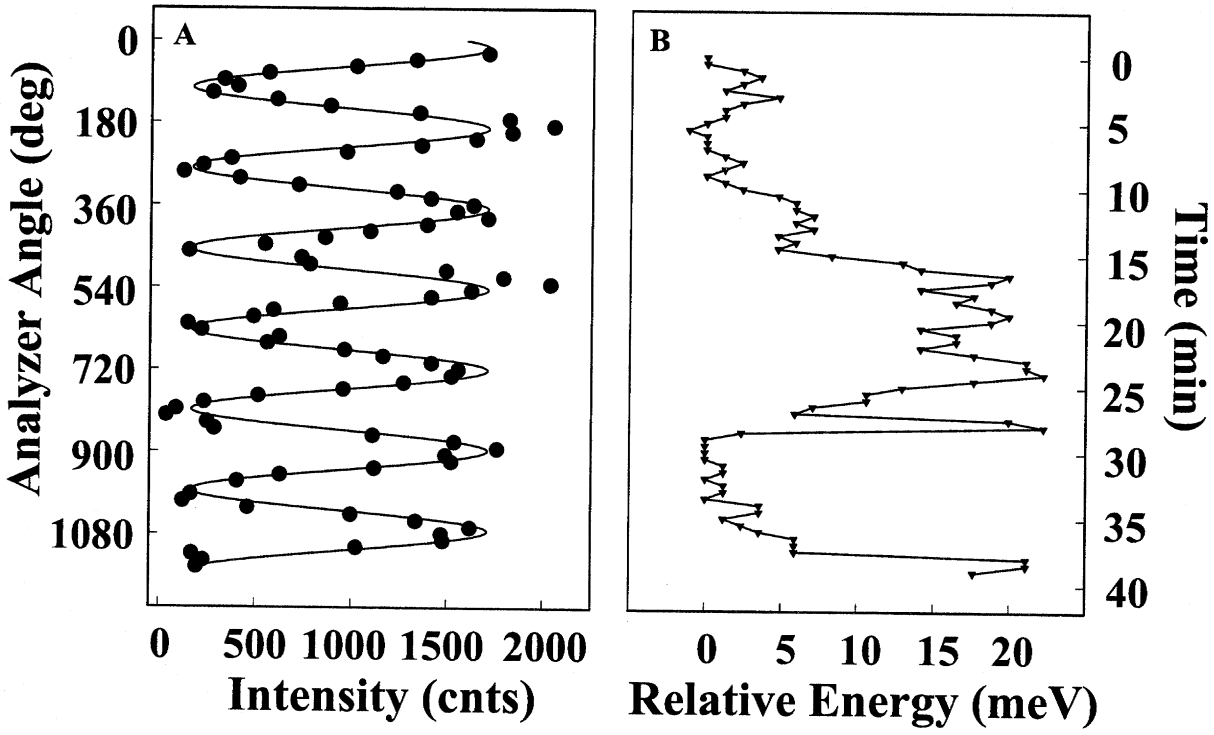

Figure 9.6: Polarization versus spectral diffusion. (A) Total emission intensity of a single 52Å overcoated nanocrystallite as a function of analyzer angle with fit. (B) Relative emission energy of the zero phonon line of the nanocrystallite in (A) as a function of time. The data in (A) and (B) were taken simultaneously so that changes in emission energy and polarization could be monitored concurrently. Data in figure 9.6 was taken with an integration time of 30 seconds, an excitation intensity of 60W/cm^2 and an excitation polarization of 0 degrees.

9.2.3 Ionization and Local Electric Fields

Ensemble dielectric dispersion measurements have suggested the presence of a ground state dipole in CdSe nanocrystallites[4]. However, while the data presented above does not preclude a contribution to the excited state dipole from intrinsic structural or charge asymmetries in the ground state[4,5], it does indicate that a large portion of this dipole arises from an extrinsic source. In fact, the changes in the excited state dipole observed in figure 9.3 are of the same order of magnitude as the average dipole measured for that sample.

If we assume that the excited state dipole is the result of local electric fields (either intrinsic or extrinsic), the magnitude of this average field is found to be quite large, comparable to that produced by a point charge (electron or hole) trapped on or near the surface of the nanocrystallite. As discussed in chapter 4, photoionization is thought to be the source of fluorescence intermittency. At room temperature, fluorescence intermittency is thought to result from ionization of the nanocrystallite followed by the return of the ionized carrier to the CdSe core. At 10K, however, there is little thermal energy available to promote the return of an external charge. Instead, neutralization may occur through an additional ionization event, resulting in an emitting nanocrystallite in the presence of a potentially large and randomly oriented local electric field.

Additional ionization or recombination events, as well as relocalization of external charges, could result in changes in both the zero-field energy as well as the excited state dipole of a single nanocrystallite. This is consistent with what is observed in figures 9.3 and 9.4. The magnitude of the spectral diffusion shifts observed in figure 9.3 implies variations in the local electric field on the order of 10^5 to 10^6 V/cm (unscreened). This is consistent with the addition or removal of an electron from the surface of the nanocrystallite.

Within the framework described above, large spectral shifts may result from ionization and recombination of carriers, while small shifts may result from slight field modulations due to movement of charges between local trap sites. While a complete discussion of small spectral diffusion shifts will be deferred until chapter 10, some predictions can be made regarding large spectral diffusion shifts:

9.2.4 Intermittency and Large Spectral Diffusion Shifts

Both intermittency and large spectral diffusion shifts are thought to have a common origin: Ionization. As a result, a correlation should exist between fluorescence intermittency and large shifts. Preliminary results confirm this conclusion. Figure 9.7 presents data taken from a single nanocrystallite over time. The time evolution of the spectrum is displayed (figure 9.7b), along with the total emission intensity as a function of time (figure 9.7c). For each period of intermittency, there is a corresponding spectral diffusion shift, consistent with the hypothesis that local electric fields result, in part, from ionization of the nanocrystallite.

While fluorescence intermittency is typically considered a binary process, the data in figure 9.7 shows that this is not strictly true. Relative emission intensities before and after a spectral diffusion shift are often different. This is easily explained as the result of spectral diffusion, which was shown to affect the relative emission intensity. As in figure 7.7, the relative emission intensity plotted in figure 9.7c decreases as the spectrum shifts to lower energy, consistent with the Stark mechanism of spectral diffusion.

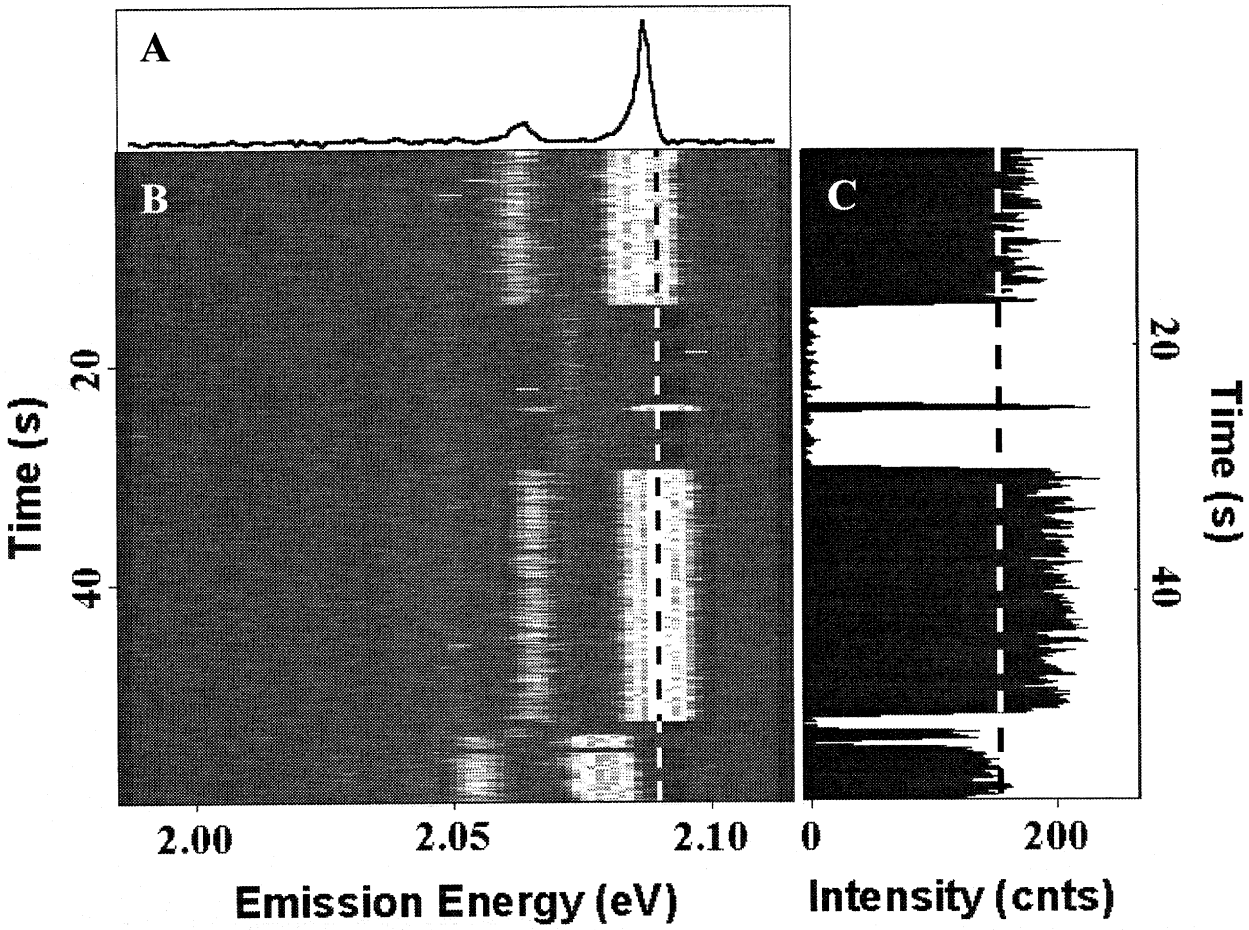

Figure 9.7: Correlated intermittency and large spectral diffusion shifts. (A) Spectrum of a single 56Å overcoated nanocrystallite. (B) Time evolution of the spectrum in (A). Horizontal stripes correspond to consecutive spectra of the same nanocrystallite taken with a 100ms integration time. (C) Intensity time trace for the nanocrystallite in (B). Dashed lines are a guide to the eye. Excitation intensity was 200W/cm^2. Data was take with the Pentamax CCD camera.

The correlation between intermittency and large spectral diffusion shifts is not perfect. For instance, near the bottom of figure 9.7b, there is an intermittency without an observable shift. Figure 9.8 shows a second nanocrystallite that blinks without shifting (thin arrow) and shifts without blinking (dotted arrow)*. These instances, however, may simply represent shifts

* Note that the spectrum in figure 9.8 appears to shift somewhat continuously during the intervals between "large shifts". These are "small" spectral diffusion shifts, as described in section 7.3.2. As we will see in Chapter 10, the local electric field fluctuations responsible for small spectral diffusion shifts are not the result of ionization and should therefore not be correlated with blinking.

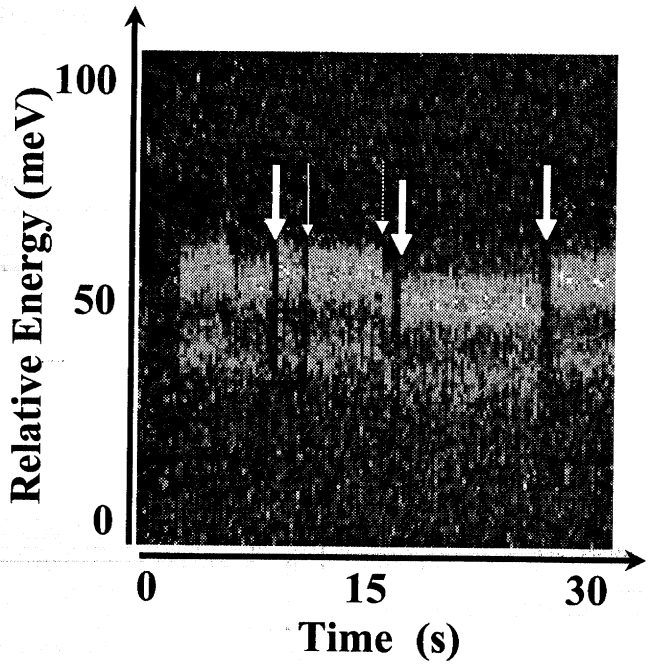

Figure 9.8: Uncorrelated intermittency and spectral diffusion. Three-dimensional plot showing emission energy of a single nanocrystallite spectrum as a function of time. Each spectrum appears as a vertical stripe within the image. Intermittency and diffusion events are marked by arrows as indicated in the text. Each spectrum was taken with a 100ms integration time using the Pentemax CCD camera. Excitation intensity was 200W/cm^2.

below our resolution limit and intermittency on a timescale faster than 100ms respectively. As always, many correlated shifts are also observed (Thick arrows) While further investigation is required in order to quantify the correlation between spectral diffusion and fluorescence intermittency, these and other similar results support the conclusion that the local electric fields responsible for spectral diffusion are the result of nanocrystallite ionization.

9.2.5 Ensemble Effects

Spectral diffusion and the presence of local electric fields in ensemble nanocrystallite samples represents an additional form of inhomogeneous broadening. Even if samples could be fabricated with an infinitely narrow size distribution, the presence of

different local fields around individual nanocrystallites would shift spectra away from the zero-field energy, broadening the ensemble spectrum. In fact, the large shifts observed in these experiments are on the same order of magnitude as the peak widths measured in ensemble samples. This suggests that a reduction in the size distribution may not significantly narrow ensemble spectra. In order to reduce ensemble peak widths, it may be necessary to reduce not only the size distribution, but also the electric field distribution within each ensemble sample. Modifications of the ionization barrier[6,7], changes in the surrounding matrix, or both may be necessary in order to reduce this local field distribution.

9.3 Conclusion

In this chapter, we have uncovered the role of local electric fields in the production of large spectral diffusion shifts. A direct comparison between spectral diffusion and single nanocrystallite Stark shifts suggests that spectral diffusion is the result of changing local electric fields which perturb single nanocrystallite spectra. Changes in the magnitude of the excited state dipole accompanying spectral diffusion shifts further support this Stark model of spectral diffusion. Polarization studies confirm that it is the local field changing around individual nanocrystallites, and not the nanocrystallite rotating within a static field that is responsible for spectral diffusion. The magnitude of the measured local electric fields suggests the presence of charge carriers on or near the nanocrystallite surface. The magnitude of the observed changes in the local field and the correlation of large spectral diffusion shifts with fluorescence intermittency suggests that the source of these local fields is ionization of the nanocrystallites. In addition to spectral diffusion, the presence of strong

local electric fields may also contribute to inhomogeneous broadening in ensemble samples.

9.4 References

[1] M.G. Bawendi, *Confined Electrons and Photons*, (Plenum Press, New York, 1995), p 339.
[2] F. Hache, D. Richard and C. Flytzanis, Appl. Phys. Lett. **55**, 1504 (1989).
[3] Sacra, A.; Norris, D.J.; Murray, C.B.; Bawendi, M.G. J. Chem. Phys. **103**(13), 5236 (1995).
[4] Blanton, S.A.; Leheny, R.L.; Hines, M.A.; Guyot-Sionnest, P. Phys. Rev. Lett. **79**(5), 865 (1997).
[5] Schmidt, M.E.; Blanton, S.A.; Hines, M.A.; Guyot-Sionnest, P. J. Chem. Phys. **106**, 5254 (1997).
[6] Hines, M.A.; Guyot Sionnest, P. J. Phys. Chem. **100**, 468 (1996).
[7] Dabbousi, B.O. et al., J. Phys Chem B **101**, 9463 (1997).

Chapter 10: Spectral Diffusion - Small Shifts

10.1 Introduction

In chapter 9, large spectral diffusion shifts were found to result from changes in the local electric field around individual nanocrystallites. These local fields were thought to result from ionization, depositing charges on or near the surface of the nanocrystallites. In this chapter we discuss a mechanism for the small spectral diffusion shifts described in section 7.3.2. We have seen that spectral diffusion plays a dominant role in the lineshape of single nanocrystallites. By understanding the origins of spectral diffusion, it may be possible to control this effect, providing additional control over the optical properties of this material.

Nanocrystallite ionization is a relatively rare event ($\sim 10^{-7}$/excitation)[1] which produces a large change in the local electric field. As a result, large spectral diffusion shifts correspond to discrete changes in the emission energy that occur on a relatively slow timescale (minutes). Small spectral diffusion shifts, however, are characterized by an almost continuous shifting of the emission spectrum on a timescale which is relatively fast compared to the acquisition time of a single spectrum. In addition, fluorescence intermittency is not commonly associated with small spectral diffusion shifts (recall figure 9.8). These characteristics suggest that small spectral diffusion shifts do not result from ionization and recombination of charges. In keeping with the results of chapter 9, however, small spectral diffusion shifts can be described in terms of fluctuations in the local electric field produced by the movement of charge carriers between local trap sites.

In what follows, we investigate this mechanism by examining the effects of various experimental parameters on small spectral diffusion shifts. Section 7.3.2 revealed that the

lineshape of a single nanocrystallite spectrum arises primarily from spectral diffusion. In order to quantify the effects of experimental conditions on spectral diffusion, linewidths are therefore used as a measure of the magnitude of small spectral diffusion shifts. In this chapter, changes in linewidth as a function of excitation intensity, wavelength, integration time and sample temperature are analyzed and found to be consistent with the activated movement of external charges in response to thermal and excess excitation energy released following each photo-excitation.

10.2 Experimental

Sample preparation and all experimental apparatus used in these experiments was identical to that described in chapter 3. Spectra were taken from single nanocrystallites under a number of different experimental conditions. Linewidths were determined by direct measurement of the full width at half maximum (FWHM) of each peak and not by a fit to a functional form (such as a Lorentzian), since single nanocrystallite spectra rarely fit a standard form.

In these experiments, we are primarily interested in the *average* effect of the applied conditions on the linewidth of single nanocrystallite spectra. For integration times, an excitation intensity of 85W/cm^2 was used to acquire spectra with times of 5, 10, 20, 30, 40, 50, 60, 90 and 120 seconds. For intensities, a time of 30 seconds was used to acquire spectra at intensities of 11, 23, 40, 85, 130, 175, 220, 355 and 450 W/cm^2. In determining the effect of integration time and excitation intensity, all points within a time or intensity series were measured on each individual nanocrystallite. As such, the average *change* in linewidth for a single nanocrystallite sample can be measured, and not merely the change in *average* linewidth. This is a subtle difference which

allows for more precise statistical analyses, since the distribution of absolute linewidths is much larger than the distribution of the changes in linewidth within a given sample.

Temperature data were taken on different days with fresh samples to insure no degradation with time. Intensity and time series were taken in non-sequential order to insure that the observed spectral changes were not caused by light induced degradation.

10.3 Results

Figure 10.1 plots the average linewidth as a function of excitation intensity for a sample of single 56.5Å non-overcoated nanocrystallites and an overcoated sample with the same size CdSe core. Figure 10.2 plots the average linewidth for a sample of single 56.5Å overcoated nanocrystallites as a function of excitation intensity, integration time and sample temperature.

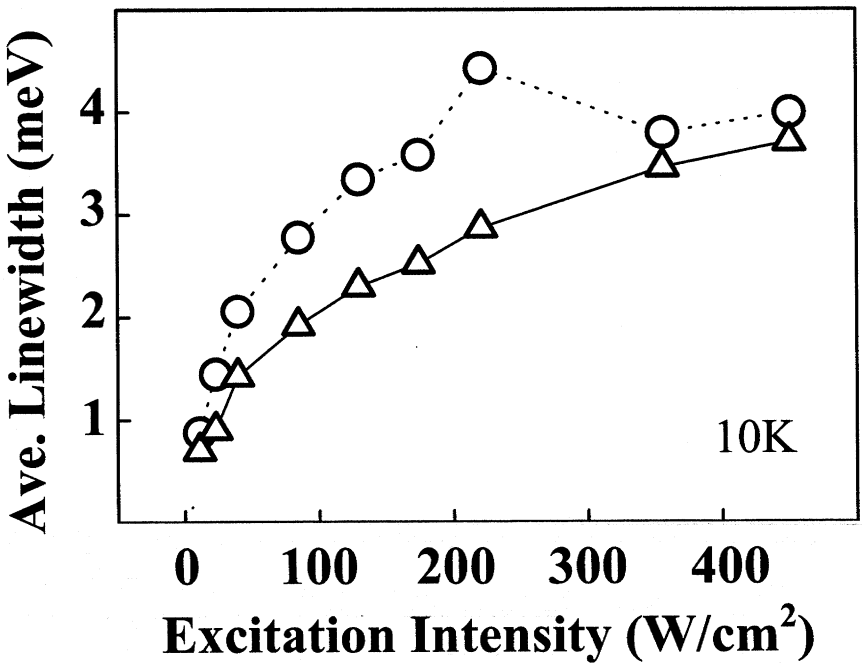

Figure 10.1: Average linewidth for 34 single overcoated nanocrystallites and 25 non-overcoated nanocrystallites (triangles and circles respectively) as a function of excitation intensity at 10K. Integration time was 30 sec.

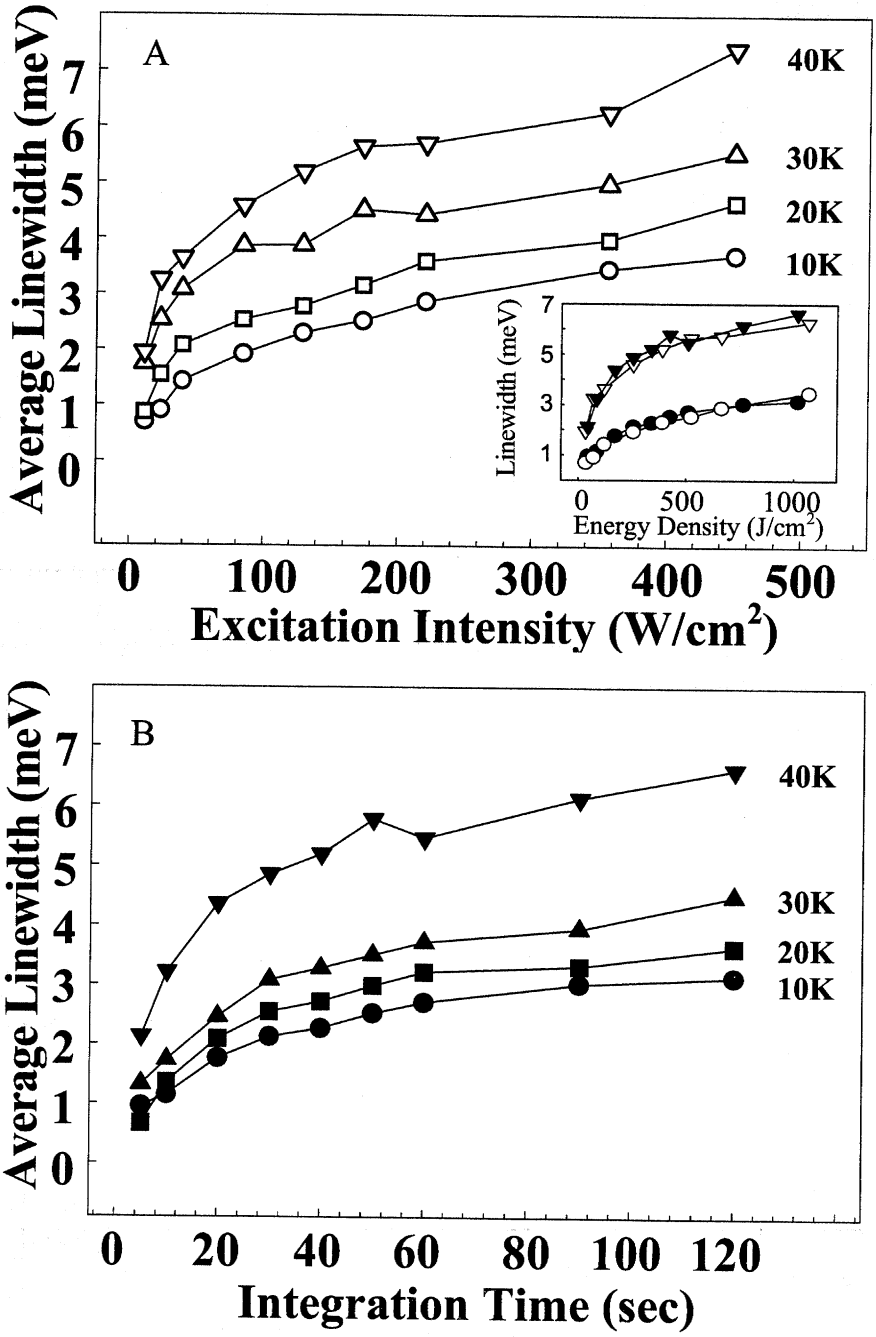

Figure 10.2: (A) Average single nanocrystallite linewidth as a function of excitation intensity and temperature for a 56.5Å overcoated sample. Circles (10K), squares (20K), upward triangles (30K) and downward triangles (40K) represent the average linewidths of 34, 53, 38 and 24 nanocrystallites respectively. Data was taken with an integration time of 30 sec. (B) Average single nanocrystallite linewidth for the same sample as a function of integration time and temperature. Circles (10K), squares (20K), upward triangles (30K) and downward triangles (40K) represent the average linewidths of 40, 47, 38 and 23 nanocrystallites respectively. Data was taken with an excitation intensity of 85W/cm^2. (Inset) Time and intensity data from (A) and (B) (open and closed symbols respectively) at 10K and 40K (circles and downward triangles respectively). Inset data is plotted as a function of excitation energy density (time × intensity) in order to normalize for the total number of photons absorbed per spectrum.

It should be noted that the average linewidths at the lowest intensities and shortest integration times in figures 10.1 and 10.2 are inflated due to many individual spectra falling below the resolution limit of our spectrometer (~0.4meV). In addition, while the average linewidth curves show a smooth saturation character, many individual nanocrystallites have a much more linear change in width as a function of time and excitation intensity, followed by a region of saturation (figure 10.3). The smooth average curves are the result of differences in the slope and saturation linewidth of individual nanocrystallites which represent the effects of different local environments on spectral diffusion.

The electric field studies described in chapter 9 suggested that small spectral diffusion shifts may result from small fluctuation in the local electric field. For electric

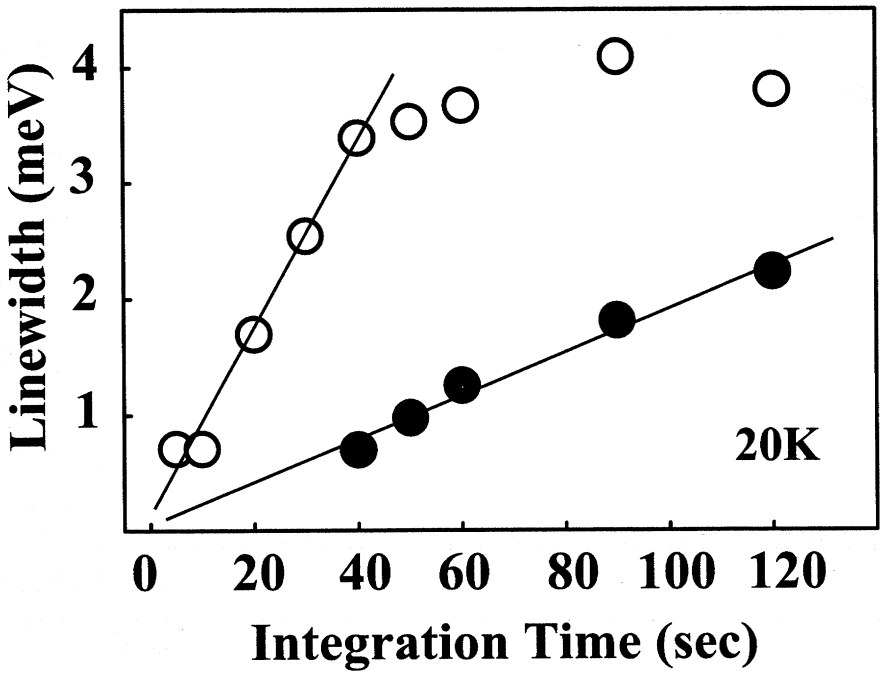

Figure 10.3: Linewidth as a function of integration time for 2 different single nanocrystallites from a 56.5Å overcoated sample at 20K. Lines indicate a least-squares fit to the linear region approaching the origin.

fields on the order of the local fields measured in those experiments, the dependence of the Stark shift (ΔE) on electric field (F) was found to be in the quadratic regime ($\Delta E \propto F^2$) (see figure 8.4b). This implies that in the presence of a fluctuating field (ΔF), the magnitude of the change in the Stark shift [$\Delta(\Delta E)$], and therefore the observed linewidth, also depends on the average field present [$\Delta(\Delta E) \propto F \cdot (\Delta F)$]. Consistent with this prediction, Stark shifted emission spectra such as those in figure 8.3 are seen to broaden as they shift to lower energies (higher total internal fields).

A similar broadening in quantum wells results from a decrease in the excited state lifetime due to field ionization of the exciton. However, if the observed broadening in CdSe nanocrystallites was lifetime limited, implying an excited state lifetime of $\sim 10^{-14}$s, the very slow radiative relaxation ($\sim 10^{-6}$s) would be completely quenched (quantum yield $\sim 10^{-8}$). The observed high emission intensity suggests that field ionization is not a significant contribution to the observed broadening, consistent with the Stark mechanism described above.

Since Stark shifts are quadratic in the average *total* electric field, and the linewidth changes linearly with the average *total* electric field, the linewidth in the presence of an applied electric field should change as the square root of the resulting Stark shift [$\Delta(\Delta E) \propto (\Delta E)^{1/2}$]. Figure 10.4 plots the linewidth of a single nanocrystallite as a function of relative shift in the presence of an applied field. As predicted, this data can be roughly fit with a function that varies as the square root of the observed shift. This result is consistent with the hypothesis that small spectral diffusion shifts result from fluctuations in the local electric field. From data such as figure 10.4, the magnitude of the change in the local electric field can be extracted (~36 kV/cm). This is the magnitude of the change in the *local* field along

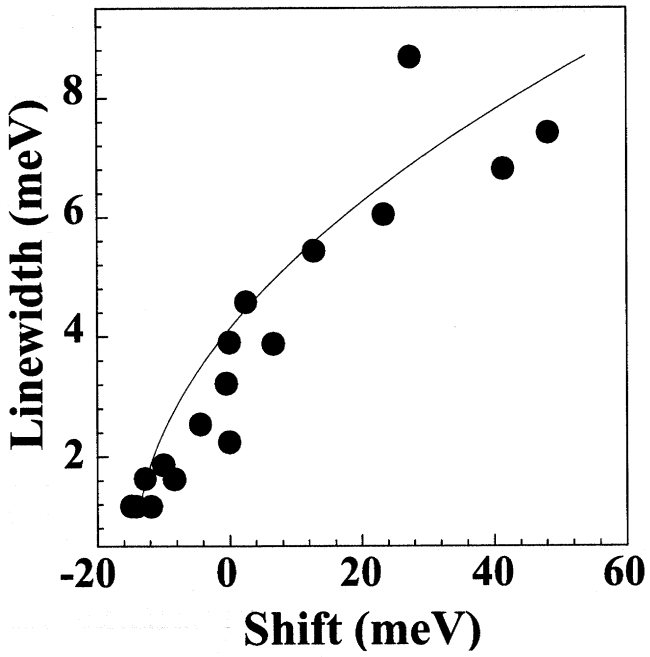

Figure 10.4: Linewidth of a single nanocrystallite emission spectrum versus shift from the zero-field position in response to an applied electric field. Solid line is a square root fit to the data. Excitation intensity was 25 W/cm^2 and an integration time of 30 seconds.

the *applied* field axis. If we assume that these changes result from charges moving around the circumference of a sphere, this change in field is comparable to that produced by a charge moving approximately the distance between 2 atomic sites on the surface of the nanocrystallite. Of course, this calculation makes many assumptions, including the assumption that there is only one charge that contributes to the local field fluctuation. As such, this should not be used as a quantitative measure of the charge movement, but rather as a confirmation that the movement of charges around the nanocrystallite could reasonably produce the observed field fluctuations.

A second consequence of the relationship between linewidth and average local electric field is that overcoated nanocrystallites, which were found to have a smaller total internal field than non-overcoated nanocrystallites (see figure 8.6) should also have

narrower diffusion induced linewidths in the presence of similar local field fluctuations. Figure 10.1 confirms that this is the case over a range of excitation intensities for a sample of overcoated and non-overcoated nanocrystallites with the same size CdSe core. This result is consistent with the hypothesis that small spectral diffusion shifts result from local field fluctuations.

10.4 Discussion

10.4.1 Model

Spectral diffusion in single molecules is typically attributed to changes in the host matrix (represented by a system of double welled potentials) which interact with individual chromophores through short range strain fields[2-4]. As described above, the fluctuating electric fields responsible for spectral diffusion in CdSe nanocrystallites are thought to result from the presence of charge carriers trapped on or near the surface of individual nanocrystallites. In what follows, I speculate that this spectral diffusion can be described in terms of point charges in a system of many welled potentials (trap sites). Small fluctuations in the local electric field result from individual charges moving between different trap sites. As a result, single nanocrystallite lineshapes are determined by the number and type of external charges, the number and depth of available trap sites, and the frequency and pattern of shifts between sites during the acquisition of a single spectrum.

10.4.2 Time and Excitation Intensity Dependence

The time dependence of the average linewidth observed in figure 10.2, which occurs over a very long timescale, can only be explained as an effect of spectral diffusion. The excitation intensity dependence, which is not the result of traditional power broadening since excitation occurs far from the emitting state (~350meV), can also be understood within the framework of spectral diffusion. The data in figure 10.2 suggests that the observed broadening is actually related to the number of excitations that occur during the acquisition of a given spectrum. The inset of figure 10.2 shows the time data (at fixed excitation intensity) and intensity data (at fixed time) for two temperatures, plotted as a function of the time integrated intensity (energy density = time × intensity). Plotted in this way, it is easy to see that changing the excitation intensity has the same effect as changing the integration time by the same relative amount. Assuming that we are in the linear absorption regime (<100kW/cm^2)[5], this implies that it is the number of absorbed photons per spectrum that is related to the observed broadening. It therefore follows that excess excitation energy, released as the exciton relaxes to the emitting state, may be responsible for the movement of external charges.

10.4.3 Wavelength Dependence

In order to verify that excess excitation energy is responsible for small spectral diffusion shifts, the average single nanocrystallite linewidth for a 56.5Å overcoated sample was studied with 514nm excitation and with 573nm excitation from an Ar^+ pumped dye laser. In this experiment, time, temperature and the number of excitations were held constant. To normalize for the number of excitations, emission intensity was

used as a measure of excitation rate. The excitation intensity was adjusted so that the average emission intensity was the same at both wavelengths. Since quantum yield has been found to be relatively wavelength independent in the region that we are exciting, each photon emitted should correspond to a fixed number of photons absorbed. Data for all nanocrystallites were collected at both wavelengths and the change in linewidth for each nanocrystallite was measured. For the 126 nanocrystallites studied, decreasing the excitation energy by ~250meV caused an average decrease in linewidth of 25%, suggesting that spectral diffusion is dependant on the amount of energy released upon each excitation. This, combined with the overlap of the time and intensity curves seen in figure 10.2(inset), implies that the lineshape of a single nanocrystallite spectrum depends on the number of excitations, and therefore the amount of energy released, during its acquisition.

A second implication of the wavelength data is that the energy responsible for the movement of external charges primarily results from the excess excitation energy released as the exciton relaxes to the emitting state, and not the energy released via non-radiative recombination of the exciton state. Assuming that these nanocrystallites do not have 100% quantum yield, some number of excitations relax non-radiatively, releasing the full excitation energy (~2.4eV). However, if non-radiative relaxation was an important contribution to the observed linewidths, the small change in excess energy resulting from the change in excitation wavelength (~250meV) would have a negligible effect relative to the large non-radiative contribution (~2000meV). The fact that this small change in energy significantly affects the measured linewidths indicates that the

energy involved in spectral diffusion is small, consistent with the energy released as the exciton relaxes to the emitting state.

10.4.4 Heating

It is possible that spectral diffusion is affected by an isotropic increase in the temperature of the nanocrystallites, which results from the release of excess excitation energy. This possibility can be evaluated by calculating the increase in temperature per excitation along with the rate of heat dissipation into the surrounding matrix. Assuming that all of the energy is released as heat, the change in temperature of the nanocrystallite upon the addition of excess excitation energy is:

$$\Delta T = \frac{\Delta U}{C_{nc}}, \qquad [10.1]$$

where ΔU is the amount of energy added to the system and C_{nc} is the heat capacity of the nanocrystallite. As an approximation, bulk CdSe has a heat capacity of ~40mJ/g·K at 25K. Therefore, for a single 56.5Å non-overcoated nanocrystallite with a mass of ~2.5×10^{-19}g, $C_{nc}\approx10^{-20}$J/K = 63meV/K. Assuming that all of the energy released as the exciton relaxes from its absorbing state is in the form of heat, the change in temperature per excitation would be ~6K (ΔU =380meV for 514 excitation with 610nm emission). By itself, this does not represent a significant increase in temperature and is unlikely to be responsible for spectral diffusion, however, if the rate of heat dissipation into the surrounding matrix is slower than the excitation rate, the cumulative increase in temperature could be substantial.

The rate of heat dissipation for a single nanocrystallite into the surrounding polymer matrix can be estimated from the rate of heat transfer from a thermally

conducting sphere with a constant surface temperature. In order to simplify the calculations, we will assume that the temperature of the surrounding matrix is 0K. In that case, the average temperature of the sphere as a function of time is[6]:

$$T(t) = \frac{6T_{init}}{\pi^2} \cdot \sum_{n=1}^{\infty} \frac{1}{n^2} \cdot e^{-\frac{n^2 \cdot K \cdot \pi^2 \cdot t}{r^2 \cdot \rho \cdot C}} \qquad [10.2]$$

where T_{init} is the initial temperature (assumed constant across the sphere), and K , ρ, C and r are the thermal conductivity, density, heat capacity, and radius of the sphere. If we use bulk parameters for CdSe (K=316mW/cm·K, ρ=5.66g/cm^3, and C=40mJ/g·K), a nanocrystallite with a diameter of 56.5Å should equilibrate with its surroundings within 10^{-12} seconds. This indicates that heating should be insignificant in these experiments since the dissipation rate is 7 orders of magnitude faster than the excitation rate (~10^{-5} seconds).

From these calculations, we can conclude that the effect of excess excitation energy is not the result of an isotropic increase in the temperature of the nanocrystallite. Instead, phonons emitted as the exciton relaxes to its lowest excited state may couple directly to trapped charges. Following each excitation, there is a certain probability that an external charge will overcome the potential barrier between adjacent trap sites as a result of the released energy. The more often the nanocrystallite is excited, the more chances a charge has to escape, and the more changes in the local field configuration will occur. The result is a broadening of the observed single nanocrystallite spectrum as time or excitation intensity is increased.

10.4.5 Saturation

Saturation occurs when spectral diffusion has reached a steady state condition. At this point, the linewidth is no longer dependent on the kinetics of charge movement, but only on the relative probability that the nanocrystallite has experienced each available

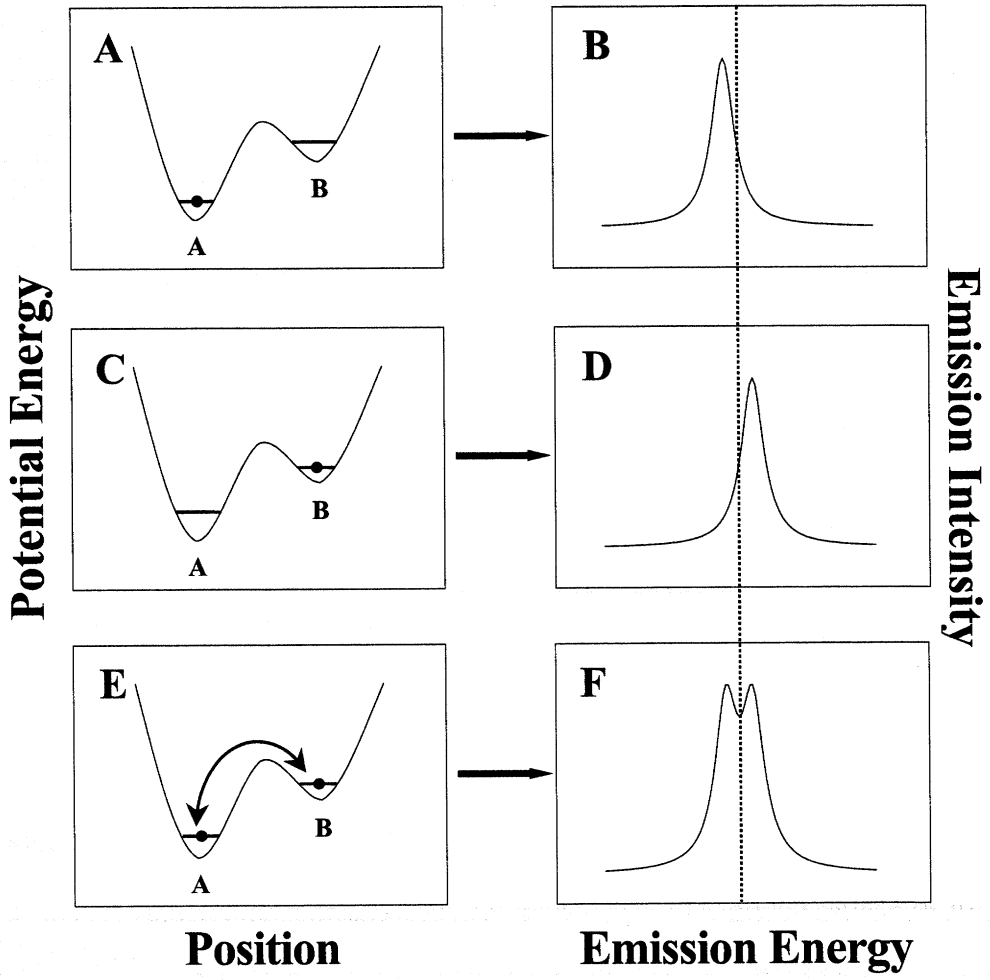

Figure 10.5: (A) and (B) Potential energy curve and resulting single nanocrystallite spectrum for a charge trapped in the left half of a double welled potential. (C) and (D) Same as (A) and (B) with the charge trapped in the right hand well. (E) Potential energy diagram in which the charge can freely move between the wells so that the observed spectrum is dependent on the relative occupancy of each well. (F) The resulting spectrum if the charge in (E) were to spend approximately equal time in each trap (this is the "high energy" limit where the available thermal and excess excitation energy is much larger than the difference in energy between the two wells). The emission energy of the peaks in figure 5(B) and (D) were arbitrarily chosen and are not expected to relate, in a direct way, to the energy of the corresponding trap site.

charge configuration. The saturation linewidth is then a function of the equilibrium distribution of trap occupancies, and will therefore depend on the number and type of external charges, the relative energies of each trap site and the available thermal and excess excitation energy.

To illustrate the effect of changing temperature or excitation energy on a single nanocrystallite spectrum, consider the simple case of a two trap system, containing a single charge (figure 10.5). In this case, the equilibrium occupancy of sites A and B ([A] and [B]) can be expressed as an exponential function of the available thermal and excess excitation energy. If we assume that the local electric field experienced by the nanocrystallite depends on the location of the trapped charge, with the resulting spectra shown in figure 10.5b and d, then the saturation linewidth of a single nanocrystallite spectrum depends on the relative amount of time that the charge spends in each trap. When the available thermal and excitation energy is small compared to the difference in energy between A and B, then $[B] \ll [A]$ and the saturation linewidth is dominated by the contribution from site A. In this case, the observed spectrum is that of figure 10.5b. When the available energy is high relative to the difference in energy between A and B, then $[B] \approx [A]$ and the observed saturation linewidth is that of figure 10.5f. Increasing the amount of available energy not only increases the saturation linewidth, it also increases the rate at which saturation is reached. From this simple example, it is clear that both the slope and saturation linewidth of a single nanocrystallite spectrum should be strongly dependent on the amount of available energy. Figure 10.2 demonstrates that this is the case for increasing temperature, consistent with the proposed mechanism.

10.4.6 Zero-Shift Limit

At very short times the number of changes in the local electric field becomes small, and spectra should approach an intrinsic width. Consistent with this, individual single nanocrystallite linewidths become very narrow as the integration time approaches zero. Two examples are presented in figure 10.4 along with linear fits to the non-saturation region. Within the measurement error, both fits intercept the y-axis at zero linewidth. This is consistent with theoretical predictions which suggest that the intrinsic linewidth of a single nanocrystallite should be extremely narrow, with a lower bound placed by the emitting state lifetime. The zero-time intercept values measured in figure 10.4 are not intended as a quantitative measure of the intrinsic width, but are only used to demonstrate the consistency between experimental results and theoretical predictions. Similar results are also observed at low excitation intensity, consistent with the proposed model.

10.4.7 Temperature Dependence

The thermal broadening observed in figure 10.2 does not result from coupling of the emitting state to acoustic phonons. Figure 7.4 shows that, under normal conditions, broadening due to dephasing is insignificant relative to the contribution of spectral diffusion. Similar to time and excitation intensity, the effect of temperature can be explained in terms of spectral diffusion. The overlap of the time and intensity curves in figure 10.2(inset), however, indicates that broadening as a direct result of thermally activated movement of external charge carriers is insignificant in this temperature range. Broadening due to direct thermal motion would result in a divergence of the time and

intensity curves, with the time curve saturating more quickly than the intensity curve, since thermal motion represents an additional time related broadening mechanism. This is not observed. At room temperature, however, the average linewidth of 31 overcoated nanocrystallites (67meV, σ=18meV) was found to be independent of excitation intensity, suggesting that direct thermal movement is the dominant broadening effect at room temperature.

The data in figure 10.2 is consistent with a thermally assisted process. What is meant by "assisted" is that while thermal energy alone may not result in significant spectral broadening, the exponential dependence of the escape probability from a given trap site implies that the total available energy (thermal + excess excitation) can have a much larger effect than either one alone. As the temperature is increased, trapped external charges populate a higher energy within each potential well (figure 10.6).

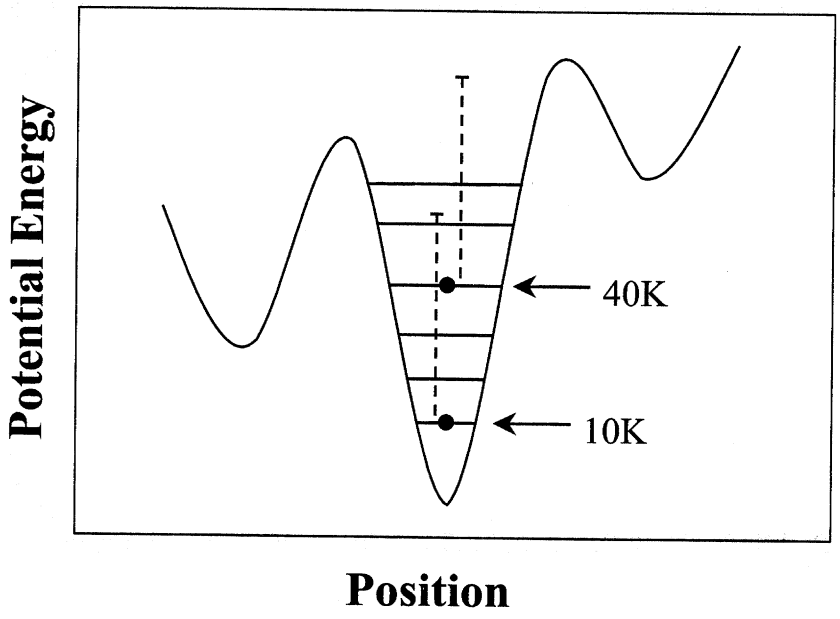

Figure 10.6: Thermally assisted charge movement. A graphic representation of a charge in a trap site at two different temperatures. Dotted lines indicate the energy added to the system from excess excitation energy.

Following each excitation, a higher energy charge has a greater probability of escaping a given trap. The observed thermal broadening is the result of a larger number of excitations resulting in a successful change in the local field configuration.

10.4.8 Notes on Modeling

It is important to point out that it is the change in the local electric field resulting from the movement of charges between trap sites, and *not* the relative energies of the traps, that determines the magnitude of a spectral diffusion shift. As a result, there is not necessarily a correlation between the energy difference between trap sites and the magnitude of the resulting spectral diffusion shift that occurs when a charge moves between these sites. While it may be possible to model the movement of charges between trap sites as an exponential function of the available energy, the resulting linewidth (the observable measured in these experiments) does not necessarily follow such a simple behavior since it also depends on the relative location of each trap. Also, it should be noted that while the number of potential trap sites around a nanocrystallite must be finite, the fact that multiple charges can contribute to the local field may result in a quasi-continuous distribution of potential field configurations.

10.4.9 Single Nanocrystallite Linewidths

In this chapter, the lineshapes of single nanocrystallite spectra were found to be strongly dependent on experimental and environmental factors. This can explain a mystery that has existed within the relatively small community of single nanocrystallite researchers. Our early work in this field[7] uncovered extremely narrow emission

linewidths for single nanocrystallite spectra (~100μev). Soon after, subsequent studies by other research groups also acquired spectra from single nanocrystallites, however, these linewidths were found to be much larger than those consistently observed in our lab. From the data in figures 10.1 and 10.2, the reported differences are consistent with variations in the experimental procedures used for each study. For instance, work by Tittel *et al.*[8] reported a minimum linewidth of ~5meV at 25K with an excitation intensity of 25W/cm^2 and an integration time of 10 minutes. Similarly, Banin *et al.*[9,10] report linewidths on the order of 2-3meV at 15K with an integration time of 1 minute and an excitation intensity of 1000W/cm^2. These results are consistent with the data presented in figure 10.2 suggesting that these reported linewidth differences are simply the result of variations in spectral diffusion arising from different experimental procedures.

10.4.10 Trap Sites

In this chapter, additional evidence of changing local electric fields around individual nanocrystallites has been presented. So far, the fields have been described in terms of charges moving between local trap sites. This is a reasonable assumption since evidence suggests that the large local field changes described in chapter 9 result from ionization of the nanocrystallites. What has not been discussed, however, is the nature of the trapped charges (i.e. where are they?). To our knowledge, no evidence currently exists which can conclusively locate these charges, however, some speculation can be made. Both spectral diffusion and the Stark results shown in chapter 9, have been observed in nanocrystallites embedded in a polymer matrix as well as ones deposited onto a quartz substrate with no surrounding matrix. Since these effects are present in the

absence of a surrounding matrix, it is likely that charges may reside in trap sites on the surface of the nanocrystallites. While this is just speculation, it is consistent with the experimental evidence currently available.

10.4.11 Non-Nanocrystallite Quantum Dots

While the experiments described in this chapter were performed on nanocrystallites, the spectral diffusion effects observed may also be relevant in other quantum dot systems. Linewidths in single GaAs quantum dots formed by potential fluctuations in thin quantum wells are found to be significantly broader for dots close to the surface of the quantum well structure[11,12]. In addition, linewidths are found to dramatically broaden if the protective AlGaAs layer is etched away from the quantum well structure, introducing a surface near the quantum dot[13]. This broadening in the presence of an exposed surface where charges can reside is consistent with spectral diffusion and the effects described in this chapter.

10.5 Conclusion

The results of this chapter suggest that the small spectral diffusion shifts responsible for measured single nanocrystallite lineshapes are actually the result of small fluctuations in the local electric field, producing Stark shifts in single nanocrystallite spectra. The magnitude of the change in the local field is found to be consistent with charges moving between local trap sites on the surface of the nanocrystallite. These spectral shifts are activated by excess energy released following each photo-excitation, with the shift probability being related to the temperature and the excitation energy.

While thermal effects are found to play an indirect role in linewidths at temperatures below 40K, they are a dominant effect at room temperature.

From the results of this chapter, a general model has been proposed to describe the linewidths of single nanocrystallite spectra in terms of the movement of charges between external trap sites around each nanocrystallite. In recent years, extensive theoretical work has been devoted to explaining the lineshapes observed in single molecular chromophores in terms of fluctuating environmental factors[2-4]. It is my hope that the experimental work presented in this chapter will inspire similar enthusiasm on the part of theorists to study the more complex mechanics involved in the lineshapes of single nanocrystallites.

10.6 References

[1] Nirmal, M. et al., Nature **383**, 802 (1996).

[2] Koedijk, J.; Wannemacher, R.; Silbey, R.; Volker, S. J. Phys. Chem **100**(51), 19945 (1996).

[3] Geva, E.; Skinner, J.L. J. Phys. Chem. B **101**(44), 8920 (1997).

[4] Pfluegl, W.; Brown, F.L.H.; Silbey, R.J. J. Chem. Phys. **108**(16), 6876 (1998).

[5] D.J. Norris, A. Sacra, C.B. Murray and M.G. Bawendi, Phys. Rev. Lett. **72**(16), 2612 (1994).

[6] H.S. Carslow and J.C. Jaeger, *Conduction of Heat in Solids*, (Oxford University Press, 1986), p235.

[7] S.A. Empedocles, D.J. Norris and M.G. Bawendi, Phys. Rev. Lett. **77**(18), 3873 (1996).

[8] J. Tittel W. Gohde, F. Koberling, Th. Basche, A. Kornowski, H. Weller, and A. Eychmuller, J. Phys. Chem. B **101**(16), 3013 (1997).

[9] U. Banin, M. Bruchez, A.P. Alivisatos, T. Ha, S. Weiss, and D.S. Chemla, J. Chem. Phys. **110**(2), 1195 (1999).

[10] U. Banin, private communication.

[11] H. Hess, E. Betzig, T.D. Harris, L.N. Pfeiffer, and K.W. West, Science **264**, 1740 (1994).

[12] D. Gammon, E. Snow and D. Katzer, Appl. Phys. Lett. **67**, 2391 (1995).

[13] D. Gammon, private communication.

Chapter 11: Summary

11.1 What have we learned?

So, after 4 years and many thousands of dollars, what have we learned about CdSe nanocrystallites that we didn't know before? The answer is: A lot! In fact, taken within the context of research being performed in our lab and others at the time, the results presented in this thesis have provided a completely new picture of these nanostructures. It is now understood that these are not simply static "artificial atoms". Rather, they are a dynamic system, with changes in the electronic and optical properties that occur over a wide range of time and energy scales. From a fundamental standpoint, these newly discovered phenomena hold considerable interest, providing new insight into the practical physics of quantum confinement. From an applications standpoint, these effects demonstrate a level of imperfection that could complicate their use in quantum confined devices. At the same time, by uncovering and understanding phenomena such as spectral diffusion and fluorescence intermittency, it may be possible to devise schemes by which to reduce or eliminate these effects, potentially resulting in a more perfect material. In fact, control over the occurrence of fluorescence intermittency and spectral diffusion is already possible through the incorporation of a ZnS overcoating. This provides an additional level of control over the optical and electronic properties that would not otherwise have been sought since these effects are unobservable in ensemble measurements. In addition, by understanding these effects, it may also be possible to harness them, allowing researches to change the emission energy and intensity of single or ensemble nanocrystallite samples at will.

Ionization appears to be a significant factor in the dynamics of CdSe nanocrystallites. While the exact mechanism for ionization is still uncertain, it seems clear that the removal of charges from the CdSe core is responsible for many of the effects observed on the single nanocrystallite level, including fluorescence intermittency and spectral diffusion. Ionization is also likely to be responsible for a significant portion of the local electric field and resulting excited state dipole moment that are measured in these nanocrystallites. The frequency of ionization can be controlled by the addition of a ZnS shell around the nanocrystallites, which acts as a barrier to ionization. Some of the effects of ionization, such as the magnitude of the induced excited state dipole, and the size of the resulting spectral diffusion shifts, can also be controlled by adding a ZnS shell or by increasing the nanocrystallite size. In these cases, the average internal electric field is decreased due to screening of the external charges and/or placement of the charges farther from the center of the exciton wavefunction respectively.

Once ionized, external charges continue to play a role in the behavior of nanocrystallites. Movement of charges between local trap sites is thought to be responsible for measured single nanocrystallite lineshapes. Charge movement is coupled to the excitation-emission cycle of each nanocrystallite as well as the temperature of the sample. In addition, excitation closer to the band edge reduces the amount of energy available to activate charge movement, decreasing its frequency. Once again, an increase in size, or the addition of a ZnS shell can reduce the resulting effects of charge movement by decreasing the average local electric field. The application of an appropriately oriented external electric field can also reduce these effects by opposing and reducing the average internal field.

In addition to dynamic effects, the existence of external charges can help explain some of the static nanocrystallite physics observed in both ensemble and single nanocrystallite studies. The magnitude of the local electric field, and the resulting induced excited state dipole moment arising from a charge on or near the surface of the nanocrystallite can explain not only the anomalously large phonon couplings measured in ensemble samples[1], and the range of phonon couplings measured in single nanocrystallite samples, it can also explain the state mixing that has been observed in ensemble non-linear optical experiments[2].

The Stark experiments that identified the existence of local electric fields around nanocrystallites have also resolved a controversy that has existed within the nanocrystallite community for many years: Are the excited states in CdSe nanocrystallites polar or polarizable? This debate arose from the question of whether emission in CdSe nanocrystallites originates from a localized surface trap state, or a delocalized exciton state. While independent ensemble Stark experiments have concluded that the excited states are either polar[3,4] or polarizable[5,6] depending on the modeling used to interpret the data, the single nanocrystallite experiments described in this thesis conclusively reveal that the emitting state has *both* polar and polarizable character. This is consistent with a delocalized exciton state in the presence of a strong local electric field.

In addition to identifying the presence of local electric fields, Stark measurements have also revealed a highly polarizable excited state, with Stark shifts of the emission spectrum that are up to 2 orders of magnitude larger than the linewidths measured for this state at 10K. These shifts are also on the same order of magnitude as room temperature

linewidths. Such large shifts suggest the potential of this material for use in highly efficient electro-optic modulation devices.

Under conditions that reduce spectral diffusion, single nanocrystallite emission spectra as narrow as ~100μeV are observed. These peaks are 600x narrower than measured ensemble peak widths and 50x narrower than linewidths extracted from ensemble size selective optical experiments such as fluorescence line narrowing. Such narrow solid state linewidths confirm theoretical predictions, reinforcing the description of these nanocrystallites as "artificial atoms". These results also support the use of nanocrystallites in potential devices such as highly efficient quantum dot lasers, electro-optic modulators, and infrared detectors, all of which rely on a narrow density of states.

In addition to the affects observed in single nanocrystallites, ionization and local electric fields may also affect observed ensemble measurements. For instance, absorption saturation measurements may be dominated by fluorescence intermittency at high excitation intensities. In this case, what is typically interpreted as saturation of an absorbing state is, in fact, a type of saturation in the emitting state. This is an entirely new perspective on an issue that would otherwise have been interpreted incorrectly, if not for these single nanocrystallite experiments. Also, the local electric fields (and changes in field) discovered in these experiments may represent a form of inhomogeneous broadening in ensemble spectra. Evidence suggests that ensemble broadening resulting from local electric fields could potentially be on the same order of magnitude as the broadening produced by the size distribution in most samples. This implies that efforts to reduce ensemble peak widths should include not only improvements in size distribution, but also improvements in the electric field distribution around individual nanocrystallites.

Again, it is important to control ionization and movement of external charges. These types of results give us a new way to think about certain ensemble characteristics that could only be obtained through single nanocrystallite detection.

Polarization measurements have demonstrated the power that simple experiments can have when applied to single nanocrystallites. Where little, if any, information is obtained on the ensemble level, polarization spectroscopy of single nanocrystallites has revealed a unique, degenerate transition dipole that is oriented isotropically in 2 dimensions. While theoretical treatments have predicted the presence of both 1D and 2D dipoles in CdSe nanocrystallites[7,8], these single nanocrystallite studies are the first direct evidence confirming the existence of a 2D dipole. In addition, the observation of such a dipole in emission provides insight into the physics of relaxation from the lowest excited state, indicating that this optically inactive state relaxes through an interaction with a degenerate dipole state. This is an important discovery, since the mechanism of relaxation from the lowest excited state in CdSe nanocrystallites has been of considerable interest in recent years[9-15]. This information should allow a more complete theoretical understanding of this mechanism. In addition, the fact that an electric field, which strongly alters the symmetry of the exciton envelope function, does not affect the orientation of the measured transition dipole moment, confirms that, for CdSe nanocrystallites, it is valid to separate the envelop and unit cell wavefunctions within the transition dipole matrix.

Finally, emission from a 2D transition dipole allows the determination of the 3D orientation of individual nanocrystallites. This has already had a substantial impact on

our ability to probe the physics of these structures, and will continue to do so in future experiments, especially in situations where directional perturbations are of interest.

11.2 Conclusion

By studying individual nanocrystallites, one at a time, it was possible to uncover exciting new physical characteristics and phenomena that were not even considered based on ensemble experiments. In addition to revealing these new characteristics, these studies have also provided a basis on which to attempt to control them. It should be stressed that the information obtained in these experiments is not merely more detailed than the information obtained on the ensemble level, it is fundamentally different. In fact, the elimination of ensemble averaging and inhomogeneous broadening have lead to a new perspective regarding the physics and dynamics of this system, and have expanded our ability to understand and manipulate this novel material.

11.3 References

[1] D. Norris, Al. Efros, M. Rosen and M. Bawendi, Phys. Rev. B, **53**, 16347 (1996).
[2] M.E. Schmidt, S.A. Blanton, M.A. Hines and P. Guyot-Sionnest, J. Chem. Phys. **106**(12), 5254 (1997).
[3] Colvin, V.L.; Alivisatos, A.P. J. Chem. Phys. **97**(1), 730 (1992).
[4] Colvin, V.L.; Cunningham, K.L.; Alivisatos, A.P J. Chem. Phys. **101**, 7122 (1994).
[5] Hache, F.; Richard, D.; Flytzanis, C. Appl. Phys. Lett. **55**, 1504 (1989).
[6] Sacra, A.; Norris, D.J.; Murray, C.B.; Bawendi, M.G. J. Chem. Phys. **103**(13), 5236 (1995).
[7] Al.L. Efros, Phys. Rev. B **46**(12), 7448 (1992).
[8] A. Zunger, Private communication.
[9] M.G. Bawendi, W.L. Wilson, L. Rothberg, P.J. Carroll, T.M. Jedju, M.L. Stegerwald, and L.E. Brus, Phys. Rev. Lett. **65**, 1623 (1990).
[10] M. O'Neil, J. Marohn, and G. McLendon, J. Phys. Chem. **94**, 4356 (1990).
[11] A. Hasselbarth, A. Eyuchmuller, and H. Weller, Chem Phys. Lett. **203**, 271 (1993).
[12] P.D.J. Calcott, K.L. Nash, L.T. Canham, M.J. Kane, and D. Brumhead, J. Lumin. **57**, 257 (1993).
[13] M. Chamaro, C. Gourdon, P.L. Lavallard, and A.I. Ekimov, Jpn. J. Appl. Phys. **34**, Suppl. 34-1, 12 (1995).
[14] M. Nirmal, D.J. Norris, M. Kuno, M.G. Bawendi, Al. L. Efros, and M. Rosen, Phys. Rev. Lett. **75**, 3728 (1995).
[15] M. Chamaro, C. Gourdon, P Lavallard, Ol Lublinskaya, and A.I. Ekimov, Phys. Rev. B **53**, 1 (1996).

Appendix 1

Evidence of Single Nanocrystallite Detection

While the impact of this work lies primarily in the information that was obtained, it should not be overlooked that one of the most significant accomplishment was that we were actually able to detect the fluorescence from single nanocrystallites. Within the context of the current field of single chromophore detection, this result may seem trivial, however, at the time this research began this represented a significant accomplishment. In fact, one of the most important aspects of the research presented here was verifying that what was being observed in these experiments were actually single CdSe nanocrystallites. Since the evidence for this is dispersed throughout the chapters of this thesis, it seems appropriate to compile them here. Taken together, this evidence represent a compelling argument for the validity of the results presented in this thesis:

1) "Single nanocrystallite" images appear as discrete, resolution limited spots on a dark background, with an areal density that is comparable to the expected density calculated from the concentration of nanocrystallites in the initial solution.
2) The total emission intensity collected in "single nanocrystallite" images is approximately what is expected, based on the excitation intensity and the absorption cross-section of a single nanocrystallite.
3) The fluorescence from individual "single nanocrystallites" is observed to blink on and off over time, in a binary fashion that is indicative of single chromophore detection (fluorescence intermittency).

4) Permanent (irreversible) photo-bleaching of "single nanocrystallites" also occurs in a single, binary step.

Of the first four points, the most compelling evidence for the detection of single nanocrystallites are 3 and 4. It should be noted, however, that while fluorescence intermittency and binary photo-bleaching are strong evidence of single chromophore detection, they do not specifically identify this chromophore as a CdSe nanocrystallite. True material identification requires the addition of spectral evidence.

5) "Single nanocrystallite" spectra reveal characteristics that are qualitatively similar to fluorescence line narrowed ensemble spectra.
6) The convolution of "single nanocrystallite" lineshapes with the distribution of zero phonon energies measured within a sample reproduces the full ensemble spectrum for that sample.

Points 5 and 6 are strong evidence that the single chromophores detected in these experiments are actually CdSe nanocrystallites. In addition, they also indicate that the nanocrystallites detected in these experiments are representative of the ensemble distribution. This is important, since the possibility exists that only a small, anomalous subset of nanocrystallites are detectable on the single nanocrystallite level. It also implies that the harsh excitation conditions used in these experiments ($>25 W/cm^2$) do not fundamentally change the spectral information obtained.

7) "Single nanocrystallite" spectra are very narrow, making it trivial to separate spectra from different nanocrystallites even when the fluorescence originates from within the same diffraction limited region of the sample.

8) Spectra from different "single nanocrystallites" display qualitatively similar spectral characteristics.

Points 7 and 8 are somewhat subtle, and require some additional explanation. In general, the dispersion of "single nanocrystallite" spectral energies observed within any sample is found to be comparable to the ensemble peak width for that sample (see point 6). At the same time, the "single nanocrystallite" spectra observed in these experiments are all found to be relatively narrow and uniform in their spectral characteristics. If the emission originating from a single spot within the image were to result from several nanocrystallites at once, the spectrum would not, in general, be narrow or uniform. In fact the resulting lineshape would have an infinite number of potential variations, depending on the emission energy of the contributing nanocrystallites. In instances where two or more nanocrystallites fall within the same diffraction limited spot, however, it is normally trivial to identify and separate the two spectra (recall figure 6.5). As such, the nature of the spectra obtained in these experiments indicates not only that these are CdSe nanocrystallites, but that they are actually spectra from *single* nanocrystallites.

9) Spectral diffusion does not, in general, result in a splitting of the "single nanocrystallite" spectra. Since no correlation is found between the spectral

diffusion shifts of different nanocrystallites within a sample, multiple overlapping spectra are expected to separate over time. This is not observed.

10) The application of an external electric field does not, in general, result in a splitting of the "single nanocrystallite" spectra. Stark characteristics for single nanocrystallites are found to be highly varied, and an applied field should shift different nanocrystallites to different degrees, separating overlapping spectra.

Similar to points 7 and 8, points 9 and 10 argue against the possibility that individual spectra result from multiple nanocrystallites.

11) The average Stark shift for a sample of "single nanocrystallites" is found to reproduce the ensemble measured value.

12) The distribution of "single nanocrystallite" polarization characteristics is representative of an isotropic distribution of single "dark axis" chromophores. The symmetry required to create a "dark axis" transition dipole is somewhat uncommon in molecular systems, indicating emission from CdSe nanocrystallites.

Similar to point 5, points 11 and 12 indicate that not only are we detecting single CdSe nanocrystallites, but also that the conditions of the experiment do not change, in a fundamental way, the physical characteristics of the nanocrystallites being observed.

Appendix 2

Effect of a Surface and Finite Numerical Aperture on the Polarization Dependence of Single Chromophores

In Chapter 5, a simple discussion of the polarization dependence as a function of out-of plane angle expected for 1-D "bright axis" and 2-D "dark axis" transition dipoles was presented. For this qualitative discussion an assumption was made that the collection angle of the detection system was infinitely small, and that the dipoles were radiating in free space. Obviously both of these assumptions are false since the dipoles are located on the surface of a quartz substrate and are being observed with a high numerical aperture microscope objective. As such, a slightly more complicated polarization dependence is expected. In order to quantify the data in figure 5.6, it was necessary to include these effects. In what follows, I describe why and how these effects contribute to the observed polarization dependence of both "bright" and "dark" axis chromophores.

Collection Angle

For a radiating dipole in free space, what is seen by the detection system is simply the projection of the dipole onto a plane that is normal to the collection axis (the line intersecting the dipole and the center of the detector – this plane will be referred to as the "sample plane"). This is strictly true, however, only if we assume an infinitely small collection angle, since a finite collection angle is capable of detecting some component of the dipole oriented perpendicular to the sample plane.

In order to envision this, imagine a dipole that is oriented parallel to the collection axis. In this case, the projection of the dipole onto the sample plane is zero (figure A.1a). If the detector is repositioned, allowing it to "see" the dipole from an angle, the projection onto the new "sample plane" is non-zero and can be detected (figure A.1b). For a microscope with a finite collection angle, the detection optics are able to "see" the dipole from a range of angles (figure A.1c). In order to calculate the total detected emission intensity, it is simply necessary to integrate over the entire solid collection angle of the microscope objective.

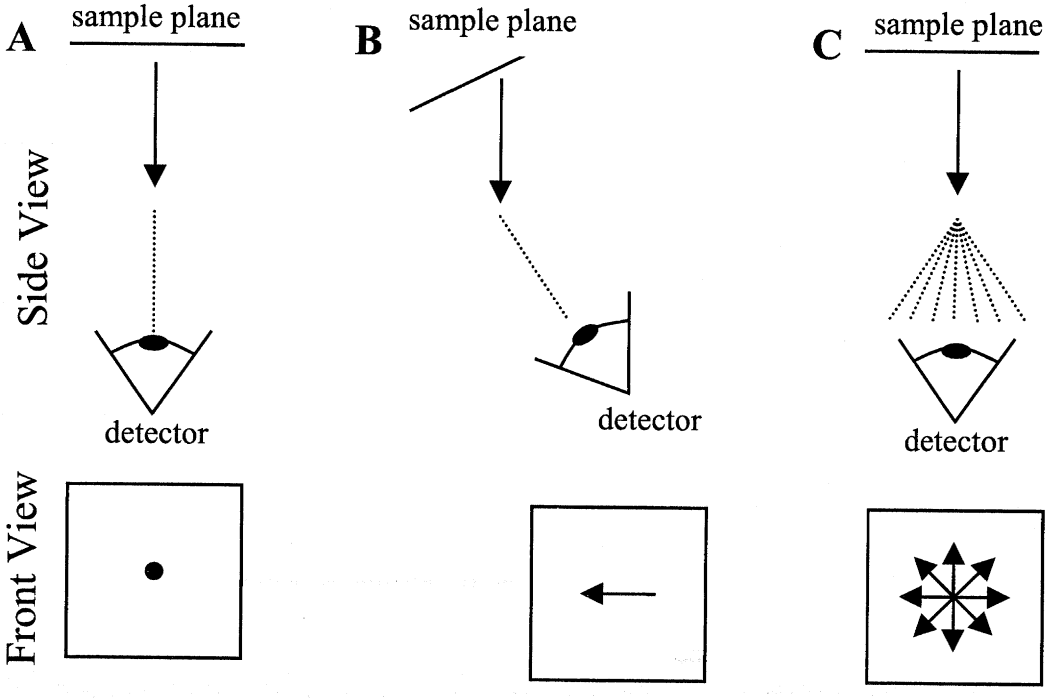

Figure A.1: Effect of collection angle on the detection of a radiating dipole. In each part, a dipole, which is oriented parallel to the collection axis, is observed by a detector. "Side view" displays the configuration of the dipole-detector system. "Front view" represents what is seen by the detector. (A) For an infinitely small collection angle, no light is emitted in the direction of the detector. (B) If the detector is moved off axis, it can "see" the dipole from the side. (C) Detection with a finite collection angle is equivalent to detection with an infinitely small collection angle, integrated over all off-axis orientations within the solid collection angle of the microscope objective.

The microscope objective used in our experiments has a large numerical aperture. The relation between numerical aperture and collection angle is:

$$N.A. = n \cdot \sin\sigma \qquad [A.1]$$

where n is the index of refraction of the medium between the sample and the microscope objective, and σ is the maximum collection half-angle for the objective. The microscope used in these experiments (N.A.=0.7) has a maximum collection half-angle of ~45° from normal.

To calculate the degree of polarization expected for any given dipole orientation, it is necessary to know the *polarization radiation pattern* emitted by the dipole (i.e. for light emitted in a direction $\vec{k}$ from the dipole, what is the polarization?). Each polarization component must then be transformed from object space (the region on the sample side of the microscope) to image space (the region on the detector side of the microscope). From this, we can determine the relative polarization of the light falling on the detector.

For a coordinate system in which the z-axis corresponds to the collection axis, and the dipole lies in the x-z plane with an out-of-plane angle θ relative to the z-axis (figure A.2a), the polarization radiation pattern for a dipole in free space is well known[1]. The polarization of the light emitted in a direction $\vec{k}$, defined by the S and P components of the light relative to the $\vec{k}$ -z plane, is

$$S(\alpha,\phi,\theta) = \frac{3}{8\pi} \cdot \sin^2\theta \cdot \sin^2\phi \qquad [A.2]$$

$$P(\alpha,\phi,\theta) = \frac{3}{8\pi}\left(\cos\theta \cdot \sin\alpha + \sin\theta \cdot \cos\phi \cdot \cos\alpha\right)^2. \qquad [A.3]$$

where the spherical coordinates ϕ and α are defined by $\vec{k}$, as shown in figure A.2b.

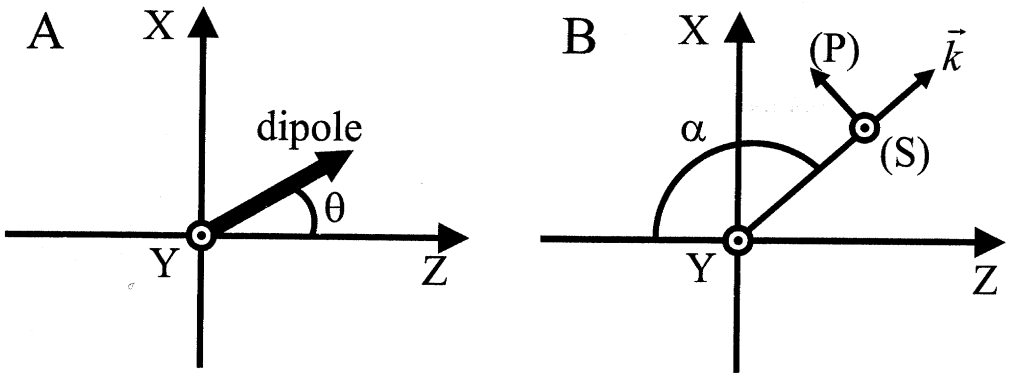

Figure A.2: Coordinate system for polarization calculations. The x-y plane corresponds to the sample plane, and is normal to the collection axis (z-axis). (A) Dipole orientation. The dipole lies in the x-z plane at an angle θ from the z-axis. (B) Emission direction and polarization. For light emitted in a direction $\vec{k}$, defined by the spherical coordinates α and ϕ, where α is defined relative to the –z axis, and ϕ is the azimuth angle defined relative to the x-axis, the orientation of the S and P polarizations is defined relative to the $\vec{k}$ -z plane as shown (⊙ indicates an orientation pointed out of the page).

In order to make the transform from object to image space, one assumption is made: The light propagating in image space is collimated. While not strictly true, this assumption is appropriate for the tube length of the microscope used in these experiments (160mm). The transform that occurs upon light passing from object to image space is that each ray is bent radially inward (toward the detector), remaining within the same $\vec{k}$ -z plane defined in object space. The S and P components retain their orientations relative to $\vec{k}$ and the $\vec{k}$ -z plane upon transformation.

Since the frame of reference used for equations A.2 and A.3 is relative to the $\vec{k}$ -z plane, and not the polarizer axis, the projection of the S and P components of $\vec{k}$ onto the polarizer frame of reference must be calculated. For this calculation, the polarizer is assumed to be parallel to the sample plane and alligned parallel to the x-axis. The

intensities of the detected light oriented parallel ($I_{//}$) and perpendicular ($I_{\perp}$) to the polarizer axis as a function of dipole orientation are

$$I_{//}(\theta) = \left(\sqrt{S(\alpha,\phi,\theta)}\sin\phi - \sqrt{P(\alpha,\phi,\theta)}\cos\phi\right)^2 \qquad [A.4]$$

$$I_{\perp}(\theta) = \left(\sqrt{S(\alpha,\phi,\theta)}\cos\phi + \sqrt{P(\alpha,\phi,\theta)}\sin\phi\right)^2 \qquad [A.5]$$

where S and P are the radiation polarization pattern for the dipole.

In order to calculate the measured polarization dependence, these functions are integrated over all $\vec{k}$ within the solid collection angle of the microscope:

$$I_{//}(\theta) = \int_{\pi}^{\pi-\sigma} d\alpha \int_{0}^{2\pi} d\phi \cdot \left(\sqrt{S(\alpha,\phi,\theta)}\sin\phi - \sqrt{P(\alpha,\phi,\theta)}\cos\phi\right)^2 \cdot \sin\alpha \qquad [A.6]$$

$$I_{\perp}(\theta) = \int_{\pi}^{\pi-\sigma} d\alpha \int_{0}^{2\pi} d\phi \cdot \left(\sqrt{S(\alpha,\phi,\theta)}\cos\phi + \sqrt{P(\alpha,\phi,\theta)}\sin\phi\right)^2 \cdot \sin\alpha \qquad [A.7]$$

where σ is the maximum collection half-angle of the microscope as defined in equation A.1. Combining equations A.2, A.3, A.6 and A.7, the measured degree of polarization as a function of out of plane angle (θ) can be calculated for a lens with an arbitrary numerical aperture:

$$D(\theta) = \left(\frac{I_{//}(\theta) - I_{\perp}(\theta)}{I_{//}(\theta)}\right). \qquad [A.8]$$

The solid line in figure A.3 shows the measured degree of polarization for a single "bright axis" dipole in free space, as a function of the out-of-plane angle. This calculation assumes a numerical aperture of 0.7. Also plotted are the relative detected peak emission intensities as a function of out-of-plane angle assuming far-field excitation (dashed lines) and isotropic excitation (dotted lines). "Peak intensity" refers to the maximum detected emission intensity as the polarizer is rotated (i.e. the peak of the sine-squared curve). The relevance of the intensity curves is to give the reader an idea of how bright the emission

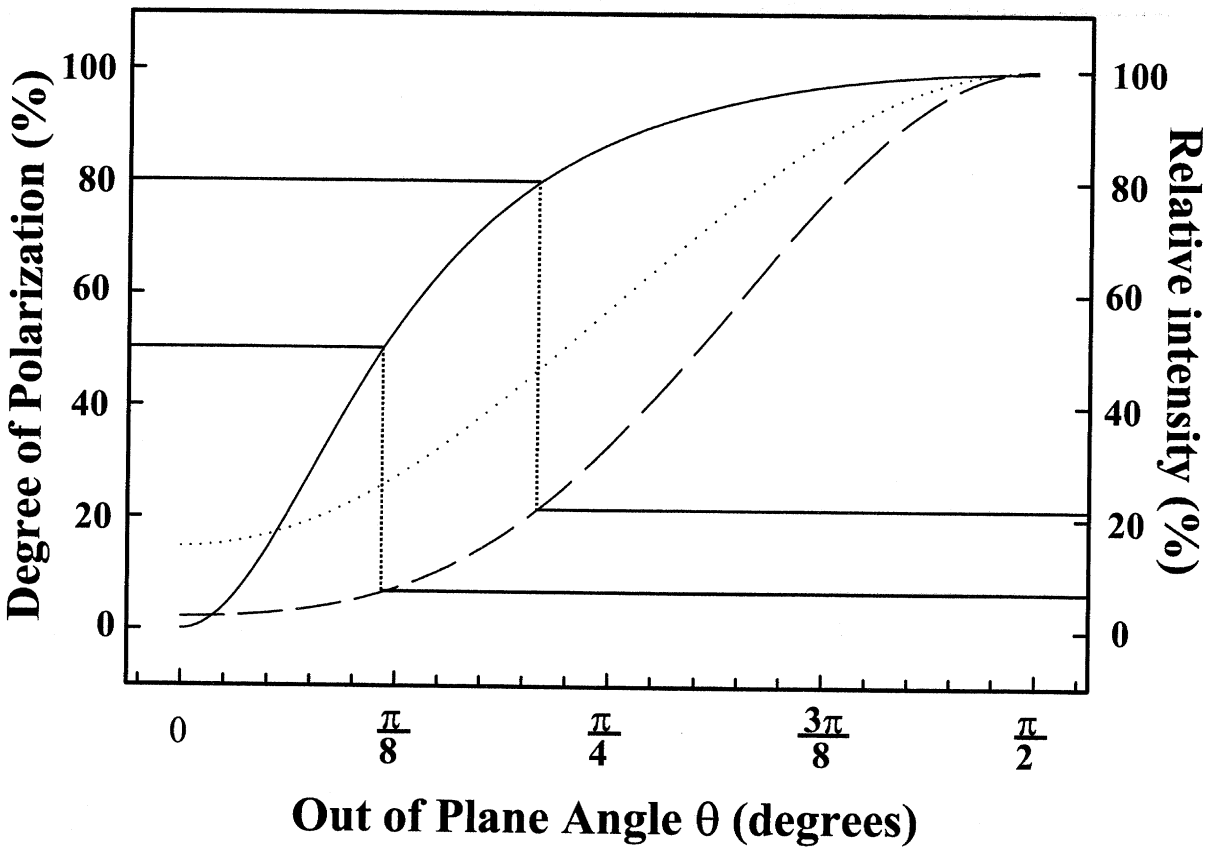

Figure A.3: Polarization and peak intensity of a "bright axis" dipole as a function of out-of-plane angle. The solid line represents the degree of polarization as a function of angle. Dotted and dashed lines represent the maximum emission intensity detected when the polarizer is oriented parallel to the projection of the dipole, assuming isotropic or far-field excitation respectively. The horizontal and vertical lines indicate the relative emission intensity for dipoles with 80% and 50% polarization.

from a dipole appears as the degree of polarization decreases. "Isotropic excitation" refers to the situation where the dipole is excited equally, regardless of orientation. "Far-field" excitation is subject to the same orientation dependence in excitation as in emission. Electroluminescence is an example of isotropic excitation, as is excitation with equal components of x, y and z polarized light. The dotted line is a simple calculation of the collection efficiency as a function of dipole orientation, and does not include the probability of excitation. The dashed line includes the fact that in order for the dipole to

emit, we must first excite it, following equations A.2-A.7. The dashed line in figure A.3 assumes that the excitation and emission dipole are collinear and that the polarization of the excitation light is parallel to the projection of the excitation dipole. This curve is what is expected experimentally.

As expected, figure A.3 indicates that dipoles with the lowest degree of polarization also emit the fewest photons in the direction of the detector. In fact, for "bright axis" dipoles having an 80% degree of polarization, the relative detected emission intensity is only ~20% of that for a dipole with 100% polarization. For a dipole with 50% polarization, the relative detected emission intensity is only 6%, and for the very small number of chromophores with 0% polarization (oriented normal to the sample plane), the total emission intensity is only 2% of the total for a dipole oriented parallel to the sample plane. From this plot, it is no surprise that the majority of all single "bright axis" chromophores observed experimentally have a degree of polarization that is close to 100%.

A comparison between figure A.3 and calculations by Axelrod[2], for the measured polarization dependence of a dipole in free space detected with a finite collection angle, reveals that they are identical. This confirms the validity of this technique for determining the measured degree of polarization for a single chromophore, which can now be adapted to incorporate the modified radiation pattern of a dipole on the surface of a dielectric interface.

Surface Effects

In order to calculate the actual degree of polarization measured for a single chromophore, we must also consider the true radiation pattern of a dipole on a surface.

Theoretical[1] and experimental[3] measurements by Lukosz *et al.* have demonstrated that the radiation pattern of a dipole on the surface of a dielectric interface is significantly different than that of a dipole in free space. For a dipole on a substrate surface, being detected from the air side of the substrate, the radiation patterns are*:

$$S(\alpha',\phi,\theta) = \frac{3}{2\pi} \cdot \frac{\cos^2\alpha' \cdot \sin^2\theta \cdot \sin^2\phi}{\left\{\cos\alpha' + n \cdot \cos\left[\sin^{-1}\left(\frac{1}{n} \cdot \sin\alpha'\right)\right]\right\}^2} \qquad \text{[A.9]}$$

$$P(\alpha',\phi,\theta) = \frac{3}{2\pi} \cdot \frac{\cos^2\alpha' \cdot \left\{n \cdot \cos\theta \cdot \sin\alpha' - \sin\theta \cdot \cos\phi \cdot \cos\left[\sin^{-1}\left(\frac{1}{n}\sin\alpha'\right)\right]\right\}^2}{\left\{n \cdot \cos\alpha' + \cos\left[\sin^{-1}\left(\frac{1}{n} \cdot \sin\alpha'\right)\right]\right\}^2} \qquad \text{[A.10]}$$

where θ and ϕ are defined as before, $\alpha' = \pi - \alpha$, and $n = \frac{n_2}{n_1}$ where n_2 is the index of refraction of the sample substrate and n_1 is the index of refraction of air.

Using equations A.6-A.10, it is trivial to calculate the measured degree of polarization as a function of the out-of-plane angle (θ) for a dipole on the surface of a dielectric interface. Figure A.4 displays the degree of polarization and relative emission intensity as a function of angle for a dipole on an air-glass interface, viewed from the air side, with NA=0.7. While these curves differ slightly from those in figure A.3, the general conclusions remain the same. In this case, for a dipole with 80% polarization, the relative detected emission intensity is ~47%. 50% polarization will result in ~22% emission intensity, and 0% will have only ~9% of the emission intensity of a dipole lying in the sample plane. As before, it is no surprise that the majority of the single "bright axis" chromophores observed have a very high degree of polarization.

* Note that equations A.9 and A.10 only describe the radiation patters for a dipole on the low index side of a dielectric interface, being detected from the low index side of the interface. The radiation patterns for other configurations (e.g. detection from the high index side) are different and can be found in reference 1.

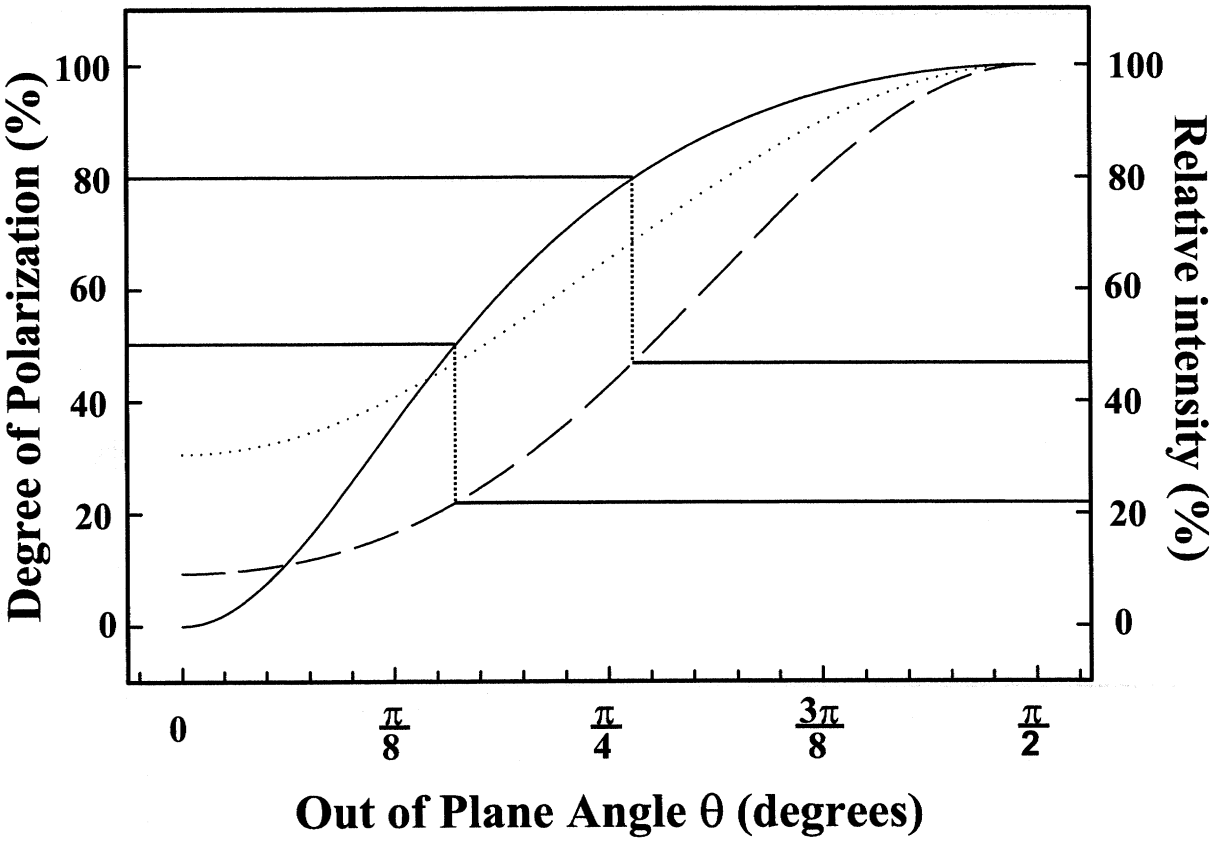

Figure A.4: Polarization and peak intensity as a function of out-of-plane angle for a "bright axis" dipole on a dielectric surface ($n_2 = 1.51$). Lines and markings are the same as in figure A.3.

"Dark Axis" Dipoles

Regardless of the orientation, the radiation pattern for a "dark axis" dipole can always be decomposed into the sum of two perpendicular "bright axis" dipoles, one that is parallel to the sample plane, and one that is oriented at some angle to the sample plane. This second "bright axis" dipole is at an angle of 90 degrees from the "dark axis" orientation, so that $\theta = 90 - \theta'$ where θ' is the out-of plane angle of the "dark axis"*.

* Note that this is a slightly different coordinate system than that used in chapter 5, since θ' is defined relative to the z-axis and not the x-y plane.

Equations A.2-A.7 and, A.9-A.10 can be used to calculate the radiation pattern of a "dark axis" dipole as follows: The relative intensities oriented parallel ($I_{//}^{D}$) and perpendicular ($I_{\perp}^{D}$) to the polarizer as a function of the "dark axis" orientation (θ') are

$$I_{//}^{D}(\theta') = I_{//}(90^{\circ}) + I_{\perp}(\theta) \qquad [A.10]$$

$$I_{\perp}^{D}(\theta') = I_{//}(\theta) \qquad [A.11]$$

where $I_{//}$ and $I_{\perp}$ are defined as in A.6 and A.7. The rationale for these equations is that the maximum detected emission intensity ($I_{//}^{D}$) occurs when the polarizer is parallel to the component of the "dark axis" dipole that is lying in the sample plane[$I_{//}(90^{\circ})$]. This intensity, however, has an additional contribution from the out of plane component, which is oriented perpendicular to the polarizer [$I_{\perp}(\theta)$]. The minimum detected emission intensity ($I_{\perp}^{D}$) occurs when the polarizer is perpendicular to the component of the "dark axis" that is lying in the sample plane [$I_{\perp}(90^{\circ})$], and parallel to the component that is oriented out of the plane[$I_{//}(\theta)$]. In this case, however, the in-plane component does not contribute to the total intensity [$I_{\perp}(90^{\circ}) = 0$].

The measured degree of polarization for a "dark axis" dipole (D^{D}) as a function of the "dark axis" orientation (θ') is

$$D^{D}(\theta') = \left(\frac{I_{//}^{D}(\theta') - I_{\perp}^{D}(\theta')}{I_{//}^{D}(\theta')} \right). \qquad [A.12]$$

The solid line in figure A.5 plots the measured degree of polarization for a "dark axis" dipole in free space as a function of θ'. The dashed line shows the peak emission intensity as a function of "dark axis" orientation. Unlike the case for the "bright axis" chromophore in figures A.3 and A.4, the dashed line in figure A.5 assumes isotropic excitation, consistent with

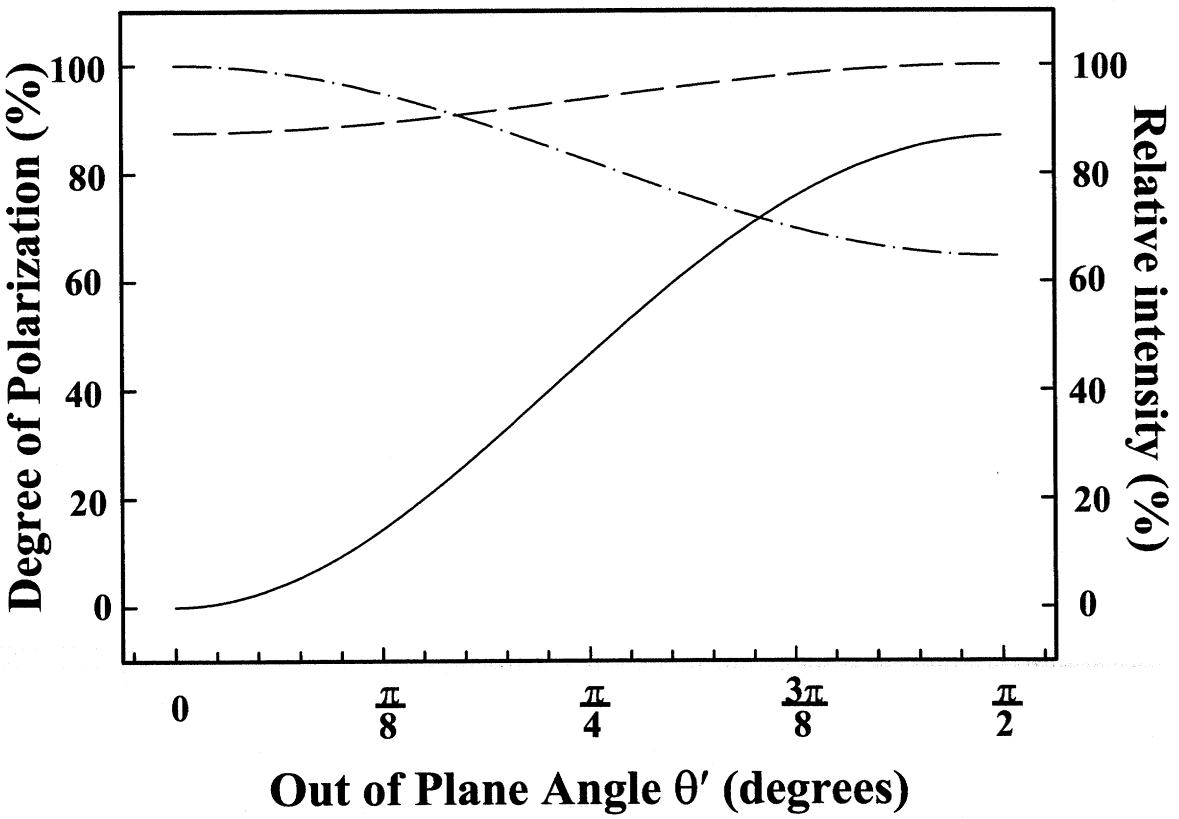

Figure A.5: Polarization, peak intensity and total intensity as a function of out-of-plane angle for a "dark axis" dipole in free space. The solid line represents the degree of polarization measured for the "dark axis" dipole as a function of angle. The dashed line plots peak emission intensity as a function of angle. The dot-dash line plots the total emission intensity as a function of angle in the absence of a polarizer in the detection pathway.

experimental results (see section 5.4.4 for details). Results for a "dark axis" dipole on a surface are derived in a similar fashion.

As expected, the maximum emission intensity for a "dark axis" dipole is relatively insensitive to changes in orientation. If the polarizer is removed, however, allowing light to be collected at all polarization angles, the results are quite different. The dot-dash line in figure A.5 indicates that for a "dark axis" oriented out of the plane, a higher total emission intensity is measured. This makes sense, since both "bright axis" components of the "dark axis" dipole are parallel to the sample plane and therefore contribute to the detected

emission intensity. For a "dark axis" lying in the plane, however, only one of the two "bright axis" dipoles contributes, resulting in a lower total emission intensity.

Warning

For anyone trying to run these calculations, beware! For some reason, Mathcad (even the newest version 8) cannot solve the integrals in these equations numerically. For many days, I thought that my formulation of the predicted polarization dependence was flawed since my answer differed from results of Axelrod[2], and from the qualitative results expected for this system. Eventually, I tried to solve the integrals symbolically, followed by a numeric solution of the evaluated integrals. This technique gave the desired (and correct) results. The worst part was that Mathcad did not display an error message when solving the integrals numerically, it simply gave the wrong answer. An example of this is displayed below.

SYMBOLIC SOLUTION

$\sigma := .77 \qquad \theta := 0, .1 .. \frac{\pi}{2}$

X(θ) = l-parallel
Y(θ) = l-perpendicular

$$X(\theta) := \int_0^{\sigma} \int_0^{2\cdot\pi} \left[\sqrt{\frac{3}{8\cdot\pi}\cdot(\cos(\theta)\cdot\sin(\alpha)+\sin(\theta)\cdot\cos(\phi)\cdot\cos(\alpha))^2}\cdot\cos(\phi) + \sqrt{\frac{3}{8\cdot\pi}\cdot\sin(\theta)^2\cdot\sin(\phi)^2}\cdot\sin(\phi) \right]^2 \cdot\sin(\alpha)\,d\phi\,d\alpha$$

symbolic evaluation of X(t)

$$X(\theta) := \frac{-3}{32}\cdot\sin(\theta)^2\cdot\cos(\sigma)^2 - \frac{3}{32}\cdot\sin(\theta)^2\cdot\cos(\sigma)^3 - \frac{1}{8}\cdot\cos(\theta)^2\cdot\sin(\sigma)^2\cdot\cos(\sigma) - \frac{1}{4}\cdot\cos(\theta)^2\cdot\cos(\sigma) - \frac{9}{32}\cdot\sin(\theta)^2\cdot\cos(\sigma) + \frac{15}{32}\cdot\sin(\theta)^2 + \frac{1}{4}\cdot\cos(\theta)^2$$

$$Y(\theta) := \int_0^{\sigma} \int_0^{2\cdot\pi} \left[\sqrt{\frac{3}{8\cdot\pi}\cdot(\cos(\theta)\cdot\sin(\alpha)+\sin(\theta)\cdot\cos(\phi)\cdot\cos(\alpha))^2}\cdot\sin(\phi) - \sqrt{\frac{3}{8\cdot\pi}\cdot\sin(\theta)^2\cdot\sin(\phi)^2}\cdot\cos(\phi) \right]^2 \cdot\sin(\alpha)\,d\phi\,d\alpha$$

symbolic evaluation of Y(t)

$$Y(\theta) := \frac{-1}{32}\cdot\sin(\theta)^2\cdot\cos(\sigma)^3 - \frac{1}{8}\cdot\cos(\theta)^2\cdot\sin(\sigma)^2\cdot\cos(\sigma) - \frac{1}{4}\cdot\cos(\theta)^2\cdot\cos(\sigma) - \frac{3}{32}\cdot\sin(\theta)^2\cdot\cos(\sigma) + \frac{3}{32}\cdot\sin(\theta)^2\cdot\cos(\sigma)^2 + \frac{1}{32}\cdot\sin(\theta)^2 + \frac{1}{4}\cdot\cos(\theta)^2$$

$$D(\theta) := \frac{X(\theta) - Y(\theta)}{X(\theta)}$$

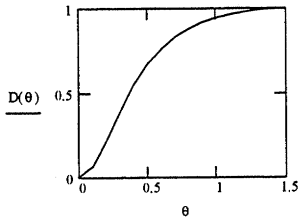

The symbolic solution to this function is correct. The answer should approach 1 as θ approaches π/2.

NUMERIC SOLUTION

$$X(\theta) := \int_0^{\sigma} \int_0^{2\cdot\pi} \left[\sqrt{\frac{3}{8\cdot\pi}\cdot(\cos(\theta)\cdot\sin(\alpha)+\sin(\theta)\cdot\cos(\phi)\cdot\cos(\alpha))^2}\cdot\cos(\phi) + \sqrt{\frac{3}{8\cdot\pi}\cdot\sin(\theta)^2\cdot\sin(\phi)^2}\cdot\sin(\phi) \right]^2 \cdot\sin(\alpha)\,d\phi\,d\alpha$$

$$Y(\theta) := \int_0^{\sigma} \int_0^{2\cdot\pi} \left[\sqrt{\frac{3}{8\cdot\pi}\cdot(\cos(\theta)\cdot\sin(\alpha)+\sin(\theta)\cdot\cos(\phi)\cdot\cos(\alpha))^2}\cdot\sin(\phi) - \sqrt{\frac{3}{8\cdot\pi}\cdot\sin(\theta)^2\cdot\sin(\phi)^2}\cdot\cos(\phi) \right]^2 \cdot\sin(\alpha)\,d\phi\,d\alpha$$

X(t) and Y(t) are identical to those above, but without the symbolic evaluation.

$$D(\theta) := \frac{X(\theta) - Y(\theta)}{X(\theta)}$$

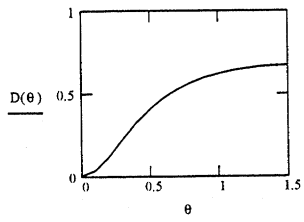

The numeric solution is wrong.

References

[1] E. Lukosz, J. Opt. Soc. Am. **69**(11), 1495 (1979).
[2] D. Axelrod, Biophys. J. **26**, 557 (1979).
[3] C. Fattinger and W. Lukosz, L.Lumines. **31&32**, 933 (1984).

List of publications

1. Empedocles, Neuhauser and Bawendi, "Three-Dimensional Orientation Measurements of Symmetric Single Chromophores Using Far-Field Polarization Microscopy", Nature (in press).
2. Empedocles, Neuhauser and Bawendi, "Spectroscopy of Single Quantum Dots", *Biblioteque Scientifique Francqui,* (De Boeck-Univeristy, 1999), (Invited – in press).
3. Empedocles and Bawendi, "Influence of Spectral Diffusion on the Lineshapes of Single CdSe Nanocrystallite Quantum Dots", J. Phys. Chem. **103**(11), 1826 (1999).
4. M.A. Pimenta, P. Corio, A. Marucci, S.D.M. Brown, E.B. Hanlon, S.A. Empedocles, M.G Bawendi, G. Dresselhaus, M.S. Dresselhaus, "Anomalous Dispersion of the Second Order Raman G'-Band in Carbon Nanotubes", (submitted).
5. C.A. Leather, N.Y. Morgan, C.R. Kagan, S.A. Empedocles, M.G. Bawendi, and M.A. Kastner, "Charge Generation and Transport in CdSe Semiconductor Quantum Dot Solids", (submitted).
6. Shimizu, Empedocles, Neuhauser and Bawendi, "Stark Spectroscopy Investigation of Spectral Diffusion in Single CdSe Quantum Dots", Proceedings of the 194th meeting of the Electrochemical Society (in press).
7. Empedocles, Neuhauser, Shimizu and Bawendi, "Photoluminescence from Single Semiconductor Nanostructures", *Characterization of Nanophase Materials,* (Wiley-VCH, Weinheim, Germany), (Invited - in press).
8. Empedocles and Bawendi, "Spectroscopy of Single CdSe Nanocrystallites", Accounts of Chemical Research (Invited - in press).
9. Pimenta, Marucci, Empedocles, Bawendi, Hanlon, Rao, Eklund, Smalley, Dresselhaus and Dresselhaus, "Raman modes of Metallic Carbon Nanotubes", Phys. Rev. B **58**(24), R16016 (1998).
10. Empedocles and Bawendi, "Quantum Confined Stark Effect in Single CdSe Nanocrystallite Quantum dots", Science **278**, 2114 (1997).
11. Empedocles, Norris and Bawendi, "Photoluminescence Spectroscopy of Single CdSe Nanocrystallite Quantum Dots", Phys. Rev. Lett. **77**(18), 3783 (1996).
12. Empedocles, Norris and Bawendi, "Spectral Diffusion of Ultra-Narrow Fluorescence Spectra in Single Quantum Dots", Materials Research Society Symposium Proceedings - Fall 1996, **452**,335 (1996).
13. Thomas, Empedocles, Morrison and Bing, Journal of the Experimental Analysis of Behavior, **60**, 313 (1993).
14. Thomas and Empedocles, Journal of Experimental Psychology: Animal Behavioral Processes, **18**, 22 (1992).

15. Thomas and Empedocles, Journal of the Experimental Analysis of Behavior, **55**, 267 (1991).

Papers in Preparation:

16. R. Neuhauser, S.A. Empedocles, K. Shimizu, and M.G. Bawendi, "Non-Binary Blinking and Correlated Spectral Diffusion: A Highly Parallel Study of Semiconductor Nanocrystals", (in preparation)
17. C.A. Leather, N.Y. Morgan, C.R. Kagan, S.A. Empedocles, M.G. Bawendi, and M.A. Kastner, "Photoconductivity in CdSe Quantum Dot Solids", (in preparation).

Acknowledgments

As with any large body of work, there are many people who have contributed to the completion of this thesis; most have added in ways that are far more significant than merely adding content to the text on these pages:

Most important to me have been the efforts of my loving wife Marianne, who moved across country and has endured many long days and missed weekends in support of my career as a scientist. She has been my anchor in life, helping me remember that there are many things that are far more important than science (yes, it's true!). For all of your patience, love and support, I am forever grateful, and will spend the rest of my life happily repaying you.

Other contributions to this thesis began long before my time at MIT. I am profoundly thankful to my mother, who, in the face of great adversity was still able to raise a "good boy" and teach him the value of hard work, both with his mind and with his hands (even if it meant missing the James Bond Film Festival to study for an algebra test at age 13). I am also greatly indebted to my Grandfather who, either through experience or genetics, has instilled in me the desire to invent and pursue my ideas with originality and creativity.

I was never a particularly motivated student until after entering college. For affecting that change, I would like to thank Dr. David Chiszar who taught me that oftentimes you have to work hard to accomplish a worthwhile goal, and sometimes it's only later that you truly realize the value of your efforts. I would also like to thank Dr. David R. Thomas for introducing me to the world of scientific research. While it may be hard to imagine how our work on *leaning and memory in pigeons* lead to my career as a physical chemist, he was able to teach me the excitement of designing and implementing original research and the wonder of being the first person in the world to learn something, or see something new.

It has been an honor and a privilege to work with my thesis advisor, Moungi Bawendi. In addition to providing a wealth of suggestions (many of which were good), he has given me the support, confidence and freedom that I need to grow and to be successful. He has always given me the opportunity to pursue my ideas (even when they were not so good) and to make and learn from my mistakes. It is because of Moungi that I have evolved from someone who likes to tinker with ideas into an actual scientist who could potentially fall on the positive side of Irwin Oppenheim's scientific value curve (thank goodness I'm not a theorist).

My experience at MIT has been shaped by my friends and colleagues in the Bawendi group: David, Manoj, Chris, Bashir, Cherie, Ann, Fred, Ken K., Hedi, Catherine, Dima, Jin-Kyu, Wing, Ken S., Vic, Robert, Sungjee and Nathan, it has been an honor to work with all of you and learn from you over the years. To the original members of the lab, I thank you for building this group into something that I have been proud to be a part of for the past 5 years. To the more recent additions, I encourage you to take advantage and enjoy being a part of such an extraordinary research environment.

Robert and Ken S., I have truly enjoyed our time together. I feel privileged to have been able to work with such exceptional scientists and to have had the opportunity to benefit from your ideas, your experience and your friendship.

While Robert has convinced me that under normal circumstances, life can be adequately sustained with only "science and air", for those occasional moments of weakness when I have required more, I am deeply indebted to my non-academic friends. Matt and Anu, Bill and Heather, Kamuran and Anna, Jon and Mara, Luke and Julie, and Jon O'Brien, thank

you for grounding me in reality and confirming for me that the only true measure of success is found in the list of people who you consider your true friends.

Since everyone knows that you really need "air, science and basketball" for a healthy and happy life, I would also like to thank the loyal attendees of Thursday afternoon basketball, especially the ones who made it through the "lean" years when we never had enough people to play a real game.

Finally, I would like to express my heartfelt gratitude to the inventor of the EREQ system, who has allowed me the freedom to spend money without leaving my seat.